Tulane University Medical Center

SCHOOL OF MEDICINE
Department of Pathology
and Laboratory Medicine SL79
1430 Tulane Avenue
New Orleans, Louisiana 70112-2699
(504) 588-5224
(504) 587-7389 FAX

cfermin@mailhost.tcs.tulane.edu
ht.//www.tmc.tulane.edu/ferminlab/
http://www.tmc.tulane.edu/imaging/

Thursday, April 09, 1998

Charles Winget, Ph.D.
NASA-Ames Research Center
MS 236-5
Moffett Field, CA 94035-1000

Dear Dr. Winget:

This is the final report to close activities of grant NASA NAG-2-999 "Effect of microgravity on afferent innervation" submitted in response to NRA 93-OLMSA-06 and funded as part of the SLM-MIR program for a period of three years. As part of report and in fulfillment of the requirements of the award I am enclosing copies of presentations and publication listed below. An explanation for each document is underlined.

1. **Fermin**, C.D. An audiovisual summary web presentation on results from SLM-MIR avian experiments. A color presentation summarizing results from the SLM-MIR and STS-29 avian experiments is located at [http://www.tmc.tulane.edu/ferminlab]. A black and white copy is enclosed now. This presentation explains the modifications that were made to the objectives of the original application. Of importance was the change in specimen sharing, malfunctioning of the Slobak incubator used in the space station MIR, and sub-optimal fixation of specimens returned for analysis. These variables were out of the control of the investigators and the final outcome of the experiments, and hence data returned, do not reflect lack of planning or proper design. Rather, it is an unfortunate side effect of politics mixing with science. In other words, the MIR program had to be conducted under the constraints of the exchange between the US and Russia. Furthermore, MIR was the only space station around at the time the experiments were planned. Fortunately, analysis of ground controls was part of the original objectives and the reports presented in this closing document resulted from evaluating samples processed at 1.0G. These ground-derived results are necessary for future evaluation of space returned samples. Additional information from the ground experiments will be published separately and will be provided as an addendum to this final report.

APR 2 7 1998

CA: C.A.S.I.
VIA
202A-3

2. **Fermin**, C.D. and Martin, DS. & H. Hara. Color threshold and ratio of S100ß, MAP5, NF68/200, GABA and GAD. I Distribution in inner ear afferents. *Cell Vision 4(5): 280-295,1997.* This paper correlated immunological expression of S100ß, MAP5, NF68/200, GABA and GAD in the VIIIth nerve afferents of the chick at 1.0G and fulfilled a very important part of the original objectives. These data characterized immunohistochemically these essential molecules during neuronal development, maturation and subsequent function of adults vertebrates. Of significance is the association of S100ß with cytoskeletal proteins. S100ß data was submitted on the original application, and implicated in the development of chick afferents that convey information about the environment to the brain centers. Most importantly however is that these data made possible by NASA support, permitted us to pursue molecular experiments at the DNA and RNA levels, and we are now able to clone gene segments that are differentially regulated before and after hatching.

3. Hara, H. Chen, X, Hartsfield, JF, Hara, J, Martin, D. and **Fermin**, CD Chicken (*Gallus domesticus*) inner ear afferents. Primary Sensory Neuron, Vol 4: **In Press, 1998**. This paper evaluated morphometrically the VIIIth nerve afferents of the chick at 1.0G in order to accumulate normative data needed for comparative evaluation of space returned samples and that was not available at the time the proposal was approved. There is a well known differences between the neurons of the auditory and vestibular branches of the VIIIth nerve in mammals and other vertebrates. The difference is relevant to each branch of the nerve response to damage and it could influence differential expression of macromolecules in the afferent neurons. Most importantly is however that these results are useful to interpret functional modifications of the afferent innervation at 1.0G as well. Similar morphometric analysis was published by us for primates and frogs by others, but this is the first comprehensive analysis of inner ear afferent in birds. Reprints of the results presented at the international meeting of the Association for Research in Otolaryngology were already requested.

4. **Fermin**, CD, Martin, DS, Jones, T, Vellinger, J, Deuser, M, Hester, P and Hullinger, R. Microgravity in the STS-29 Space Shuttle Discovery affected the vestibular system of chick embryos. Histol Histopath 11 (2):407-426, 1996. This paper consolidated results from the STS-29 experiments. Specimens from that flight and some data were collected by several investigators. Only minimal funds ($5,000) were given to PI of the project for data analysis. Since such funds were not sufficient for evaluating the results and did not provide any fund for inter investigator data evaluation, data was not published until bundled up with the SLM-MIR results due to relevance to the avian program and the similarity between quails and chickens. Additional samples await analysis and will be published when funds become available for that purpose.

5. **Fermin**, CD. and Martin, DS. Expression of S100ß in sensory & secretory cells of the vertebrate inner ear. *Cellular and Molecular Biology,* 41:213-225,1995. This paper evaluated the immunological expression of S100 beta in the VIIIth nerve afferents of the chick at 1.0G. S100ß is a calcium binding protein and neurotrophic factor that is expressed on the nuclei of some vestibular neurons and terminal dendrites. S100ß expression increases toward hatching and remains elevated thereafter. We know that S100ß expression changes after deafferentation and that patterns of expression at 1.0G may be different from those observed in space flown samples exposed to altered gravity. Based on observations above, we recently obtained transcript profiles from PCR amplified products that suggest a differential upregulation of S100ß after the VIIIth nerve was damaged to simulate changes that may occur to the vestibular system in altered gravity.

6. **Fermin**, CD, Lychakov, D, Campos, A, Hara, H, Sondag, E, Jones, T, Jones, S, Taylor M, Meza-Ruiz, G and Martin, DS. Otoconia biogenesis, phylogeny, composition & functional attributes. Histol & Histopath ***In Press, 1998***. This paper compiled data on each one of the topics above with vertebrate otoconia. Otoconia contribute greatly to the detection of linear

acceleration in all vertebrates. Thus, analysis of otoconia is of paramount importance to the understanding of underlaying sensory and non-sensory structures of the maculae that house the otoconia. Review of the literature and new data presented in this work demonstrate that otoconia of higher vertebrates recapitulate during phylogeny morphological features of older species. In addition, analysis of the work suggests that crystal forms of newer species retained the most energy efficient mechanisms present in older forms. This work, which was conducted cuncurrently with the SLM-MIR work and funded by NASA in previous grants, is not part of the original SLM-MIR objectives but very significant to the functional attributes of the afferent fibers whose analysis was the main goal of the SLM-MIR application.

7. **Fermin**, CD, Martin, DS, Li, Y-T & Li, S-C. The glycan keratan sulfate in inner ear crystals. *Cellular and Molecular Biology*, 41: 577-591, 1995. This Paper is complimentary to the otoconia review and it combined molecular and morphological approaches to in the characterization of the organic and inorganic components of otoconia. This work, which was conducted concurrently with the SLM-MIR work and funded by NASA in previous grants, is not part of the original SLM-MIR objectives but very significant to the functional attributes of the afferent fibers whose analysis was the main goal of the SLM-MIR application.

8. **Fermin**, CD, Lee, DH and Martin DS. Elliptical-P cells in the avian perilymphatic interface of the tegmentum vasculosum. *Scanning Microscopy 9(4)*:1207-1222, 1995. This work characterized specialized cells that in the inner ear may contribute to the separation of the endolymph from perilymph, two compartment fluid filled conduits that house the cells responsible for detection of gravity, linear and angular acceleration. This work is not part of the original SLM-MIR objectives but very significant to the functional attributes of the afferent fibers whose analysis was the main goal of the SLM-MIR application.

•**Hara,** H, Martin, D, Garry, G and Fermin, CD. LAMP2c & S100ß upregulation in brain stem after VIIIth nerve deafferentation. This portion of the report is the most exciting one, because it provides supporting data for my lab's transition between histological and molecular research. A small supplement to the last year of grant NAG-2-999 permitted pursuing molecular analyses of S100ß in the developing and deafferentated VIIIth cranial nerve. As discussed above the S100ß protein may have important effects on the developing, maturation and functioning of the afferent neurons of the VIIIth nerve, reason why we considered support of the study via a supplement to the grant warranted.

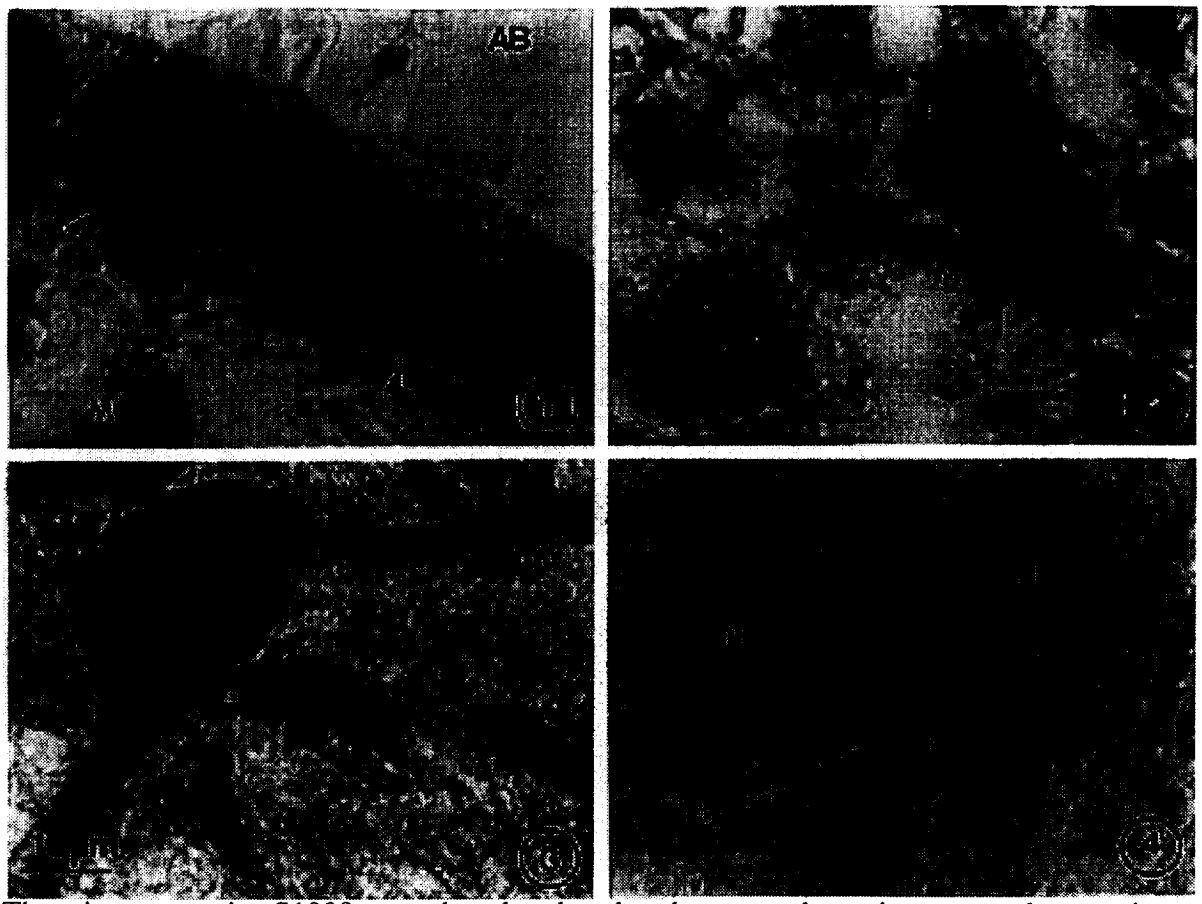

There is not an avian S100ß gene cloned to date, but there are other avian genes whose aminoacid sequence shared homology with mammalian S100ß. We designed and constructed primers and cDNA and used them to amplify S100ß related messages from normal and from deafferentated nerves. In these photographs we show S100ß expression over the terminal dendrites of the afferent neurons (arrowheads) and myelin (M) which serves as a positive built in control in the inner ear (FIGURE 1). Expression of S100ß over afferent neurons of the VIIIth nerve is very pronounced over nuclei of vestibular neurons and myelin (FIGURE 2), whereas in certain vestibular nuclei of the brain stem neurons contacted by the peripheral nerve also express S100ß abundantly (FIGURE 3), but negative control (FIGURE 4) neurons do not express S100ß. These results are a recapitulation of work published and submitted as enclosures, and are shown here for comparison with the in situ data that has not been published yet and it **should be treated as confidential and privileged**. Afferent dendrites surrounding hair cells hybridized with four cDNA probes constructed from the M126 gene mentioned above (FIGURES 5-8). The in situ data with these probes suggest that the M126 gene is a good candidate for and avian S100ß gene or close to it. We are presently sequencing the bands shown in the gels below and will complete the work when funds become available.

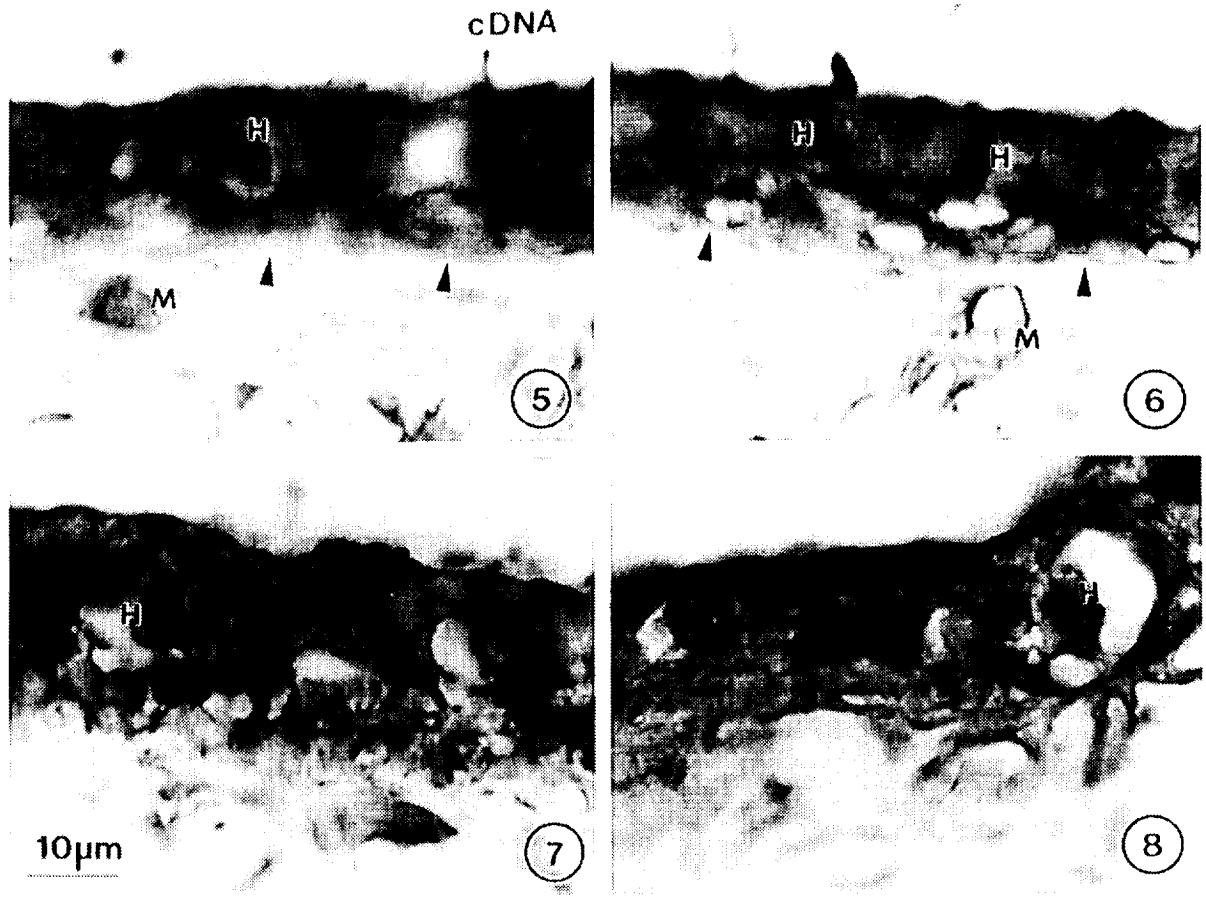

In situ protocol developed with cDNA constructed from sequence homology between mammalian S100ß and presumptive avian equivalent M126 gene.

1. Deparaffinize formalin fixed-tissue sections mounted on slides.

2. Deproteinize for 15 minutes at room temperature with Proteinase K.

3. Rinse slides with deionized water.

4. Dehydrate slides by immersing in alcohols and dry at room temperature for 5 minutes.

5. Add one drop of labeled DNA Probe/Hybridization Solution, (Biotinylated S100b oligomer diluted to 0.5ug/ml in SSC, formamide, and dextran sulfate), to tissue section and place a coverslip overslide.

6. Denature at 95C, 10 minutes.

7. Hybridize at 37C in a humidity chamber overnight.

8. Soak off coverslip with Tris/Saline wash buffer (0.1M Tris buffer, pH9.5, 0.1M NaCl).

9. Wash in Tris/Saline wash buffer, 2x2 minutes.

10. Incubate with horseradish peroxidase-labeled streptavidin, (BioGenex Laboratories), for 1 hour at room temperature.

11. Wash in Tris/Saline buffer, 2x2 minutes.

12. Develop color with AEC (3-amino-9-ethylcarbazole), counterstain with haematoxylin and aqueous mount.

Isolation of RNA from tissues. (Analytical Biochemistry 1987;162:156-159).

1. Homogenize 1mg of tissue in 1ml denaturing solution (4M guanidinum thiocyanate, 25mM sodium citirate, pH7; 0.5% sarcosyl, 0.1M 2-mercaptoethanol) at 4C.

2. Add sequentially to the homogenate 0.1ml of 2M sodium acetate, pH4, 1ml phenol, and 0.2ml of chloroform-isoamylalcohol(24:1) mixing thoroughly by inversion after each addition. Cool on ice for 15 minutes, and centrifuge at 10,000g for 20 minutes at 4C.

3. Collect aqueous phase in fresh tube and precipitate RNA with 1ml of isopropanol at -20C overnight or at least1h. Centrifuge at10,000g for 10 minutes at 4C.

4. Wash RNA pellet in 75% ethanol, sediment, vacuum dry for 15 minutes, and dissolve in 50ul of sterile nuclease free water. Aliquot and store at -70C until use.

Reverse Transcription-Polymerase Chain Reaction.

1. First strand cDNA synthesis using SuperScript II from Life Technologies (Grand Island, NY). Add to a nuclease-free microcentrifuge tube 1ul Oligo (dT), 1-5ug total RNA, and sterile distilled water to12ul. Heat to 70C for 10 minutes and chill on ice. Add 4ul 5x First strand buffer, 2ul 0.1M DTT, 1ul 10mM dNTP mix. Gently mix contents of the tube and incubate at 42C for minutes. Add 1ul of Superscript II, pipet gently and incubate 50 minutes at 42C. Heat at 70C for 15 minutes to inactivate and use the cDNA for amplification in PCR.

2. PCR using AmpliTaq DNA Polymerase from Perkin Elmer (Foster City, CA).
Add the following components of the reaction mix to a sterile microcentrifuge tube: 5ul 10x PCR buffer, 1ul 10mM dNTP mix, 0.5-2.5ul each of primer1 and primer2 (0.2-1.0 uM), 0.5ul AmpliTaq DNA polymerase, 2-8ul 25mM MgCl2, cDNA template <0.5ug/50ul, and sterile distilled water to a total volume of 50ul. Overlay with 30ul oil and perform the PCR reaction in a DNA thermal cycler. Heat at 94C for 1 min then for 25 cycles consisting of denaturation at 94C for 30 sec , primer annealing at 60C for 3 min and primer extension at 72C for 1 min. End with a final extension at 72C for 7-10 minutes Analyse 10ul of the PCR product by electrophoresis on a 2% agarose gel, stain with ethidium bromide and visualize with UV fluoresence.

Cloning of PCR Products.

1. Excise PCR products from gel and purify using QIAquick Gel Extraction Kit Protocol from Qiagen (Santa Clarita, CA). Briefly, dissolve agarose completely, apply to column, wash, and elute.

2. Ligate PCR product and pCR-TOPO vector using TOPO TA Cloning Kit from Invitrogen (Carlsbad, CA). Mix gently 0.5-2 ul of PCR sample (10ng/ul), 1ul pCR-TOPO vector, and sterile water to a final volume of 4ul, incubate at room temperature for 5 minutes and place on ice. Add 2ul of this cloning reaction to competent cells and incubate on ice for 30 minutes. Heat shock the cells for

30 seconds at 42C and chill on ice for 2 minutes. Add 250ul of room temperature SOC medium and shake horizontally at 37C for 30 minutes. Spread100ul on LB plates containing 50ug/ml ampicillin and incubate overnight at 37C. Pick white colonies and culture in 5ml LB medium containing 50 ug/ml ampicillin.

3. Isolate plasmid DNA using QIAprep Miniprep for purification of plasmid DNA from Qiagen (Santa Clarita,CA), and analyse with PCR and gel electrophoresis.

Sequencing of PCR Product

1. Sequence with T7 Sequenase v2.0 Quick-Denature plasmid sequencing kit from Amersham LIFE SCIENCE (cleveland, Ohio).
Alkaline denature 2ug DNA in the presence of primer(0.1ug M13 reverse primer, Invitrogen) and plasmid reaction buffer, and anneal at 37C. Mix with labeling mix and incubate at room temperature for 5 minutes, then terminate the reaction by transferring 4.5ul of the labeling reaction to tubes containing 2.5ul of the respective ddNTPs at 37C and continuing incubation for 5 minutes at 37C. Stop reactions by adding 4ul of stop solution and heat samples to 72C for 2 minutes before loading onto sequencing gel.

S100ß Avain candidates

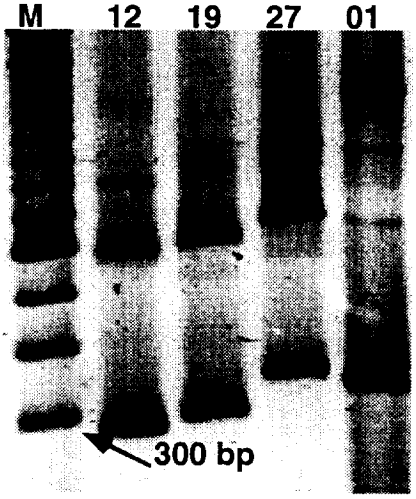

[5'-3']
S1 CGCTGCTTCACCAACATGAG
AS1 ACAGAAGTGGAGGTGCTCGT

S12 GGGGACAAAGACACCCTGAC
AS12 CAAGCACAGCCCTCCTCAGT

S19 CTCCGAGCTGGAGAAAGCCA
AS19 CTGTTGCTGGTGGTCCTCAC

A27 ATGAGCAAGGGCTGCCAGAC
AS27 GTGTTGGTGTTGGTGCTGTT

Four primer pairs synthesized were design with the Tetra Molly computer program by matching the sequence of a chicken M126 gene (Oncogene 7:527-534, 1992) to that of rodent and human S100ß published sequences and deposited in the gene bank.

Two gel bands were obtained from PCR of each primer pair with chick brain cDNA. Approx. 300 bp and 600 bp from S 12,19 and 27, and approx. 300 bp and1000 bp from S1. The 300 bp PCR product from S27 is being sequenced. The expected product lengths for the primer sets are S1; 321 bp, S12; 279 bp, S19; 292 bp, and S27; 339 bp.

The following is a brief summary of experiments that were possible with the small supplement to the last year of the grant:

Total RNA was extracted from three chickens' brainstem and used for differential display PCR to amplify genes that may be related to vestibular neural plasticity observed within one hour after

deafferentation. Surgical deafferentation produces a chronic non reversible effect afferent neurons with instant drastic effect on the brain stem areas to which the nerve connects. Chemical deafferentation such as that produced by TTX is acute temporary and reversible. Fifteen chickens underwent the surgical procedure and functional measures before and after deafferentation. Twelve chickens including TTX controls will be evaluated later. Chickens received left unilateral labyrinthectomy under general anesthesia and were killed 30minutes after surgery. The brain (cerebrum, cerebellum, brain stem and spinal cord) were dissected and cut along the saggital line and collected separately. After total RNA extraction and reverse transcription, cDNA fragments were amplified with PCR using DD-PCR primer sets (supplied with RNA map kit by GenHunter Co.). DD-PCR was performed with non-radioactive labeling of left and right brain stem samples. One of the differential displayed bands between right and left brain stem, 309bp fragment (which was expressed only on the left brainstem of all three chickens), were collected from Agarose gel and reamplified. After the subcloning with TOPO TA cloning kit (supplied by Invitrogen Co.) and sequencing with Sequenase 2.0 (supplied by Amersham Co.), the amplified product showed a 100% sequence identity with a *Gallus domesticus* lysosome-associated membrane glycoprotein (LAMP2c) mRNA. LAMP2a,b and c are major integral membrane proteins of lysosomes, but are also expressed on the cell surface. Thus, LAMP2c may provide receptor mediate signals to the affected cells. LAMP2c differential regulation on the brain stem samples ipsilateral to the deafferentation may be related to gliosis seen as early as 1 hour after surgery with immunohistochemical labeling of S100ß which is made by brain glial cells. We will investigate any relationship that may exisit between elevated S100ß and LAMP2c in ipsilateral brain stem after deafferentation of the VIIIth cranial nerve.

LAMP2c upregulation 30 min after surgery

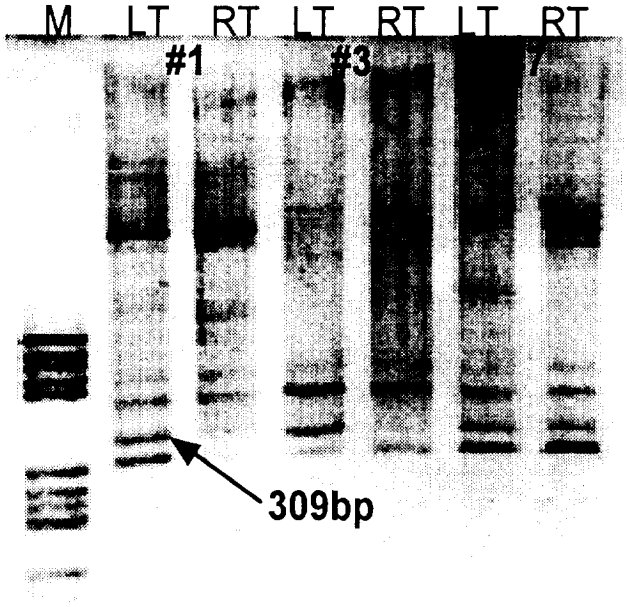

M= Marker, LT= left, RT= right, bp= base pairs

The transcripts that are upregulated on the left side of the brain stem after the left afferent fibers are severed (arrow), belong to the lysosomal associated membrane protein 2c. Experiments are now in progress to determine if LAMP2c upregulation is related to the upregulation of S100ß seen within one hour after deafferentation.

Please let me know who wish receiving this file which contains color images of the black and white now submitted.

Best regards,

César D. Fermin, Ph.D.
Professor and Director of Morphological Services
Director of Centralized Tulane Imaging Center

CDF/

cc:

1.) Mr. Kenneth L. Souza, Chief Life Sciences Division Mail/Stop: 240-10
2.) Ms. Bonnie P. Dalton, Deputy Chief Life Sciences Division Mail Stop: 240-10
3.) Mr. Paul D. Savage, Jr, Chief Science Payloads Operations Branch M/S: 240A-3
4.) Ms Venoncia A., Braxton, Grant Officer Space and University Affairs Branch M/S: 241-1
5.) Ms. Barrie A., Caldwell Space and University Affairs Branch M/S: 241-1
6.) Dr. Charles M., Winget Space Payloads Operation Branch M/S: 236-5
7.) DrVernikos, Director Life & Biomedical Sciences NASA HQ/UL
8.) Dr. Schneider, Life & Biomedical Sciences NASA HQ/UL
9.) Dr. Uri, Johnson Space Center Houston

This web audiovisual is based on a presentation given by C.D. Fermin, Ph.D. to audience of the Symposium below. Dr. Fermin is a professor of Pathology and Otolaryngology at Tulane Medical School. Phone 504 584-2521 FAX 587-7389. email:fermin@tmc.tulane.edu. In depth description of figures & scientific interpretation is available upon request.

Presented at the Phase-1 NASA-MIR Symposium, JSC Houston Tx 8/5/97-8/7/97.The Symposium was organized and supervised by J. Uri, Ph.D. and J. Valverde at JSC

The work presented in this report was made possible by a NASA grant NAGW2-999 to C.D. Fermin, Ph.D. Additional NASA grants supported the other investigators. Data in this report is © and requires permission before use! Additional references about this type of work can be extracted from selected references cited in (Dr. Fermin's Publications).

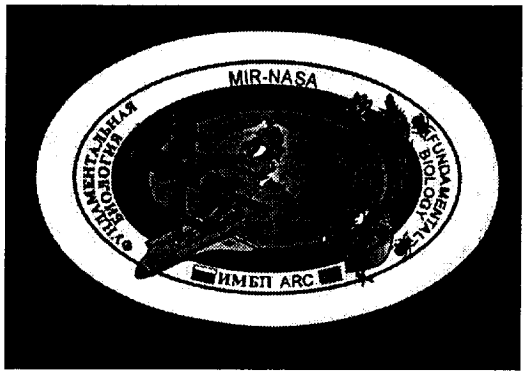

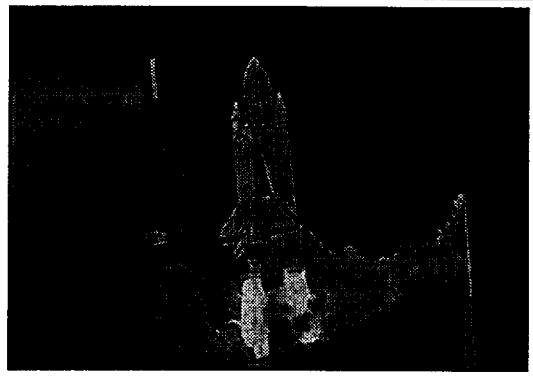

Introduction-Pair 1

In this presentation the research of 10 investigators participating in the SLM project and whom work in different fields is summarized. Special thanks to NASA AMES (ARC) personnel for their continued and devoted efforts to ensure that all investigators fulfilled the requirements needed to satisfy regulatory and governmental policies: Dr. K. Souza, Dr. G. Jahns, S. Piert, K. Lagel, & T. Schnepp; in NASA headquarters to Dr. Schneider and J. Vernikos for supporting this important avian project; and to the Russian team Dr. V. Sychev, Dr. T. Gurieva, Dr. O. Dadasheva and Dr. D. Lychakov for their invaluable help during numerous debriefing and dissection of every specimen returned.

The project

- **Rationale**: Mature organisms are affected by microgravity, and embryos may be affected too
- **Hypothesis**: Microgravity affects the normal development of avian embryos
- **Justification**: Microgravity affected the equilibrium system of chicks in STS-29

Investigators

Name	Institution	Subject
P. Anderson, M.D.	Duke Univ.	Contractile Proteins
W. Conrad, Ph.D.	Kansas S. Univ.	Eye
J.E. Barrett, Ph.D.		
S.B. Doty, Ph.D.	Hosp. S. Surgery	Bone
C.D. Fermin, Ph.D.	Tulane Medical	Vestibular Peripheral
B. Pritzsch, Ph.D.	Creighton Univ.	Vestibular Central
L.L. Bruce, Ph.D.		
P.Y. Hester, Ph.D.	Purdue Univ.	Shell-Mineral
H. Orban, Ph.D.		
P.I. Lelkes, Ph.D.	Wisconsin-Milwaukee	CAM
B.R. Unsworth, Ph.D.	Marquette Univ. "	
T. Shimizy, Ph.D.	USF	Visuo-Vestibular
B.C. Wentworth, Ph.D.	Wisconsin-Madison	Fecundity

The Project & Investigators-Pair 2

A team of investigators with diverse experience in anatomy, molecular biology and animal husbandry earned peer acceptance and approval of 10 distinct projects to investigate tissues of specimens flown to the MIR space station and returned via the US space Shuttle. Upon return of specimens from MIR, investigators met at NASA ARC to dissect and divide the specimens according to funded protocols. Specimens were shared with Russian investigators involved in the program. Studies proposed were justified by previous work on the STS-29 Shuttle that showed specific effect of microgravity upon the development of sensory structures in the inner ear responsible for the correct posture and balance of the body (Discussion of STS-29 Findings). Balance of erect animals such as bipedal birds and primates is a complex process that depends greatly on visual and vestibular cues shaped by gravity on earth. Analysis of the absence of gravity is only possible in space where it can be removed for prolonged periods of time. Brief removal of gravity possible in KC flight is not sufficient to study embryological processes that require weeks to complete.

Objectives

- To determine if **microgravity** affects avian embryonic development:
  - **Organogenesis**
  - Organization of **body axis**
  - Development of visual and equilibrium **sensory receptors**
  - **Bone** and **mineral** homoestasis
  - Nucleic acids

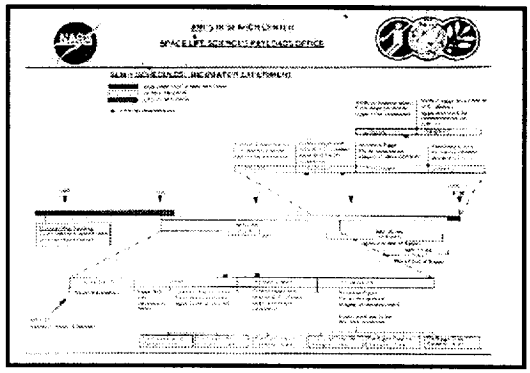

Objectives-Pair 3

The original objectives of the projects were changed slightly after unexpected problems with the performance of the Russian incubator were detected in flight. In addition, specimens were shared with the Russian colleagues reducing the available number of specimens to satisfy statistical testing of the data. The overall objectives of the SLM project were met and investigators were able to evaluate egg fertility and viability, organ formation, eye and ear structures development, bone formation, vascular development and calcium utilization. Development of US controlled hardware will infuse much needed flexibility in the development of payloads that maximize science return.

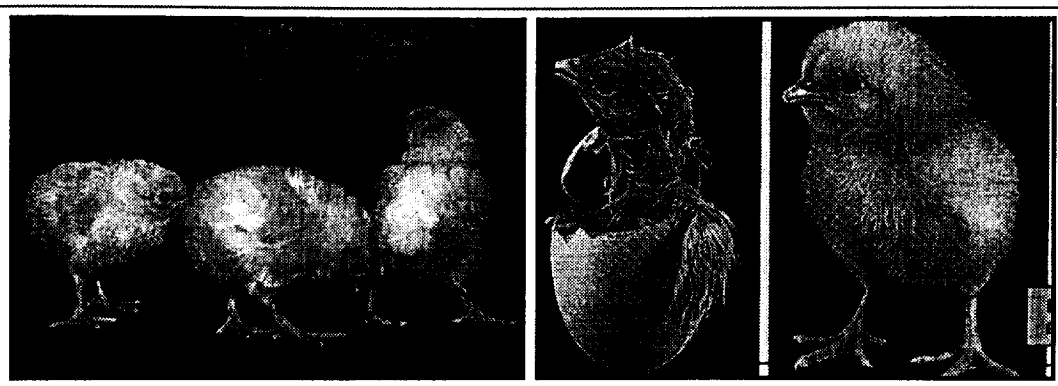

Avian Model-Pair 4

Besides being precocious, quail and chicken hatchlings are ideal models for space experimentation. Being precocious afford birds fully functional sensory structures upon hatching. Thus, hatchlings can walk and balance, and have fully functional vision. Other attractive features of the avian developmental model are that it has been studied for centuries with a wealth of information accumulated on its development, behavior and survival. Furthermore, fertile eggs can develop in space in self-contained system (shell) that do not require crew time, a valuable commodity in space. Birds can also potentially provide a rich source of protein for long duration flights.

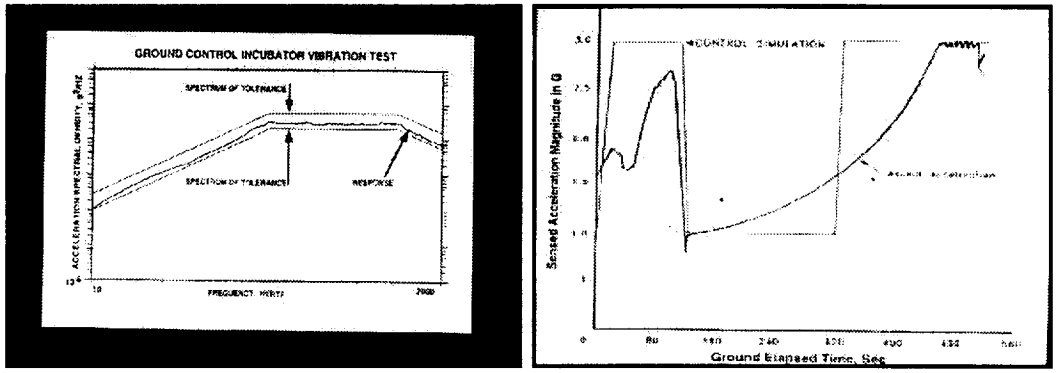

Acceleration & Vibration-Pair 5

Ascent vibration & acceleration of the space vehicles at launch demand special protection of its cargo. Eggs with fragile and thin shells would seem unsuited to withstand the forces created by the ascent acceleration of the Space Shuttle. However, controls on both variables showed that eggs withstand both physical parameters and develop normally. Synchronous controls subjected to similar vibration and acceleration as those encountered in space but developing under 1.0G load developed normally, whereas those that developed in space in the absence of gravity showed significant modifications of their sensory structures. In particular, structures responsible for balance and equilibrium.

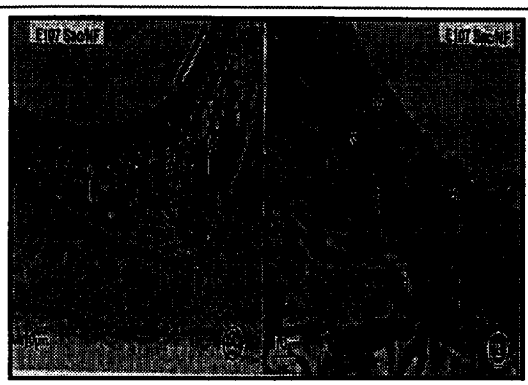

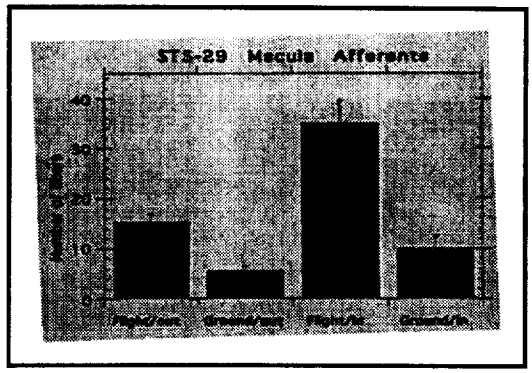

Afferent Neurons-Pair 6

Immunohistochemical staining (More on Inner Ear Antibody Labeling via this link) of inner ear afferent neurons with anti-neurofilament protein antibody suggested that chick embryos exposed to microgravity for only 5 days during development had more afferent nerve terminals in their sensory epithelia. Similar increase in afferent terminals was reported by Dr. M. Ross in rats flown in space and indicates that sensory structures responsible for keeping the body erect at 1.0G on earth are affected by reduced gravity.

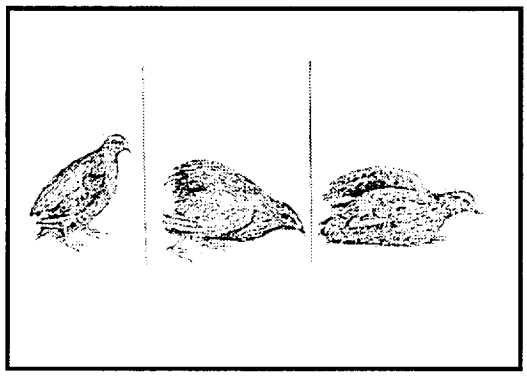

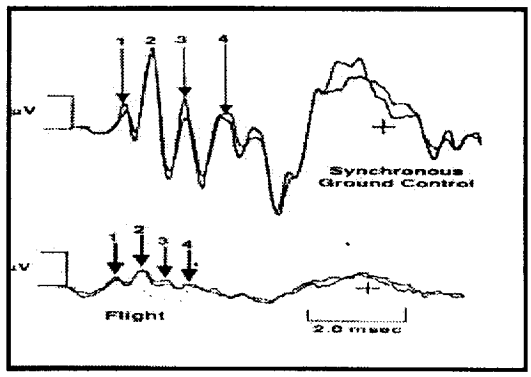

Behavioral Measures-Pair 7

One of the Russian investigator involved with this research showed previously that quails hatched in space required time to readapt to the earth environment. In addition, the quails showed ataxia and desorientation similar to that exhibited by humans upon return from space flights. It is believed that behavioral deficits of posture and balance are related to modifications induced by microgravity to the sensory neurons that process sensory perception of the environment and tell the brain the body position in space. Modifications of the sensory pathways requires time to correct. Fertile eggs flown into space and returned to earth were allow to hatch. Vestibular thresholds were measured on the hatchlings non-invasively weeks after returned to 1.0G and showed thresholds shift in space and not in ground synchronous controls. Such delayed effect suggests that readaption of certain behavior requires weeks to complete. Anecdotal accounts by Russian cosmonausts indicate that even 6 months after return to 1.0G following long term stay in the MIR station there were occasional miss judgments in sensory perception. **It is clear that future studies of the avian model should include behavioral testing for comparing responses of flight and ground synchronous controls and for validating the morphological changes already documented.**

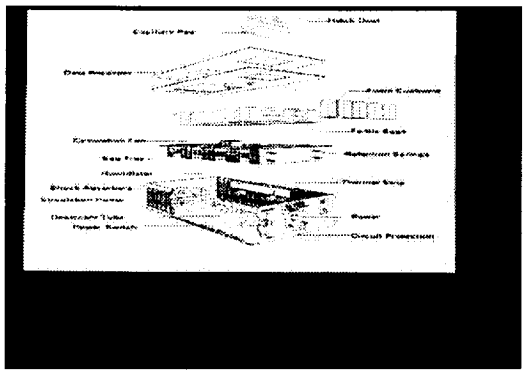

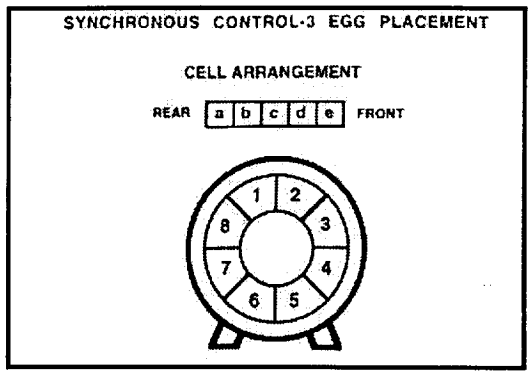

Hardware-Pair 8

There is a considerable difference between the technologies used by the US and the Russian space agencies. The incubator used for the STS-29 experiment was not available for the MIR project. Instead a Slobak incubator used by the Russian in previous flights and certify to flight on MIR was used. The Slovak incubator consisted of a cylinder with cells for positioning the fertile eggs. The US incubator approved to flight in the Shuttle was a sophisticated instrument with temperature and humidity control. Future avian experiments with fertile eggs should insist on proven technology that delivers humidity and temperature control within a reasonable and acceptable margin of error. With today technology, the incubator should be able to store data on such important parameters of egg development to evaluate upon return to earth.

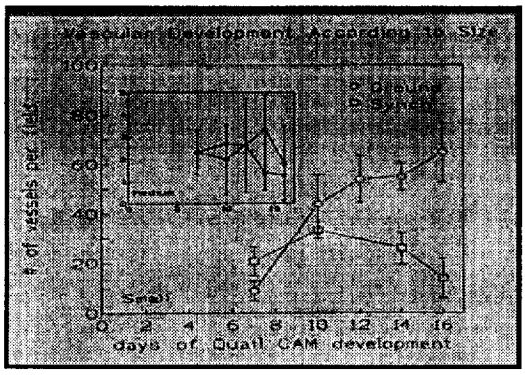

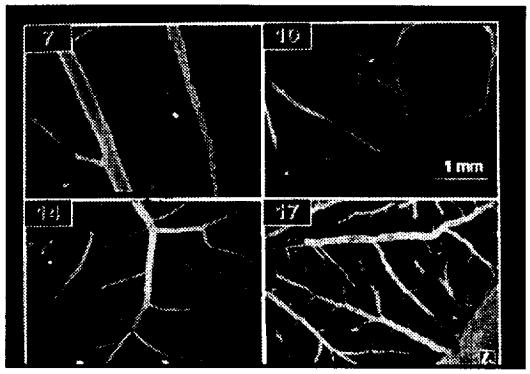

Embryonic Membranes-Pair 9

Preliminary results from Dr. Lelkes & Unsworth suggests that the vasculature in the choriollontoic embryonic membrane (CAM) of synchronous and control embryos may be affected by variables other than microgravity alone. The CAM is responsible for gas exchange/oxygenation of the embryo. This group uses morphometric analyses aided by imaging technology to study changes in the embryonic membranes that nourish the embryo development. This and other work suggest that certain critical developmental changes occur during narrow windows of time (critical periods). **Accurate knowledge of critical periods of development of cells, tissue formation and organogesis will permit investigators to design experiments that maximize embryo survival and availability of viable materials.**

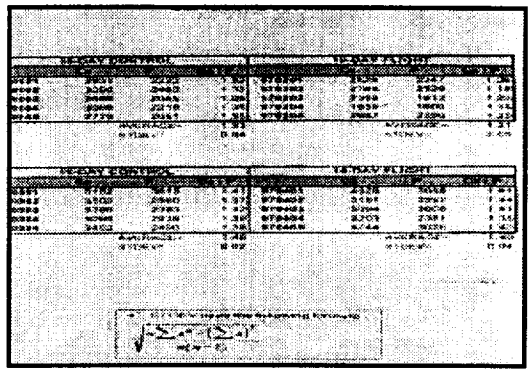

Bone-Mineral-Pair 10

Dr. Doty from the Special Surgery Hospital in NY uses Transmission electron microscopy and elemental analysis of thin sections to detect changes in mineral composition in bone of flight and synchronous controls. There seem to be critical windows of development when primarily the utilization of calcium and phosphorous differs between the two groups. This is an important part of the SLM-1 research because bone retains its structural architecture even after the sub optimal fixation that is possible in space where the hazardous chemical of ground laboratory can not be used. All fixative used on earth to produce acceptable ultrastructural preservation of cells and tissues are off-limits in the Shuttle and MIR due to their toxicity and hazardous properties. In addition, volume and weight remain important variables for space flight payloads prohibiting the volume:solid ratios of fixative:tissue required for optimal fixation. The compromise reached for the MIR project proved acceptable but not optimal and future analyses will require modifications of present protocols.

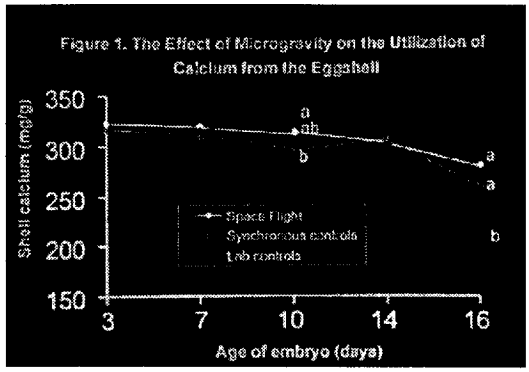

Bone-Mineral-Pair 11

Dr. Hester & Dr. Orban evaluated the mineral content of the shell to determine calcium and phosphorous utilization during development. Dr. Hester's results on calcium utilization from shell and those of Dr. Doty agree on the existence of critical periods of development for the formation and refinement of many developmental processes. Both, the study of bone and shell take advantage of the fact that bone and shell retain their structural integrity even following sub optimal fixation. Both Dr. Doty (Left Figure) and Dr. Hester/Orban analyses (Right Figure) are essential in space exploration because bone and shell retain structural integrity better than soft tissues.

Eyes-Pair 12

Dr. Conrad & Dr. Barrett takes advantage of the resilience of the cornea to withstand pressure and resist damage to determine variability in its morphology. Besides evaluating the innervation pattern of synchronous and flight embryos, this group takes advantage of an ossicle ring that surrounds the cornea of quails and provides a landmark for detecting variability in the formation of the eye. Other aspects of quail development will be evaluated and presented in future gathering. In the next slide sets I will describe properties and changes of the avian inner ear (Dr. Fermin's expertise) that justify the chick as a model for space experimentation.

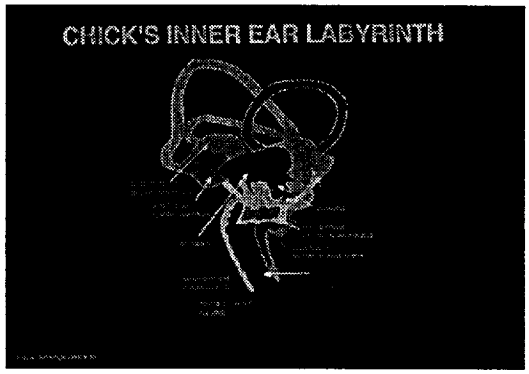

Tissue Density-Pair 13

Fixation of inner ear structures is difficult even on the earth laboratories. The temporal bone that houses the inner ear is the hardest bone of the body. The inner ear tissues are heterogeneous and surrounded by fluids. Not only are the tissues hard to reach (Left Image), but once the fixing solution reaches the inner ear it can be diluted by the endolymph and perilymph before reaching the cells. This difficulty of fixative penetration into the inner ear can be appreciated from the composite diagram illustrating several layers of hard tissue from the skin toward the brain fixing solutions must diffuse through before reaching the inner ear structures. Fixatives must also penetrate the CAMs and are diluted by unused egg white. The membranous labyrinth of birds is similar to the mammals except for the presence of an otoconia containing organ at the end of a straight auditory organ. In mammals, the auditory organ is coiled (cochlea), but the sensitivity needed to detect vestibular and auditory stimuli to keep the body in tune with the environment is comparable in birds and mammals.

Ideal-Real-Pair 14

Space experiments meant to analyze cell integrity provide a reality check to the researcher that is accustomed to ground laboratories. Even after aldehyde fixation, the structural integrity of cells fixed in space may not match that of tissues fixed on the ground because the ideal ratio of 1:20 (tissue:fluid) can not always be met due to payload restrictions. The ideal preservation of inner ear gravity detectors (linear accelerometers) is shown on the left after fixation of inner ear tissues by substituting the blood of the chicks with saline and then with fixative through a heart perfusion. The procedure delivers fixative to the space between cells where it can cross link the proteins of the cytosol and preserve the cell integrity. The distance between the epithelia and the otoliths (membrane with crystals that at 1.0G provide load to deflect the stereocilia of the receptor hair cells) was maintained due in part to the embedding of structures in methacrylate plastic instead of wax embedding (More on Inner Ear Attributes) . The slide on the right shows extraction of cytosol from the epithelia due to weak cross linking of proteins in the cytosol and extraction of wax. Wax embedding of tissues yields more reliable antibody-antigen recognition than plastic embedding and thus the compromise. Nonetheless, analysis of organs, tissues and cells is possible in space fixed tissues (Right Figure).

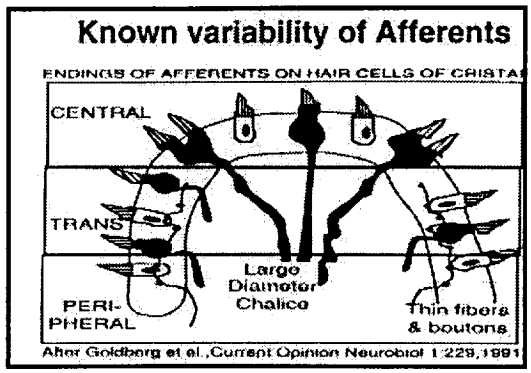

Angular Acceleration Detectors-Pair 15

The arrangement of afferent nerve fibers in the crista of the ampulla of birds is identical to that previously demonstrated for mammals shown on the right. Different types of afferent neurons contact different types of detectors hair cells to provide adequate information to the brain about the position of the body in space. Anti-neurofilament staining of the fibers on chicks returned from the STS-29 experiments (Fixed on the ground immediately after return from space) demonstrated that labeling of the fibers in well fixed samples returned from space is possible and yield important information about morphological properties of afferent neurons developed at 1.0G and in microgravity.

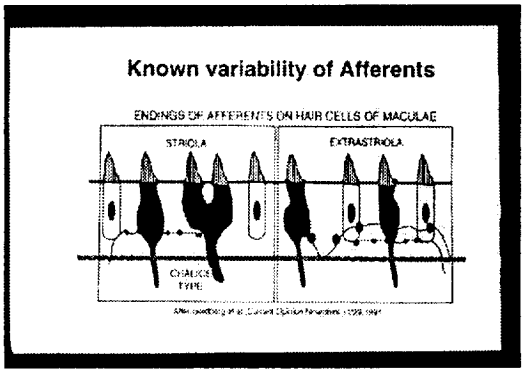

Linear Acceleration Detectors-Pair 16

The arrangement of afferent nerve fibers in the macula of the utricle and saccule of birds is identical to that previously demonstrated for mammals shown on the left. Different types of afferent neurons contact different types of detectors hair cells to provide adequate information to the brain about the position of the body in space. Anti-neurofilament staining of the fibers on chicks returned from the STS-29 experiments demonstrated that labeling of the fibers in well fixed samples returned from space is possible and yield important information. Count of fibers inside the epithelia suggests that microgravity induces sprouting of afferent terminals around the receptor hair cells. This observation requires corroboration because it may explain the delay recovery of certain vestibular functions at 1.0G after prolong space flights. In other words, rewiring of the circuits may be necessary both during flight in space and after return to 1.0G (see pair 7).

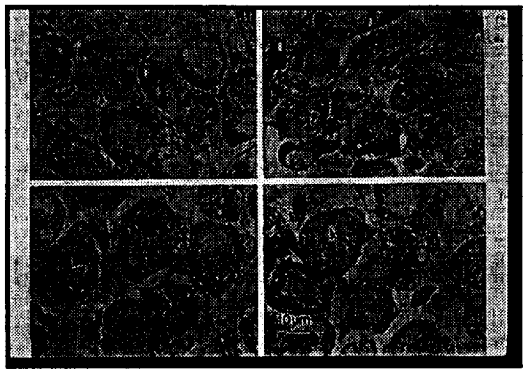

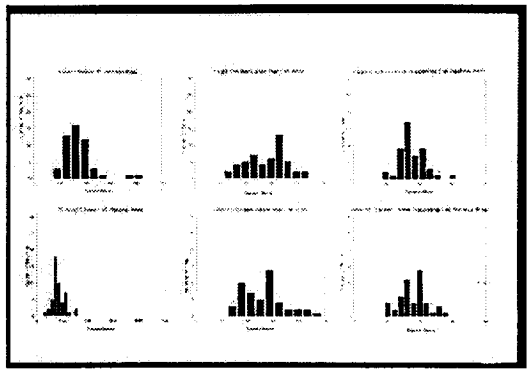

Neuronal body (Perikarya)-Pair 17

Besides the well documented sprouting of afferent fibers inside the sensory epithelia (see Pair 6), there seems to be an increase in the surface area (that may reflect an increase in volume) of the perikarya (soma) or bodies (left Figure, and left histogram of right Figure). There was however no difference in the afferent fibers (Right Figure) of the in flight (top) when compared to ground (bottom) embryos outside the basement membrane of the sensory epithelia. In the ear these bipolar neurons (two axons) connect the hair cells to the brain processing center for detection of linear and angular acceleration. An increase in volume of the perikarya where the metabolic machinery of the cell resides may be related to hastened modifications of the neuronal functioning brought about by a changed environment. These type of observations must be corroborated in future experiments that are only possible in the planned space station, where prolonged periods of reduced gravity will be possible and where an on board 1.0G centrifuge may be available.

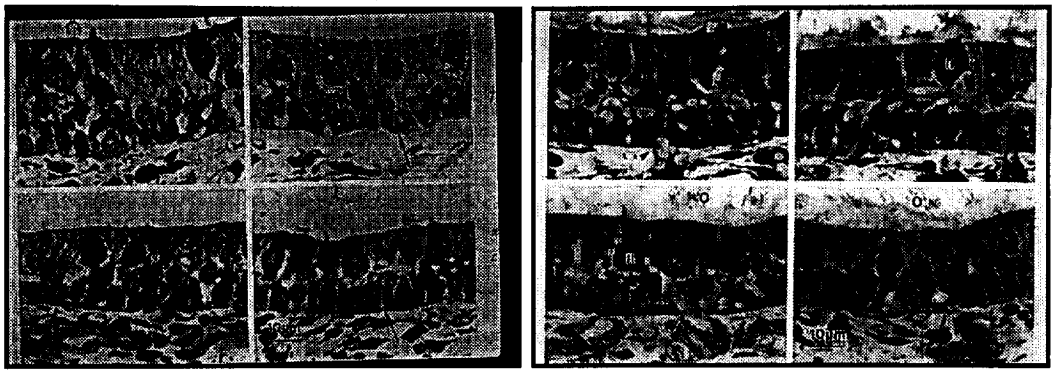

Subtle Modifications-Pair 18

The original planned morphological analyses of space and ground synchronous controls were based on the assumption that functional alteration of human vestibular system leading to motion sickness would have morphological correlates of similar magnitude. However, many of the functional modifications observed in space and after return to earth at 1.0G may be subtle and have little or no visible morphological modifications, specially those that are reversible such as latent synapse activation . It is known that inactive synapses may be activated during hastened functional demands and deactivated thereafter. Such process of activation-deactivation is economical to systems, as opposed to formation of new neurons. Subtle differences between these STS-29 macular epithelia structures are seen at the level of the support cells nuclei and the distance between the basement membrane and the lumen of the epithelia. Such changes may not yield statistically significant differences but are nevertheless representative of actual metabolic modifications of the system and justify further analyses. Left top flight and bottom control. Right top control and bottom flight.

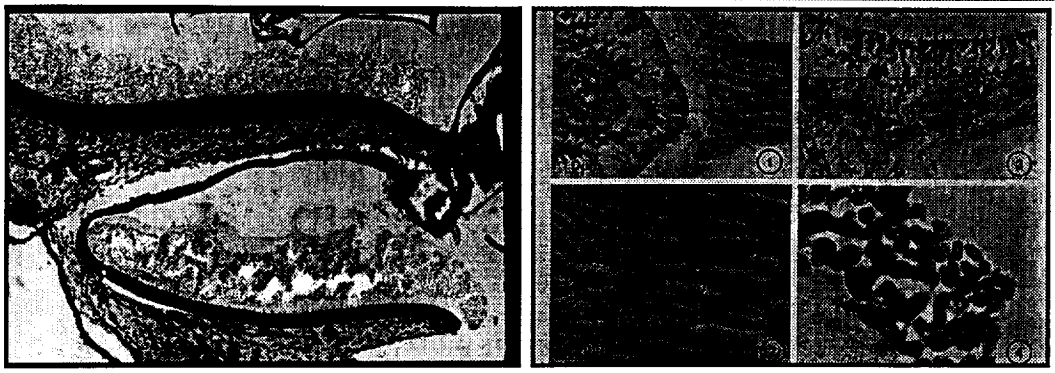

Rocks in the Ear-Pair 19

All vertebrate have crystalline structures inside the inner ear that have been retained throughout evolution as necessary loading masses to deflect the stereocilia of hair cells (More on Inner Ear). This is a requirement for proper transduction of mechanical into neural energy. If you recall the discussion introduced with the **Tissue Density**(Pair 13), the inner ear tissues are difficult to fix in space where perfusion of chemical hazardous chemical through the heart is not possible. Assuming a reasonable fixation by passive diffusion as permitted in space, one has to accept other inherent difficult to control variables of the system. On the left the crystalline nature of the otoconia (hexagonal crystal (Otoconial Membrane as loading Masses) obtained on earth fixed controls embedded in plastic un calcified. Unless the tissues are decalcified with chelators such as EDTA, sectioning at 1-10 micrometer thickness is not possible. Incomplete penetration of the plastic embedding medium (methacrylate) into the dense otoconial membrane is common. While the preservation of cells on the sensory organs of flight materials shown at right is not comparable to the grown shown at left, the architecture of components is evident, and the cupula and otoconia retain their organiztion.

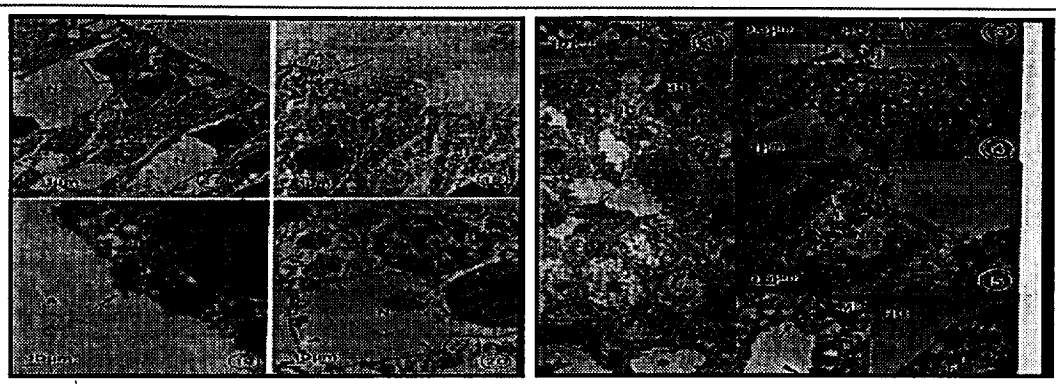

Ultrastructural details-Pair 20

The main problem with mild fixation such as is possible in flight, is that the cytosolic components are only weakly cross-linked and are therefore easily extracted during dehydration. To successfully cut soft tissues as thin as 60 nm, proteins must be fixed in place, lipids oxidized and water must be removed. All these procedures are harsh and usually extract those components of the cells that are not strongly immobilized. These transmission electron micrographs (Compare with Pairs 10-11) of space fixed tissues demonstrate that there is sufficient ultrastructural details to evaluate cellular changes. However, the axoplasm (See Pairs 15-16) of the afferent fibers was extracted. In other words, the antigens present in the sections of Pairs 15-16 were extracted by the harsh procedure needed to prepare electron micrographs. Since knowing the molecules present in cells and understanding their topography are both important, a multidisciplinary approach is needed to maximize science return from space experiments and compromises such as this are inevitable.

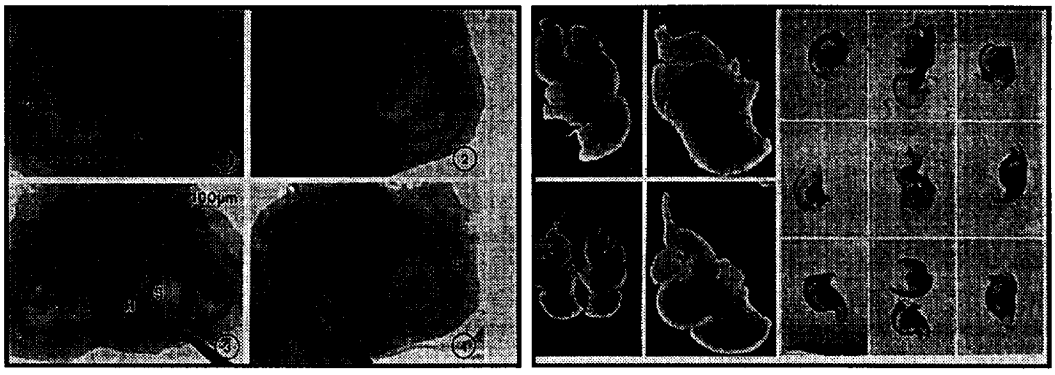

Gross morphological changes-Pair 21

On the left figure (bottom right) a flight embryo inner ear shows bending of the horizontal canal whereas the synchronous control has no such bending. Such gross morphological changes are rare and the impact of the observation must be tested statistically. Sharing of specimens among numerous investigators is a great mean to ensure a multidisciplinary approach for evaluating the effects of microgravity upon developing vertebrates, but sharing should be assessed carefully to ensure that sufficient samples remain in each group to permit acceptable and meaningful statistical tests. Gross examination of brain showed little differences between flight (Right) and ground controls. Microdissection of individual inner ear organs yield no difference either. However, the wiring of cells inside individual organs may be altered and requires further evaluation.

Results & Discussion

- Egg fertility was 99% & viability 60% with **no gross** anatomical malformations of specimens dissected
- Utilization of shell **calcium** at E16 seems higher in microgravity than at 1.0G
- Microgravity may **delay** development of certain structures
- Sensory inner ear vestibular receptors (**equilibrium**) are altered in microgravity
- The quail **avian system** is excellent model for vertebrate embryonic development because it does **not require mother's** care
- **Chicks** like human have functional sensory structures at hatching (**precocious**) & stand on two limbs (**bipedal**)

Lessons Learned

- The avian embryo is an excellent **model** system of vertebrate development in space
- **Fixation** of embryos in space should be improved
- **A1.0G control** in space is needed
- Synchronous & Lab controls should **mimic** space samples
- **Behavioral** test correlates of anatomical changes observed should be considered

Discussion & Lessons Learned-Pair 22

The results obtained from the MIR avian project are encourashing because they demonstrated that fertile eggs can be incubated and fixed in an orbiting space station and then returned to earth via the space Shuttle for scientific analyses. The ability to incubate eggs in space and eventually produce eggs in space is necessary to remove gravity from the developmental process. Fertile eggs produce at 1.0G on earth and brought to the space station via the Shuttle are already 22 hours post fertilization and thus have experience the gravity vector of the earth environment. True lack of gravity as contributing variable for vertebrate development of avian embryos will be possible with eggs produced in space. Results obtained thus far permitted scientists to focus aims to maximize the science-return from future space experimentation.

Variables to Consider

- Microgravity may produce **subtle** reversible changes capable of affecting development and not produce long lasting visible cellular alterations
- Experimental **designs** should maximize sample return that allow statistical analysis of data from at least a few projects (**sharing**)

Operational Accomplishments

- Incubation of fertile eggs on the Russian MIR & transport via the USA Shuttle was successful
- The microgravity environment of MIR affects certain development processes of quail embryos

Future Considerations-Pair 23

The complexity of the space program and the need to mix politics with scientific design for successful completion of the SLM project suggests that cooperation between the partners of the planned international space station is a reality. Life science projects that evaluate alteration that lack of gravity may cause to vertebrates tissues and cell should be a priority on the list of things to do on the upcoming international space station. If changes that lack of gravity induce to tissues and cells were only chronic, traditional histological observations would suffice to demonstrate their severity. Unfortunately, many changes are transitory, reversible or simple sporadic and their scientific evaluation requires multidisciplinary approaches that incorporate cellular, molecular & behavioral analyses.


Fermín
C.V.

Color Threshold and Ratio of S100β, MAP5, NF68/200, GABA & GAD. I. Distribution in Inner Ear Afferents

C. D. Fermin, D.S. Martin, and H. Hara
Department of Pathology & Laboratory Medicine
Tulane University School of Medicine

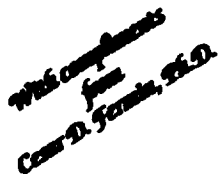

Summary

Afferents of chick embryos (Gallus domesticus) VIIIth nerve were examined at E3, E6, E9, E13, E17, and hatching (NH) for anti-S100β, anti-MAP5, anti-GABA, anti-GAD and anti-NF68/200 stain. Different ages were processed together to determine if the distribution of these antibodies changed during synaptogenesis and myelination. Color thresholding showed that saturation of pixels changed for S100β only 5%, for NF68/200 10%, and for MAP5, 10%, between E9-NH. Color ratio of NF68/200 over MAP5 was 1.00 at E13 and 0.25 at E16 and NH. S100β, GABA and GAD were co-expressed on nerve endings at the edge of the maculae and center of the cristae, whereas hair cells in the center of the maculae expressed either S100β or GABA, but not both. S100β/NF68/200 shared antigenic sites on the chalices, but NF68/200 expression was higher than S100β in the chalices at hatching. MAP5 was expressed in more neurons than NF68/200 at E11, whereas NF68/200 was more abundant than MAP5 at hatching. The results suggest that: 1) the immunoexpression of these neuronal proteins is modulated concomitantly with the establishment of afferent synapses and myelination; 2) S100β may serve a neurotrophic function in the chalices where it is co-expressed with the neurotransmitter GABA and its synthesizing enzyme GAD.

Introduction

Rapidly growing neurons when in search for targets to innervate display large numbers of microtubules, particularly at their growing tips or growth cones [65]. Transport of molecules from the soma to the growing tip is essential for neuronal growth and functioning [89]. There are highly elongated protein molecules in axons [49] that modulate intraaxonal motility [57]. Of those, the microtubule associate proteins (MAP) and *tau* [1, 13] are expressed in growing neurons and may mediate transport of molecules from the soma to the growth cone [55], a process that could be modulated by neurotrophic molecules [7, 70, 92]. Tubulin and MAP may play a role in regulation of the NGF gene [4], whereas the S100 family of proteins may inhibit polymerization of GFAP [8], and affect plaque formation in Alzheimer [80], suggesting that an association may exist between the neurotrophic function of S100ß and cytoskeletal proteins. Glioma cells undergo a reduction of S100ß mRNA after treatment with anti-microtubular drugs [23]. Besides neutrophic molecules, the establishment of synaptic contacts may halt axonal growth and initiate organ maturation, expression of intermediate filaments [46, 53, 68, 74], and the synthesis of neurofilaments [79, 99]. These events may determine axon caliber [20], modulate transport of nutrients of newly synthesized molecules from the soma to the growth cone [40], and interfere with protein dynamics eventually leading to neurofibrillary pathology [66, 67]. The MAP and NF cytoskeletal elements are discontinuous, forming segments along the axoplasm that remain in register with other axoplasmic organelles [83].

A tight association between myelination of axons and expression NF and MAP was demonstrated [51]. The cross sectional area decreases and the shape changes after a decrease in the NF gene expression [71]. In mutant quails deficient in NF there are more microtubules per axon when compared to controls [94, 99], suggesting a exquisite balance between MAP & NF for normal maintenance of axons. Anti-NF68/200 staining is decreased in brain axons after surgical injury to the brain [73], a process that may be accompanied by upregulated phosphorylation of NF proteins in the axons [95]. NF68/200 expression increases in afferent neurons of chicks exposed to microgravity [30]. Several MAP isoforms are important for assembly and disassembly of microtubules [59]. MAP2 (*tau*) and MAP5 are differentially distributed in dorsal root ganglion cells in culture both in the soma and the dendrites [75]. At the site of myelination by Schwann's cells, local modulation of NF phosphorylation could determine

Submitted February 24, 1997, accepted August 27, 1997

axonal caliber, and influence transport [20], because the caliber of myelinated axons was dependent on the number of NF present in those axons. S100 is expressed centrally in glial cells [69] where it can bind to neurocalcin, and Schwann cells peripherally [29]), and it is co-expressed with NF68/200. There are 19 types of S100 with unique tissue and cell expressions. The original two members of this family (S100a and S100ß) can regulate cell-cell communication, differentiation and transduction among other functions [102].

Expression of NF was demonstrated in the vestibular nerve of guinea pigs [88], and hair cells [5, 97] where it labels afferent dendrites in vivo. In the inner ear, maintenance of synapses and growth of the fibers may be mutually dependant events [76]; and the expression of neurotrophic molecules, e.g., S100β [29] in those neurons, could be modulated concomitantly with synapse formation and the myelination of neurons [31, 32]. Thus, in this study we examined the immunoexpression and distribution of the well characterized neurotrophic molecule S100β, the neurotransmitter GABA and its synthesizing enzyme GAD, and two of the most important cytoskeletal proteins in the axoplasm, i.e., MAP5 and NF68/200. Our results indicated that: a) S100β is differentially expressed in the nuclei of certain groups of peripheral vestibular neurons; b) expression of MAP5 in the axoplasm is highest in the axon before synapse formation around E11 (stage 37), whereas; c) expression of NF68/200 is highest after afferent synapses starting at E16, and reaching its highest expression after hatching; d) the immunoexpression of these neuronal proteins is modulated concomitantly with the establishment of afferent synapses and with myelination; e) S100β may serve a neurotrophic function at the chalices where also GABA, and its synthesizing enzyme GAD, are expressed.

Materials and Methods

Tissue Preparation: Ten embryos each at days E5, E9, E13, E17, and hatching (NH) were used for this study. three E3 and one E6 embryo were for NF68/200 and MAP5 double staining because MAP5 is expressed early in development. The use of animals was approved by Tulane Medical School Animal Care Advisory Resources. Tissues were fixed with 10% formalin, embedded in paraffin and cut at 10 μm thick. Each section was placed on a manila folder and saved. Sections with comparable inner ear structures from each stage above were place on the same slide and stained together for anti-S100β, anti-MAP5, anti-GABA/GAD and/or anti-NF68/200. Staining sections from different experimental groups together eliminates inter-individual variability, and ensures that all groups receive equal treatment [29].

Antibodies: Anti-MAP5 (1:5000 dilution) was a monoclonal mouse ascites of clone No AA6 from Sigma Chemical Co. The antibody is also known as MAP1B, MAP1X or MAP1,2 which labels dendritic trees throughout the brain. It was determined to react with human, rat, bovine, chicken and quail tissues, but does not stain tubulin or other MAPs. The antibody showed increased expression during neuronal maturation and correlated well with NGF-induced neurite outgrowth. **Anti-S100ß** (1:4000 dilution) was a rabbit polyclonal from East.acres Biologicals (lot 36 HT2-8) characterized as selective for the S100β polypeptide that has less than 1% cross-reactivity with S100β and no cross-reactivity with calmodulin (another calcium binding protein). The antibody reacts with human, bovine, rodent and avian tissues. Anti-NF68/200 (1:200 dilution) was a monoclonal (clone 2F11) from bioGenex Laboratories. The antibody was characterized to label 68kD and 200 kD polypeptides of neurofilament and to stain neurons. No cross-reactivity was observed with GFAP, keratin, vimentin or desmin. Anti-GABA (1:100 dilution) was a monoclonal mouse isotype IgG1 (catalog MAB316) from Chemicon International, Inc. The immunogen was coupled to BSA with glutaraldehyde. This antibody does not cross-react with other amino acids according to the supplier. Anti-GAD (1:200 dilution) was a monoclonal mouse isotype IgG1 (catalog MAB340) from Chemican International, Inc. The antibody showed reactivity in tissues from monkeys, rabbits, cats, rodents and chickens.

Immunohistochemistry: In our laboratory we used procedures similar to those already published [29]. Briefly: All incubations were done at room temperature in a humidity chamber with tris buffer rinse in between: 1) 20 minutes in 1% hydrogen peroxide; 2) 10% goat serum for 20 minutes; 3) primary anti-S100 rabbit IgG diluted 1:4000, or primary anti-MAP5 mouse IgG diluted 1:5000 or primary anit-NF68/200 diluted 1:200 in in 2% Bovine serum albumin-Tris (BSA-TMS/HCL) buffer for 18 hours; 4) biotinylated goat-anti-rabbit IgG for 30 minutes, 5) streptavidin-horseradish peroxidase (Biogenex Laboratories, CA) for 30 minutes; 6) 3'3'-diaminobenzidine tetrahydochloride (DAB) for 5 minutes or 3-amino-9-ethylcarbozole (AEC); 7) counterstain in hematoxylin. For double immunostaining the same procedure was repeated for each antibody. For anti-GABA and anti-GAD we used glutaraldehyde with the primary fixative.

Double immunostaining: For the first cycle we used 1) 3 minutes in tris buffer, 2) normal goat serum for 20 minutes, 3) primary anti-NF68/200 mouse as indicated above, 4) biotinylated goat anti-mouse immunoglubulin for 30 minutes, 5) streptavidin-alkaline phosphatase (Biogenex Laboratories, California) for 30 minutes, and 6) bromo-4-choro-3indolyl phophate (BCIP)/nitroblue tetrzolium (NBT) from Sigma for 5 minutes. For the second cycle: 1)20 minutes in 1% hydrogen peroxide, 2) normal goat serum for 20 minutes, 3) primary anti-MAP5 mouse IgG diluted 1:5000 in 2% BSA-TMS/HCL buffer for one hour., or primary anti-S100ß rabbit IgG diluted 1:1000 in 2% BSA-TMS/HCL buffer for 30 minutes, 4) biolinylated goat anti-rabbit immunoglubulin or biotinylated goat anti-mouse immunoglubulin for 30 minutes, 5) strepavidin-horseradish peroxidase for 30 minutes, 6) 3-amino-9-ethylcarbazole (AEC) for 5 minutes, and 7) cover slip with aqueous mounting media. Detailed in-

formation about double immunostaining was previously published in this journal [42].

Controls: Two negative controls were included: 1) omission or replacement of the primary antibody with an unrelated antisera, and 2) pre-absorption of antibody when the substrate was available. In addition different age specimens were processed together on the same slide to ensure that differences observed were due to changing expression of the antibody and not to inter-specimen variability. Two built-in positive controls exist in our preparations. First, the brain and cerebullum that contain positive reactive structures to the antibodies in question are included with the inner ear preparation. Second, differences in the expression of a single antibody between different inner ear structures was always done on the same preparation.

Video Imaging: The immuno-expression of each antibody was evaluated by determining, a) the relative concentration of each antibody in tissue sections with color thresholding, and b) by calculating the number of pixels representing each stain. The following pixel values for Red-Cyan of 168-201, Yellow-Blue 116-164 and Luma 25-92 exemplify the objectivity of color thresholding for one measure used. Values like those above for each color established objective thresholds independent of the operator bias [33].

a) Color saturation (thresholding): The hues, saturation and intensity (HSI) of reaction products was used to calculate the relative concentration of the antibody in the tissue sections in real time with a Videometric V150® (Oncor, Geithersburg, MD USA). HSI permits a pixel-by-pixel analysis of the areas that contain a given color without regard to the density of the reaction. A numerical value was assigned to each color based on its position within a color cube, and subsequent identification of pixels with similar threshold done by the computer in frozen frames or in real time. The net results is that different colors of similar intensities are separated without filters [33], a property that favors histological examination [25], and minimizes bias [26].

b) Color ratio of stain pairs (NF/S100ß and NF/MAP): Color ratio permits a pixel-by-pixel comparison of stained areas with different color thresholds. The color thresholds are to the user numerical representation of the position that each color occupies on a color cube (e.g., Red-Cyan, Magenta-blue and luma). Except for operator assisted choosing of area for measuments, the analysis is fully automated by a macro, or short program subroutine. The macro is executed directly from the main video screen of the program, and it prompts the user to: a) chose area of interest, b) focus area of interest and c) name file to store the data. Ratio of an entire screen is calculated instantly upon instruction, and numerical values stored. Macros can be modified by users and interpreted directly by a "J" compiler built into the program. A ratio of 1.0 indicates an equal number of pixel for each stain, a ratio of less than 1.0 indicates less pixels of the first color measured, whereas a ratio of > 1.0 indicates more pixel of the first color measured.

Results

Expression of the neurotrophic molecule S100ß was minimal or absent at E9 in the neurons of the VIIIth nerve (Figure 1), before those neurons synapse with hair cells inside the epithelia. The auditory ganglion neurons expressed S100ß difusely at E9 (stage 35), except over the nuclei which stained darker than the cytoplasm and Schwann's cells (Figure 2). By 17 days of incubation (stage 43) when temporary afferent synpases are being replaced with permanent synapses, the expression of S100ß was stronger in selected groups of vestibular neurons (Figure 3). By hatching, S100ß expression remained difuse over some auditory neurons (Figure 4), whereas on the vestibular ganglion the expression was restricted to the nuclei of some neurons (Figure 5). The immuno expression of S100ß was completely abolished by pre-incubation of anti-S100ß with S100 purchased from SIGMA (Figure 6).

At E6 (stage 29) before synapses formed in most axons of the VIIIth cranial nerve, neurons were unmyelinated and had large numbers of microtubules and neurofilaments (Figure 7). The ultrastructural appearance of E6 axons was different at hatching time when axons were myelinated, and there were only a few microtubules but large numbers of neurofilaments (Figure 8). Neurofilaments in the axoplasm stained with silver solutions thin (Figure 9) and thick (Figure 10) fibers. However, the characteristic segmental arrangement of neurofilaments along the axons was best demonstrated by monoclonal antibodies such as anti-NF68/200 that stained the soma and fibers, particularly somas that were transected through the axon hillock (Figures 11-12). Anti-NF stained the afferent dendrites that synapse onto the hair cells (Figure 13) providing a convenient tool for following the branching pattern of those dendrites inside the epithelia, where large dendritic afferent endings form chalices around hair cells type I (Figure 14).

The trajectory of afferent fibers into the epithelia is also revealed by anti-S100ß, which in addition to its expression over the myelin, was also expressed over the denude segment of the dendrites inside the epithelia (Figure 14). Dense immunostain of S100ß was seen over the chalice endings, but not on the hair cells, suggesting that S100ß was expressed on the chalices. The expression of S100ß over the unmyelinated segment of the dendrite under the hair cell was masked by the expression of anti-NF68/200 in double immunostain of these molecules (Figure 15), suggesting that both molecules were co-expressed in the afferent dendrites in the area of synaptic contact. Expression of the NF68/200 was restricted outside the basement membrane to the axoplasm. On the other hand, expression of anti-S100ß over the nuclei or myelin of the neurons was not completely masked by the NF expression outside the basement membrane (Figures 15-16). Double immunostain for

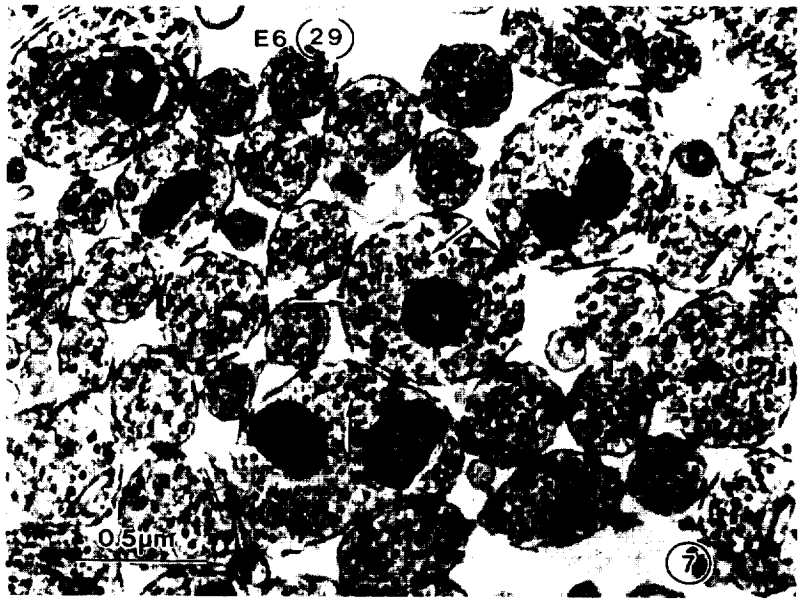

Figure 7. Electron micrograph at E6 (stage 29) with cross section through axons showing that microtubules (arrows) are more abundant than neurofilaments. At this embryonic stage there is no myelin and afferent synapses are just forming

Figure 8. Electron microscopy of axon at P1 (stage 46 plus one day after hatching) show that microtubules are scarce, whereas neurofilaments (ar rows) packed the axoplasm. A nucleated red blood cell, characteristic in birds, is seen at the upper right corner of the figure. At this stage, myelina tion is almost complete, afferent temporary synapses have been replaced by permanent synapses and afferent fibers from the brain contact hair cells.

Figure 1-6 (Color montage of S100β) demonstrating that expression of S100β is initially diffuse in neurons of the auditory and vestibular ganglia, whereas at hatching expression is diffuse only in the auditory neurons.

Figure 1. E9 (stage 35) auditory neurons (arrow) with minimal to none S100β expression.
Figure 2. E9 vestibular neurons from the same tissue section as in Figure 1 showing that S100β expression is higher in these neurons (arrows).
Figure 3. E17 (stage 43) when myelination is active, and afferent temporary synapses have been formed; S100β was expressed in the nuclei of some vestibular neurons, while other neurons (large arrow) did not express S100β at all.
Figure 4. Post-hatched day one (P1) showing that auditory neurons retained diffuse expression of S100β over the cytoplasm and nucleus of auditory neurons (arrows) even at hatching. Expression over myelinated fibers (M) was high.
Figure 5. Vestibular neurons from the same section as figure 4 (thus the same nerve) showing that expression of S100β was restricted to just some neurons, and primarily to their nuclei (small arrows), whereas other neurons were completely devoid of stain. The myelinated (M) fibers serve as positive built-in control. S100 was originally isolated from central glia and peripheral Schwann cells express it as well.
Figure 6. Pre-absorption of the antibody with pure protein purchased from Sigma abolished the reaction products over the nuclei of every neuron (arrow) and myelin.

Figures 9-14. Color montage showing the characteristic branching pattern of thin and thick fibers in newly hatched chicks (stage 46+1 or P1) inner ear organs. The branching pattern of the thin and thick fibers obtained with silver impregnation is also obtained with immunostain to phosphorylated and non-phosphorylated neurofilament antibodies.

Figure 9. Nerve fibers in the utricle silver-stained showing branching of thin unmyelinated fibers (arrows) branching inside the sensory epithelia. Staining of axons with silver is contributed by the neurofilaments in the axoplasm. The stain is contiguous because silver also stains other intermedi ate filaments non-specifically.

Figure 10. Contrary to thin fibers, thick fibers (usually myelinated) follow a more direct trajectory toward the hair cells (arrow) to form chalice and bouton synaptic contacts. Silver also stains intermediate filaments non-specifically in these fibers.

Figure 11. A subset of neurons stained with NF68/200 in the vestibular ganglion. The characteristic segmental appearance of neurofilaments in the axoplasm is also shown (arrows). Note that some neurons did not express NF68/200 and that the contiguous staining pattern of afferents by silver is not present.

Figure 12. Contrary to silver stained axons that appear uninterrupted-interrupted along the nerve, in antibody stained axons (arrows), neurofilaments and microtubules may not extend the entire length of the axon, a pattern that was previously reported for other peripheral afferents.

Figure 13. Afferent fibers entering the sensory epithelia of the inner ear are stained (arrow) permitting their tracing up to the hair cells (HC) located under the otoconial mass (O). Note that in this area of the macula where only type II hair cells are located, the NF68/200 stain only reaches the bottom of the hair cells (boutonic contacts). No chalices are present in this area.

Figure 14. Portion of the saccule with large afferent myelinated terminals (chalices) stained for S100β and contacting type I hair cells. Myelin (thick arrows) outside the habenula perforata, and after the terminal node of Ranvier (arrowhead) of these fibers do not penetrate the basement membrane in birds and mammals, but stain is robust in the entire chalice terminal (thin arrow). This suggests that staining at the chalice is contributed by S100β itself rather than by a diffusion artifact from the myelin stain.

Figure 15-20. Color montage of sections double immunostained for S100β /NF and MAP/NF illustrating that S100β and NF68/200 are co-expressed at the terminal afferent axons and that NF68/200 and MAP5 are differe ıtially expressed early and late in the inner ear afferents.

Figure 15. When sections were double immunostained, NF68/200 expression over-shac ow S100β (compare to Figure 14), where the myelin ends (large arrow), just before the fibers penetrate the basement membrane (thin arrow). NF68/200 was also present in the chalice ending around the hair cells (HC).

Figure 16. Whereas the immunoreaction of S100β was masked by neurofilaments at th : axon terminals (peripheral dendrites), the expression of S100β (red) over the nuclei of vestibular neurons was not (arrows). The stain of neurofilament (NF) was segmental along the axons.

Figure 17. Double immunostain for MAP5/NF68/200 at E3 with high expression of M AP5 (red) and almost absent NF68/200 expression (please see figures 7-8). At this stage (15), the otocyst (OT) was largely undifferentiated and the ve :tibular nerve (VG) located between the otocyst and the telencephalon (arrow) expressed MAP5.

Figure 18. By E5 (stage 28), the sensory epithelia (SEP) was still undifferentiated at the ocation of the presumptive utricle, and appeared pseudostratified. The vestibular nerve fibers expressed MAP5 up to the basement membrane of the epith lia, but not NF68/200. No myelination or mature afferent synapses are present at this time.

Figure 19. By E11 (stage 37) when myelination and synapses are ultrastructurally iden ified, a mixed staining pattern of MAP5 (red) and NF68/200 (black) was observed. Some fibers (small arrows) expressed NF68/200 outside and insi le the basement membrane, whereas other fibers expressed only S100β (large arrow).

Figure 20. By hatching (stage 46) double immunostaining for MAP5/NF68/200 showed a reversal of the pattern observed at before E11. The chick is precocious with a functional vestibular apparatus at hatching when synapses and myelination is near complete. Similar to the ultrastructural appearance shown on Figure 8, NF68/200 stain largely over shadowed the expression of the reduced number of microtubules present. NF68/200 was expressed inside the epithelia past the basement membrane (arrows).

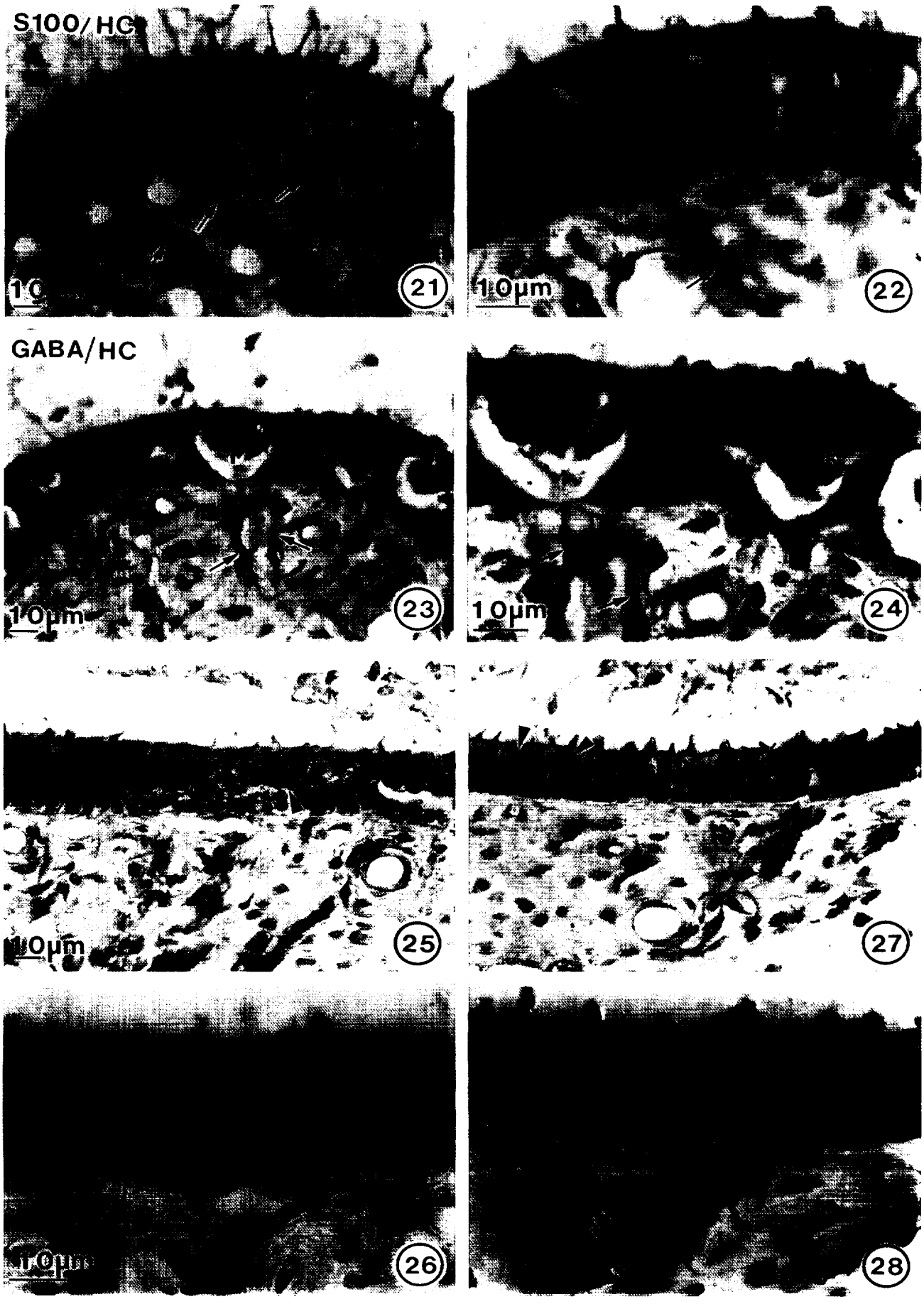
S100/HC
21
1.0μm
22
GABA/HC
23
1.0μm
24
25
1.0μm
27
26
28

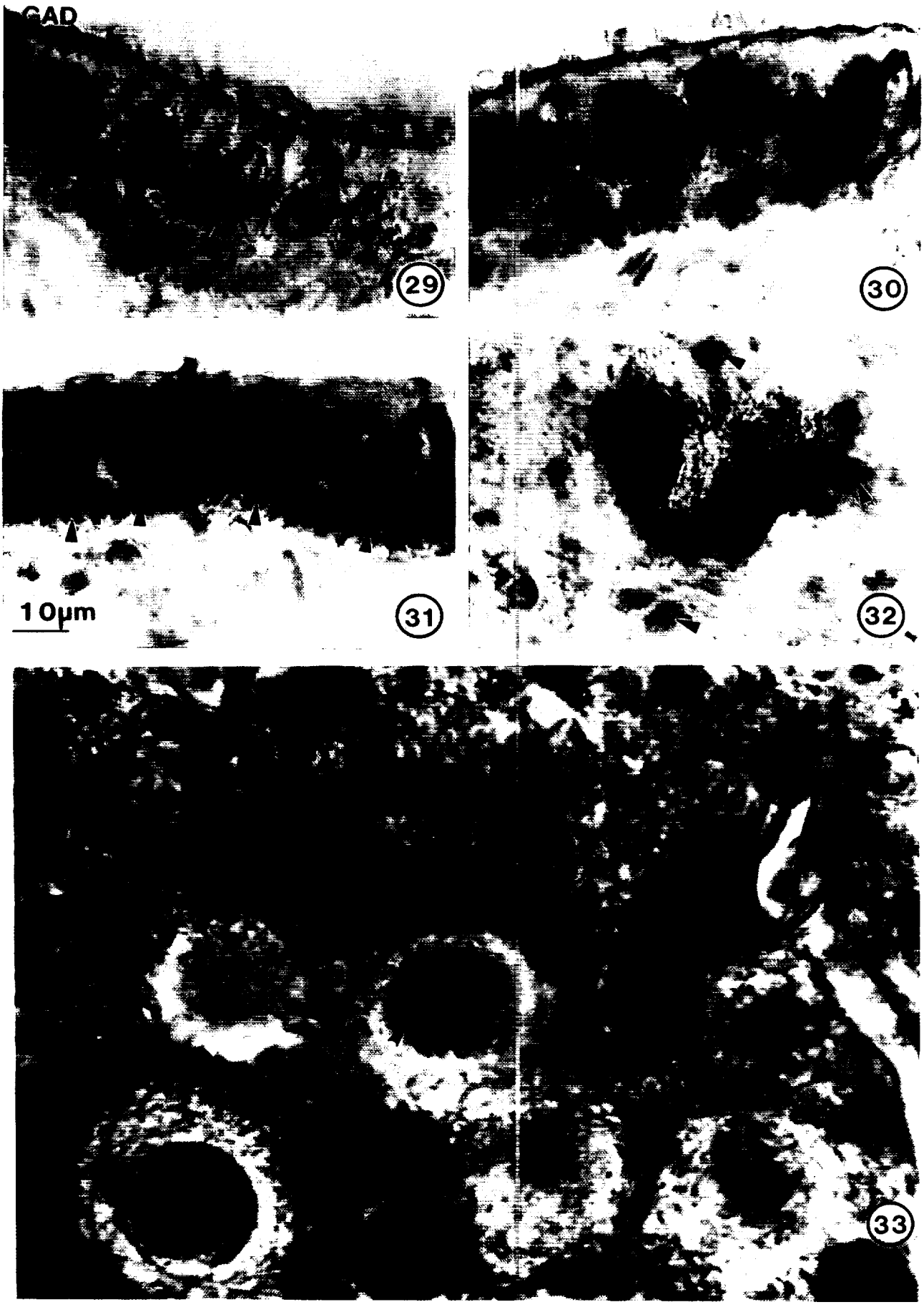
GAD
29
30
10μm
31
32
33

Figure 21. S100β expression on afferents innervating crista hair cells. Expression over the myelin (arrows) is strong and serves as a positive built in control.

Figure 22. Higher magnification from Figure 21 showing that while the terminal dendrites of afferents that form chalices expressed S100β , the hair cells themselves remain negative. In addition, expression of S100β over the myelin (arrow) contributed by Schwann cells is strong.

Figure 23. Expression of GABA, on the other hand, is prominent over the hair cells type I (I), and absent over the myelin (arrows). GABA is the most likely inhibitory neurotransmitter in the inner ear and is not normally expressed over myelin.

Figure 24. Higher magnification from Figure 23 showing that a up to 5 GABA positive hair cells can be ensheathed by a single chalice. Myelin over these large afferents does not express GABA (arrows) and serve as a negative control.

Figure 25. Double immunostain for S100β (brown) and GABA (red) of the utricular macula with co-expression of both molecules in cells of the striola. Hair cells type I with chalices (arrowhead) expressed mainly S100β (brown), whereas type II (arrow) expressed mainly GABA (red).

Figure 26. Higher magnification from Figure 25 showing the differential expression of S100β and GABA over type I (arrows) and II (arrowheads) hair cells at the boundary of the striolar region of the utricle. Note that hair cells (arrows) are negative, suggesting that S100β expression is restricted to the afferent terminal.

Figure 27. Non striolar region of the same specimen of Figure 25 showing diffuse co-expression of GABA and S100β over type I and II hair cells and/or afferent terminals.

Figure 28. Higher magnification from Figure 27 showing type I hair cells. The GABA (red) stain is restricted to the base of the hair cells. The S100β (brown) stain is located over the nerve terminal, not the hair cells.

Figure 29. Expression of GAD over hair cells type I and II in the saccule, matching the expression of GABA and suggesting that GABA is made locally. Similar results were demonstrated biochemically and immunohistochemically previously. Expression is restricted to the contact of the afferent terminals and the hair cells (arrows).

Figure 30. Expression of GAD over hair cells type I and II in the horizontal canal crista, matching the expression of GABA and suggesting that GABA is made locally. Expression is restricted to the contact of the afferent nerve terminals and the hair cells (arrows), whereas the nuclei and cytoplasms of the hair cells is negative.

Figure 31. Expression of GAD over hair cells type I and II in the utricle, matching the expression of GABA and suggesting that GABA is made locally. Note expression of the antibody in the nerve terminal between two hair cells (arrow). The supporting cell nuclei (arrowheads) mark the boundary of the basement membrane.

Figure 32. Positive control for the expression of GAD over spoon nerve endings (neuron on different focusing plane) of the tangential nucleus neurons from the same specimen as Figures 29-33. Negative control included pre-absorption and omission of the primary antibody (please see Figure 6). Note that the glial cells are negative (arrowheads).

Figure 33. Positive control for the expression of S100β /GABA in the Purkinje's cells of the cerebellum from the same specimen as Figures 29-33. Expression of S100β (brown) is apparent over the myelin fibers and the nuclei of the Purkinje's neurons (arrowheads). GABA (red) stained the terminal boutons synapsing on the neurons (arrow). Attesting to the lack of endogenous reaction are the red blood cells (asterisk) w hich lacked stain.

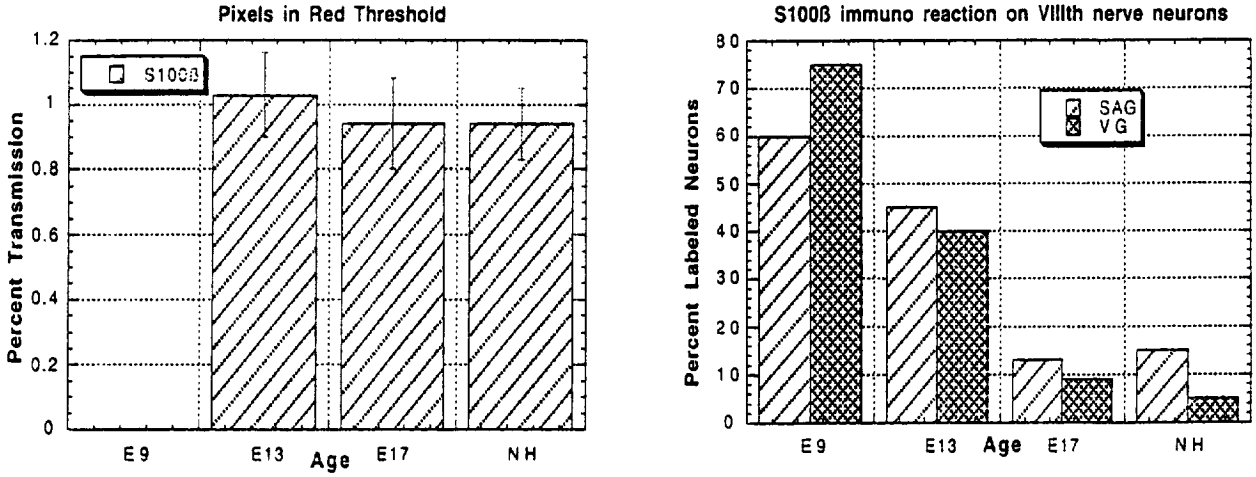

Figure 34. Color threshold measurements of S100β expression in the afferent perikarya that contact hair cells. No expression was present at E9, that is, no pixels were present in the area outlined with the mouse that corresponded to the present thresholds. The change in pixel density that color thresholding determines is always less noticeable than the visual impression of the stain. In our laboratory multiple users quizzed at random always estimated visually 2-3 times stronger differences between the immunostain for each antibody than the pixel saturation showed between stages. As the next figure shows, the percent of immunostain vestibular neurons changed with age.

Figure 35. The saturation of the immuno stain did not change much during development after it first appeared, but the number of neurons in each ganglion that expressed S100β varied with developmental age. Diffuse stain was present over auditory and vestibular neurons at E9 (35) in the majority of neurons, whereas only a small percentage express S100β at hatching (P1).

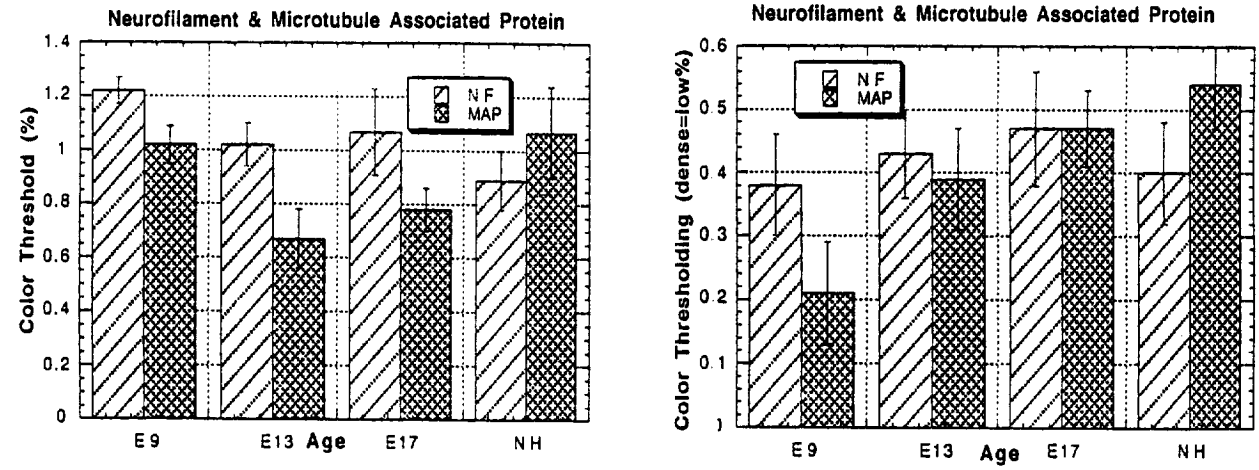

Figures 36-37. Color thresholding of S100β immunostain from two sets of slides from the same embryos, but processed separately in two batches. Saturation of pixels for the threshold used is different in the two groups even though the same antibody was used. Thus, comparison between ages or groups should only be done between sections that have been processed together.

MAP5/NF68/200 failed to show expression of NF68/200 (Figure 17) at E3 (stage15), or at E5 (stage 29) over the axons of the VIIIth nerve (Figure 18). NF expression was present at E13 (stage 39) over the myelinated and unmyelinated portions of the axon (Figure 19), and increased steadily toward hatching (stage 46) when the anti-MAP5 expression was overshadowed by that of the anti-NF68/200 antibody (Figure 20).

In the end organs, afferent chalice terminals around hair cells stained with anti S100ß. The myelin around the large fibers of the angular accelerometers of the inner ear (crista of the ampula) expressed S100ß (Figures 21-22). Portions of the hair cells and of the chalice terminals expressed GABA, and the myelin or axoplasm did not (Figures 23-24). In the linear accelerometers (maculae of the utricle and saccule), S100ß/GABA were expressed in different regions of these organs. In the center or striola of the maculae, type I hair cells with chalice endings expressed S100ß, whereas type II hair with bouton endings expressed GABA (Figures 25-26). In the periphery of these organs (areas surrounding the striola) S100ß/GABA were co-expressed in terminals to both type of hair cells (Figures 27-28). GAD was expressed in the same locations where GABA was expressed in the maculae (Figure 29), in the cristae (Figures 30-31) and in the brain neurons used as positive built-in controls (Figure 32-33).

Color thresholding analysis of S100ß immuno reaction density showed little change in the saturation of pixels from embryonic day 13 (E13) to hatching in the terminal dendrites (growth cones) that contact hair cells (Figure 34). Similar results were obtained when the neuronal bodies (perikarya) were analyzed. There was no noticeable S100ß staining at E9 in the terminal dendrites, reason why we did not examined younger embryos for S100ß expression. There was however a change in the percent of neurons with nuclear expressing S100ß (Figure 35). The intensity of the neurofilament and microtubule associated protein antibody stains was calculated in two sets of slides with varying degree of intensity to demonstrate the point made earlier in the methods that intensity of the reaction is dependant upon technical preparatory conditions. In the first set (Figure 36) color thresholding values as percent transmission of light through pixels for the preset threshold values expand from 60% to 120%, whereas in the second set (Figure 37) from 20% to 46%.

Discussion

The main purpose of this study was to determine if any anatomical relationship existed between the expression of neurotrophic molecules, neurotransmitters, cytoskeletal proteins, the formation of synapses and myelination of afferents in the VIIIth cranial nerve of the inner ear of the chick embryos. The results presented here suggest that: a) the expression of the neurotrophic factor S100ß is restricted to groups of vestibular afferent neurons (Figures 1-6), and increases slightly in the afferent chalices (dendritic afferent endings) after synapse formation (Figures 14, 21-22); b) the expression of cytoskeletal (Figures 9-13) MAP5 and NF68/200 is reversed (Figures 7-8) during early and late development (Figures 15-20); and c) S100ß expression and that of GABA (Figures 21-28) and GAD (Figures 29-32) occurs in the dendritic chalice endings of the inner ear afferents. We are aware of the diversity of growth factors and molecules involved in the embryonic remodelling of sensory tissues and recognize that those we chose and discuss here are just participants of a complex process. Nonetheless, the molecules we examined in this studied were demonstrated by others as essential components of normal neuronal development in other sensory systems and may be activated to modulate repair, regeneration and regrowth after axotomy (deafferentation). We designed this experiment to test the hypothesis that the well known neurotrophic molecule S100ß immuno expression in the inner ear may be suggestive of a neurotrophic role there if co-expressed with a well known neurotransmitter like GABA. In addition, we reasoned that the previous differentiating patterns of sensory and secretory cells in the chick inner ear [16, 32, 34] including myelination [31] could be related to the expression of S100ß, particularly, if S100ß expression was modulated concomitantly with synapse formation and myelination. We will discuss these data, provide our interpretation and relate it to other work with these molecules in other sensory systems.

Implications for S100ß role in the development and maintenance of the inner ear: Recent work suggests that many differentiating factors including proteins and cytokines with neurtrophic properties can be activated in response to injury [72]. We reported previously that S100ß expression in the developing inner ear suggested a dual function, because it was found both molecules on neurons [29] and secretory cells [28]. We hypothesized that because inner ear functions demand neurotrophic and ionic modulation of sensory and secretory cells, S100 may subserve these functions in the inner ear. First, transduction of mechanical impulses into neuronal energy requires the participation of afferent neurons to convey to the brain correct information about the body's position in space. This in turn probably requires the participation of neurons with different functional charateristics connected to different inner ear end organs. It is highly possible that the differential expression of S100ß in only selected groups of vestibular neurons may be related to the functional heterogeneity that characterizes the inner ear. Second, calcium binding proteins, including S100 are well known for their calcium modulatory actions. The inner ear endolymphatic duct and fluid contain large stores of calcium (otoliths) in the form of calcium carbonate. Calcium ions on the other hand act as second messengers in cells and induce a multitude of functions including secretion, contraction and division [78], essential properties of inner ear functioning. The S100 family includes about 16 members with unique immuno-distri-

bution patterns, and most function as intracellular calcium-modulated-target proteins in a calium dependent manner. Third, S100 binding proteins may have intracellular and extracellular functions depending on whether they form homodimers and/or heterodimers. This last property imparts to them ideal neurotrophic and ionic modulatory activities. The calcium binding proteins are characterized by a helix-loop-helix EF structural motif that binds calcium, but unlike other calcium binding proteins that act mostly as buffers, S100 acts as trigger and activator proteins [69, 78] and can induce apoptosis and regulate phosphorylation. This last condition is significant for the transformation of neurofilament proteins in the axon. In fact, over expression of S100ß in astrocytes alters synaptic plasticity and impairs spatial learning in transgenic mice [38, 39]. As it will be discussed later, cytoskeletal proteins can be regulated by S100 and similar calcium binding proteins [8]. These properties described above suggest that if S100ß is to have neurotrophic action upon afferents, it should be expressed in the perikarya and/or their axons. The immunoexpression we report over the myelin (Schawnn's cells) was expected because they are neural crest derived cells that like glial cells stain positive for S100ß. Figures 1-6 shows that vestibular afferents stained differently from auditory afferents. This is an important observation for our studies because our laboratory showed previously [27, 34, 35] that deafferentation of neurons in the auditory and vestibular ganglion of the squirrel monkey induced total degeneration of auditory neurons, whereas 40% of vestibular neurons survived three years after deafferentation. At hatching, when the chicks can walk and go about with normal balancing functions, only certain groups of afferent neurons express S100ß in their nuclei (Figure 5), whereas auditory neurons express the protein diffusibly througout nuclei and cytoplasm (Figure 4). A distinct nuclear expression versus a diffused cytoplasmic expression of S100ß could be related to yet undemonstrated function of S100ß in some vestibular neurons. From our previous observations in deafferentated squirrell monkeys we suggested that "surviving neurons could belong to a subpopulation with greater capacity for repair" [27].

A case for calcium binding proteins in the inner ear possibly serving as neurotrophic and ionic modulators is strengthened by the demonstration of the calcium binding protein calbindin-D28K in the inner ear of human, primates and rodents [18, 19, 84, 88]. These authors concluded, similar to our previous conclusions in birds [29], that such proteins may regulate calcium concentration in the perilymphatic fluid [28]. Other calcium binding proteins are expressed in the inner ear of rodents [3, 12, 58], amphibian and fishes [36, 37, 50, 77] and most central nervous system components [10]. Of the 16 known S100 subtypes, we are most interested in the S100ß isoform because of its expression in afferent neurons and secretory cells. The recent outstanding review of Schafer above emphasizes the multifunctional attributes of S100ß [52], which one would expect to be part of a heterogenous tissue as the inner ear. Among others, he noted: a) S100ß is expressed and can be isolated from Schwann and glial cells, b) it targets the proteins of *p53*, calponin, *tau*, tubulin, caldesmon, neurocalcin, neuromodulin and GAP43 among others, c) it was shown to stimulate neurite extension, to stimulate calcium fluxes, to inhibit PKC mediated phosphorylation, to induce axonal and astrocyte proliferation, d) to inhibit microbutule assembly, and e) it has been associated with a variaty of neurological diseases where it may alter neuronal functioning. Finally, the high level of structural homology in the sequences of S100ß between rodents, bovine and human species suggests that the genes responsible for the control of this protein are and highly conserved. To this end, S100 mRNA is distributed throughout the body in tissues as diverse as: brain, aorta, bladder, brown fat, color kidney, intestine, skeletal muscle, testes, skin, nerve melanoma cells and monocytes among others [101]. Thus, our original assumption that S100β may serve as a modulatory function in the inner ear besides being neurotrophic for certain afferent neurons deserves further analysis. We will report separately our recent in situ hybridization findings (data not shown) with a synthetic S100β probe made from a highly conserved region of sequence alignment match between rodent, bovine and human S100β. The probe hybridizes in the same tissues where the anti-S100βwas localized.

Differential distribution of MAP5/NF68/200: These two proteins are considered essential for axon development, for neuronal survival and proper functioning [81]. Microtubules are necessary for cell motility, transport, cells shape, cell polarity and mitosis ([59, 60], and help guide growth cones during target search [61]. Microtubules are the major cytoskeletal components of the developing neurons, where they are continuously modified, particularly at the distal locations (e.g., growth cones) where turnover is rapid [9, 24]. Besides these properties, microtubules may be related to axonal diameter [47, 48, 98], and influence development of certain pathologies [41]. Neurofilaments on the other hand are essential components of the axoplasm whose dependence on neurofilaments for proper functioning was demonstrated in mutant quails unable to express them [17, 82, 98]. In those animals, the number of neurofilaments and microtubules in myelinated fibers was smaller than in normal animals suggesting that these two cytoskeletal components act differentially upon the development of myelinated and unmyelinated axons.

Since we and others observed expression of S100ß at the peripheral dendrite of the large myelinated afferent axons, we wanted to determine if there was any relation to the expression of cytoskeletal protein particularly before, during and after synapse formation. Ultrastructurally, the axons of the VIIIth nerve are homogenous before synapse and myelination formation with characteristic abundant number of microtubules (Figure 7). This appearance is reversed at hatching after synapse formation and myelination (figure 8) when the axoplasm is packed with neurofilaments, a condition that characterizes other sensory axons in other nerves. Interme-

diate filaments including neurofilaments are responsible for the characteristic silver stain appearance (Figures 9-10) observed by us and others. However, only with antibody to certain isoforms of the NF family can the neuronal and axoplasmic distribution of intermediate filaments be specifically identified (Figures 11-13). Afferent fibers stained with anti-NF68/200 can be followed into the sensory epithelial up to the hair cells they contact (Figure 14). Those dendrites contacting hair cells also expressed the neurotrophic molecule S100ß. These and other calcium binding proteins are expressed on neural crest derived cells and in particular peripheral Schwann and central glial cells. Myelination and synapse formation and the expression of neurofilaments could be related during development, because others have shown that changes in neurofilament phosphorylation and axonal caliber are linked to myelin thickness [17]. These authors proposed that the simplest way to explain the relationship between axon caliber and myelin was to assume a ligand on the Schwann cell inner myelin face binding to an intergral membrane receptor in the axolemmal membrane face, a situation that could be aided by S100ß which is intrinsic to the Schwann cells. S100ß and NF68/200 were co-expressed in the thick myelinated axons of the VIIIth nerve (Figure 15) and in the perikarya (Figure 16). In double immunostaining for S100ß and NF/68/200 (Figures 15-16) the terminal dendrites after the last node of Ranvier expressed mainly NF68/200, and myelin up to the first node of Ranvier expressed S100ß. Since S100ß is expressed up to the terminal dendrite when used alone, it seems that the number of antigenic sites at the terminal dendrites (chalices) is higher for NF68/200 than for S100ß. It would be instructive to determine in future studies if such pattern of co-expression between a neurotrophic factor like S100ß and an intermediate filament protein like NF68/200 remain unaltered in the adult, and even more important if it changed after deafferentation of the nerve. Expression of neurofilament proteins in afferent terminals of the VIIIth nerve were reported in the cochlea [6, 74], in the rodent [84, 87, 97] and human [5] vestibular organs. The expression of GABA and GAD where S100ß is expressed (Figures 21-32) suggests that S100ß could play a neurotrophic role in the chalices as well, and studies are now underway to determine if this is the case. In dorsal root ganglia neurons there is a 50% decrease in the neurofilament mRNA [71] during axonal atrophy, and it is believed that the regulation of neurofilament protein dynamics via phosphorylation plays a major role in diseases related to neurofibrillary accumulation [66]. This last condition is opposite immediately after deafferentation, when there is a marked decrease in neurofilament triplet proteins [73, 99].

In staying with the original hypothesis that an association between the expression of S100ß and cytoskeletal proteins we chose to study could exist during development, double immunostained for NF68/200 and MAP5. We reasoned that if the microtubular drugs colchicine and vinblastine could reduce S100ß mRNA to 25% in relation to controls [23] in rat glioma cells, a relationship may exist between the expression of S100ß and neurofilaments. Early in development before synapses form and myelination takes place, MAP5 is expressed in the nerve fibers (Figures 17-18). However, at the time that myelination is taking place and synapses are actively forming (Figure 19), MAP5 and NF68/200 are co-expressed about equally in the axons and the terminal dendrites. By hatching and in parallel with the ultrastructural observation we published previously about the VIIIth cranial nerve [31, 32, 35], the expression of NF68/200 is higher than that of MAP5 (Figures 7-8). These observations are consistent with the previously described function and characteristic of MAP. The MAP proteins are very heterogeneous show stage-specific expression during development and usually subsellular-specific compartmentalization [1, 2]. For instance, projection domains of MAP2 or *tau* determine spacing between microtubules in axons [13] where there is redundancy between isoforms of MAP [44, 45]. A close interplay between NF and MAP was demonstrated in mutant quails deficient in neurofilaments. In those animals there were more microtubules per axon than in normal [98,99]. On the other hand, mechanical pressure on sensory neural induces neurite formation and the appearance of new microtubules [100]. In DRG neurons expression of MAP5 decreases following the establishment of specific connections [75], which occur in the chick afferents after 16 days (Figures 18-19). Finally, assuming that S100ß has any neurotrophic role in the afferents of the inner ear it is possible that its regulation be intimately associated to the microtubular network as is the case in L929 cultured cells [4]. We are thus encouraged to continue our studies of association between the expression of S100ß and cytoskeletal proteins and of S100ß as a potential modulatory molecule during inner ear development and post-natal life.

Importance of GABA and GAD co-expression with S100ß: γ-Aminobutyric Acid (GABA) is the major inhibitory neurotransmitter of the vertebrate peripheral and central nervous system [63, 93]. The co-localization of GABA and its synthesizing enzyme L-glutamic decarboxylase (GAD) with S100ß suggests that GABA is secreted locally rather than transported there. GABA synthesis in the vestibular tissues of the chick inner ear was demonstrated biochemically and morphologically [62]. GABA was later localized in the chick [85, 86], but to our knowledge few if any study demonstrated co-localization of GABA with any other neurotrophic factor until our results (Figures 21-28). Data that we feel is strengthened by the demonstration of GAD in the locations where GABA and S100ß were expressed (Figures 29-32). We are not suggesting that S100ß and GABA are neurotransmitters of the chick inner ear, rather that they may be some of the molecules that serve as modulators there [29]. GABA is a well studied neurotransmitter in the avian brain, including the forebrain and midbrain of pigeons [90, 96] where a regional distribution of GABA and benzodiazepine receptors in these areas was similar to mammals [22]. However, most works with GABA and avian inner ears were preformed on auditory central structures, where a considerable portion

of the GABA neurons arise locally [91], and contribute to the auditory processing there [64]. Lack of input from the cochlea modifies the expression of GABA centrally [14, 15].

Several works localized GABA in the peripheral end organs of rodents. Co-localizaton of GABA and GAD in similar areas was shown in the guinea pig vestibule [54, 56, 62] suggesting that in rodents GABA may serve a modulatory function [21]. GABA is an inhibitory neurotransmitter centrally and probably peripherally as well. Expression of GABA and GAD positive terminals were also documented in the developing mouse cochlea [93], where its embryological expression was carefully evaluated, and suggested that local GABAergic circuitry may exist wtihin the inner ear. Our previous observations that GABA and S100ß were differentially expressed in vestibular type I and II hair cells terminals [29], is now corroborated and strengthen by the demonstration of GAD in the same areas. Immuno reaction of GABA on hair cell type II of the macula lagena [86] of the chick (a vestibular organ with otoliths) was similar to the staining pattern we demonstrated on hair cells type II of the true otolithic organs utricle and saccule (Figures 25-28). Nonetheless, hair cell type I with chalice endings of the crista expressed GABA abundantly (Figures 21-24). Expression of calcium binding proteins (Calbindin,-D28K calmodulin, parvalbumin) was generally restricted to the inner ear hair cells cytoplasm in various species. Such was the case too for the expression of the S100ααßß dimer in the inner ear of fish [36, 37, 77] and frogs [50]. The expression of S100ß on the other hand was restricted to the afferent nerves fibers in the chick inner ear organs rather than to the hair cells themselves (Figures 14-15, 21-28) true to its previously characterized affinity for Schwann cells and neural crest derived cells. Similar observations were made in our previous studies in which we cautioned about the proper interpretation of S100 immunoreactivity inside the sensory epithelia of the inner ear organs. Even though fish and frogs do not have true type I and II hair cells [43], this work demonstrated a differential expression of S100aaßß in different areas of the sensory epithelia of the maculae. We emphasized such feature in our recent work [28, 29] and showed that GABA may be differentially expressed in the secretory epithelia as well. In the rat [11] co-localization of GABA and other calcium binding proteins was observed in the hippocampus, but the authors suggested that the association was probably a fortuitous observation with no neurotransmitter or neuromodulator effect. However, in the inner ear where differential functional attributes are known and well characterized for different types of hair cells and neurons, the differential expression of GABA and S100ß may be more than coincidental. Particularly in view of its expression in similar areas of evolutionarily older species. We are thus encouraged by these findings and have designed experiments aimed at evaluating the functional effect of S100ß in the developing inner ear. It would be interesting to show if S100ß is one of many modulator molecules of sensory and secretory cells in the inner ear.

In summary: The results presented in this paper illustrated the immunoexpression of the neurotrophic factor and calcium-binding protein S100β on afferent dendrites of the VIIIth cranial nerve. The VIIIth nerve conveys sensory information about body posture and equilibrium from the inner ear to the brain. The saturation of S100β stain did not change significantly immediately after the establishment of permanent afferent synapses on the chalices and the nuclei of vestibular neurons. However, the percent of neurons that in each ganglion expressed S100β changed around synaptogenesis and myelination of the fibers. Furthermore, afferent terminalsthat expressed S100β were located in different portions of the sensory organs examined. In the cristae of the ampullae (angular acceleration detecting organs), S100β was more abundant in the afferent endings of hair cells type I (chalices), whereas in the maculae of the utricle and saccule (linear acceleration detecting organs), the terminal endings of afferents to both type I (chalice) and type II (boutonic) expressed S100β abundantly. The increased expression of S100β in those areas also paralleled myelination. These changes were also related to the expression of MAP5 and NF68/200, two important cytoskeletal proteins necessary for neuronal survival and differentiation. Co-localization of S100β with NF68/200 suggested that the NF68/200 may share a higher number of antigenic epitopes at the terminal chalices than S100β. Co-localization of MAP5 and NF68/200 suggested that the expression of these two important cytoskeletal elements changes during development so that NF68/200 is more prevalent near and after hatching than MAP5, at least in chicks. Co-localization of S100β, with the known neurotrasmitter GABA and its synthesizing enzyme GAD, suggested that S100β was probably made locally raising the possibility that it served an important function there. We assume that one of the functions of S100β in the inner ear VIIIth nerve could be neurotrophic, and that additional functions could have a modulatory effect upon secretory cells that control the homeostasis of the lymphatic inner ear fluids. Moreover, the differential expression of GABA in both types of hair cells and in different regions of the utricle and the saccule may also be related to, as yet undetermined, differential functional roles of S100β and GABA in each hair cell type. We needed to establish these normative patterns to later determine if the immunoexpression of these proteins will be altered after physiological, mechanical, or chemical insults to the inner ear. It is highly possible that degeneration and de-differentiation needed for proper repair of adult of sensory neurons after insults recapitulate changes in expressions of the molecules evaluated there during development.

Acknowledgments

Supported by the Department of Pathology at Tulane, NASA grants NAGW 1516 and NAG-2-999 to CDF and funds from the NIH. Thanks to Mrs. Mary G. Fermin and Odette Marquez for correcting the manuscript, to Dr. Meza

for answering so many questions about the significance of the co-localization of GABA, GAD and S100β, and to Mr. Ellis Diaz who provided photography technical assistance. Dr. Robert Garry provided invaluable critique of the experimental design, methods, and interpretations antibody of stains.

References

1. **Avila, J., J. Dominguez and J. Diaznido**. 1994. Regulation of microtubule dynamics by microtubule-associated protein expression and phosphorylation during neuronal development. Int J Dev Biol. 38:13-25.
2. **Avila, J., L. Ulloa, J. Gonzalez, F. Moreno and J. Diaznido**. 1994. Phosphorylation of microtubule-associated proteins by protein kinase CK2 in neuritogenesis. Cell Mol Biol Res. 40:573-579.
3. **Baimbridge, K., M. Celio and J. Rogers**. 1992. Calcium-binding proteins in the nervous system. TINS. 15:303-308.
4. **Baudet, C., P. Naveilhan, F. Jehan, P. Brachet and D. Wion**. 1995. Expression of the nerve growth factor gene is controlled by the microtubule network. J Neurosci Res. 41:462-470.
5. **Bauwens, L.J.J.M., J.C.M.J. Degroot, F.C.S. Ramaekers, J.E. Veldman and E.H. Huizing**. 1992. Expression of intermediate filament proteins in the adult human vestibular labyrinth. Ann Otol Rhinol Laryngol. 101:479-486.
6. **Baxter, R., L.H. Bannister, H.C. Dodson and D.V. Gathercole**. 1993. Protein gene product 9.5 in the developing cochlea of the rat - cellular distribution and relation to the cochlear cytoskeleton. J Neurocytol. 22:14-25.
7. **Bhattacharyya, A., R.W. Oppenheim, D. Prevette, B.W. Moore, R. Brackenbury and N. Ratner**. 1992. S100 is present in developing chicken neurons and Schwann cells and promotes motor neuron survival In vivo. J Neurobiol. 23:451-466.
8. **Bianchi, R., M. Garbuglia, M. Verzini, I. Giambanco and R. Donato**. 1994. Calpactin I binds to the glial fibrillary acidic protein (GFAP) and cosediments with glial filaments in a Ca2+-dependent manner: implications for concerted regulatory effects of calpactin I and s100 protein on glial filaments. Biochemica et Biophysica Acta. 1223:361-367.
9. **Black, M. and A. Brown**. 1993. Sites of microtubule assembly in growing azons, p. 171-182. In Hirokawa, N. (Ed.). Neuronal cytoskeleton morphogenesis, transport and synaptic transmission. Vol. 16. Japan Scientific Socieiteis Press & CRC Press Tokyo, Tokyo.
10. **Braun, K.** 1990. Calcium-binding proteins in avian and mammalian central nervous system: Possible Localization, development and possible functions. Prog in Histochem & Cytochem. 21:1-64.
11. **Celio, M.** 1986. Parvalbumin in most gamma-aminobutyric acid-containing neurons of the rat cerebral cortex. Science. 231:995-997.
12. **Celio, M.** 1990. Calbindin D-28k and paralbumin in the rat nervous system. Neuroscience. 35:375-475.
13. **Chen, J., Y. Kanai, N.J. Cowan and N. Hirokawa**. 1992. Projection domains of MAP2 and tau determine spacings between microtubules in dendrites and axons. Nature. 360:674-676.
14. **Code, R.A., G.D. Burd and E.W. Rubel**. 1989. Development of GABA immunoreactivity in brainstem auditory nuclei of the chick: Ontogeny of gradients in terminal staining. J Comp Neurol. 284:504-518.
15. **Code, R.A. and L. Churchill**. 1991. $GABA_A$ Receptors in auditory brainstem nuclei of the chick during development and after cochlea removal. Hear Res. 54:281-295.
16. **Cohen, G.M. and C.D. Fermin**. 1985. Development of the embryonic chick's tectorial membrane. Hear Res. 18:29-39.
17. **De Waegh, S., V.-Y. Lee and S. Brady**. 1992. Local modulation of neurofilament phosphorylation axonal caliber, and slow axonal transport by myelinating Schwann cells. Cell. 68:451-463.
18. **Dememes, D., M. Eybalin and N. Renard**. 1993. Cellular distribution of parvalbumin immunoreactivity in the peripheral vestibular system of three rodents. Cell Tissue Res. 274:487-492.
19. **Dememes, D., J. Raymond, P. Atger, C. Grill, L. Winsky and C.J. Dechesne**. 1992. Identification of neuron subpopulations in the rat vestibular ganglion by calbindin-D 28K, calretinin and neurofilament proteins immunoreactivity. Brain Res. 582:168-172.
20. **Dewaegh, S.M., V.M.Y. Lee and S.T. Brady**. 1992. Local modulation of neurofilament phosphorylation, axonal caliber, and slow axonal transport by myelinating Schwann cells. Cell. 68:451-463.
21. **Didier, A., J. Dupont and Y. Cazals**. 1990. GABA immunoreactivity of calyceal nerve endings in the vestibular system of the guinea pig. Cell Tissue Res. 260:415-419.
22. **Dietl, M.M., R. Cortes and J.M. Palacios**. 1988. Neurotransmitter receptors in the avian brain. III. GABA-benzodiazepine receptors. Brain Res. 439:366-371.
23. **Dunn, R., C. Landry, D. O'Hanlon, J. Dunn, R. Allore, I. Brown and A. Marks**. 1987. Reduction in S100 protein beta subunit mRNA in C6 rat glioma cells following treatment with anti-microtubular drugs. J Biol Chem. 262:3562-6.
24. **Edson, K.J., S.S. Lim, G.G. Borisy and P.C. Letourneau**. 1993. FRAP analysis of the stability of the microtubule population along the neurites of chick sensory neurons. Cell Motil Cytoskeleton. 25:59-72.
25. **Fermin, C.** 1995. Anatomy, histology and color thresholding. Microscopy Today. 95-5:16.
26. **Fermin, C. and S. DeGraw**. 1995. Color Thresholding in video imaging. J. Anat. 186:469-481.
27. **Fermin, C., M. Igarashi, G. Martin and H. Jenkins**. 1989. Ultrastructural evidence of repair and neuronal survival after labyrinthectomy in the squirrel monkey. Acta Anat. 135:62-70.
28. **Fermin, C., D. Lee and D. Martin**. 1995. Elliptical-P cells in the avian perilymphatic interface of the *tegmentum vasculosum*. Scann Microsc. 9:1207-1222.
29. **Fermin, C. and D. Martin**. 1995. Expression of S100ß in sensory and secretory cells of the vertebrate inner ear. Cell Mol Biol. 41:213-225.
30. **Fermin, C., D. Martin, T. Jones, J. Vellinger, M. Deuser, P. Hester and R. Hullinger**. 1996. Microgravity in the STS-29 Space Shuttle Discovery affected the vestibular system of chick embryos. Histol Histopath. 11:407-426.
31. **Fermin, C.D. and G.M. Cohen**. 1984. Development of the embryonic chick's statoacoustic ganglion. Acta Otolaryngol (Stockh). 98:42-52.
32. **Fermin, C.D. and G.M. Cohen**. 1984. Developmental gradients in the embryonic chick's basilar papilla. Acta Otolaryngol (Stockh). 97:39-51.
33. **Fermin, C.D., M.A. Gerber and J. Torre-Bueno**. 1992. Colour thresholding & objective quantification in bioimaging. J. Microscopy. 167:85-96.
34. **Fermin, C.D. and M. Igarashi**. 1984. Dendritic growth following labyrinthectomy in the squirrel monkey. Acta Otolaryngol (Stockh). 97:203-212.
35. **Fernandez, C. and J.M. Goldberg**. 1971. Physiology of peripheral neurons innervating semicircular canals of the squirrel monkey. II. Response to sinusoidal stimulation and dynamics of peripheral vestibular system. J. Neurophysiol. 34:661-675.
36. **Foster, J.D., M.J. Drescher, J.S. Hatfield and D.G. Drescher**. 1994. Immunohistochemical localization of S-100 protein in auditory and vestibular end organs of the mouse and hamster. Hear Res. 74:67-76.
37. **Foster, J.D., M.J. Drescher, K.M. Khan and D.G. Drescher**. 1993. Immunohistochemical localization of S-100 protein in the saccule of the rainbow trout (*Salmo-Gairdnerii R*). Hear Res. 68:180-188.
38. **Gerlai, R., W. Friend, L. Becker, D. Ohanlon, A. Marks and J. Roder**. 1993. Female transgenic mice carrying multiple copies of the human gene for S100-beta are hyperactive. Behav Brain Res. 55:51-59.
39. **Gerlai, R., A. Marks and J. Roder**. 1994. T-Maze spontaneous alternation rate is decreased in S100 beta transgenic mice. Behav Neurosci. 108:100-106.

40. **Glass, J.D. and J.W. Griffin**. 1991. Neurofilament redistribution in transected nerves - evidence for bidirectional transport of neurofilaments. J Neurosci. 11:3146-3154.
41. **Goedert, M.** 1993. Tau proteins and alzheimer's disease, p. 233-246. In Hirokawa, N. (Ed.). Neuronal cytoskeleton morphogenesis, transport and synaptic transmission. Vol. 16. Japan Scientific Socieiteis Press & CRC Press Tokyo, Tokyo.
42. **Gu, J., N. Agrawal, P.-P. Wang, M. Cohen and J. Downey**. 1995. A primary-secondary antibody complex method of immunocytochemistry using rabbit polyclonal antibody to detect antigens in rabbit tissue. Cell Vision. 2:52-58.
43. **Guth, P., C. Fermin, R. Pantoja, R. Edwards and C. Norris**. 1994. Hair cells of different shapes and their placement along the frog crista ampullaris. Hear. Res. 73:109-113.
44. **Hara, A., A.N. Salt and R. Thalmann**. 1989. Perilymph composition in scala tympani of the cochlea - influence of cerebrospinal fluid. Hear Res. 42:265-271.
45. **Harada, A., K. Oguchi, S. Okabe, J. Kuno, S. Terada, T. Ohshima, R. Satoyoshitake, Y. Takei, T. Noda and N. Hirokawa**. 1994. Altered microtubule organization in small-calibre axons of mice lacking tau protein. Nature. 369:488-491.
46. **Heidemann, S.R.** 1993. A new twist on integrins and the cytoskeleton. Science. 260:1080-1081.
47. **Hirokawa, N.** 1977. Disappearance of afferent and efferent nerve terminals in the inner ear of the chick embryo after chronic treatment with bungarotoxin. J Cell Biol. 73:27-46.
48. **Hirokawa, N.** 1993. The neuronal cytoskeleton: Its role in neuronal morphogenesis and organelle transport, p. 4-32. In Hirokawa, N. (Ed.). Neuronal cytoskeleton morphogenesis, transport and synaptic transmission. Vol. 16. Japan Scientific Societies Press & CRC Press Tokyo, Tokyo.
49. **Hirokawa, N. and L.G. Tilney**. 1982. Interactions between actin filaments and between actin filaments and membranes in quick-frozen and deeply etched hair cells of the chick ear. J Cell Biol. 95:249-261.
50. **Kerschbaum, H. and A. Hermann**. 1993. Calcium-binding proteins in the inner ear of the *Xenopus laevis* (Daudin). Brain Res. 617:43-49.
51. **Kirkpatrick, L.L. and S.T. Brady**. 1994. Modulation of the axonal microtubule cytoskeleton by myelinating Schwann cells. J Neurosci. 14:7440-7450.
52. **Kligman, D. and D.C. Hilt**. 1988. The S-100 protein family. TIBS. 13:437-443.
53. **Lankford, K.L. and P.C. Letourneau**. 1991. Roles of actin filaments and three second-messenger systems in short-term regulation of chick dorsal root ganglion neurite outgrowth. Cell Motil Cytoskel. 20:7-29.
54. **Lo, Y.-J. and M.-M. Poo**. 1991. Activity-dependent synaptic competition in vitro: heterosynaptic suppression of developing synapses. Science. 254:1019-1022.
55. **Lockerbie, R.O.** 1987. The neuronal growth cone: A review of its locomotory, navigational and target recognition capabilities. Neuroscience. 20:719-729.
56. **Lopez, I., J.-Y. Wu and G. Meza**. 1991. Glutamate decarboxlase: GABA-transminase localizationin the guinea pig vestibule, immunocytochemical support for an efferent GABAergic neurottransmission. Soc Neurosci Abstr. 1:632.
57. **Macrae, T.H.** 1992. Towards an understanding of microtubule function and cell organization - an overview. Biochem Cell Biol. 70:835-841.
58. **Maeda, T., U. Hiroshi, A. Kazuaki, R. Kuwano, T. Yasuo and Y. Suzuki**. 1991. Structure and expression of rat S-100 ß subunit gene. Mol Brain Res. 10:193-202.
59. **Mandelkow, E. and E.-M. Mandelkow**. 1995. Microtubule and microtubule-associated proteins. Current Opinion in Cell Biol. 7:72-81.
60. **Mandelkow, E. and E.M. Mandelkow**. 1994. Microtubule structure. Curr Opin Struct Biol. 4:171-179.
61. **Mercer, J.A., J.P. Albanesi and S.T. Brady**. 1994. Molecular motors and cell motility in the brain. Brain Pathol. 4:167-179.
62. **Meza, G., A. Carabez and M. Ruiz**. 1982. GABA synthesis in isolated vestibulary tissue of chick inner ear. Brain Res. 241:157-161.
63. **Mohler, H., P. Schoch and J.G. Richards**. 1987. Structure and location of a $GABA_A$ receptor complex in the central nervoux system. J Recept Res. 7:617-628.
64. **Muller, C.M.** 1987. γ-Aminobutyric acid immunoreactivity in brainstem auditory nuclei of the chicken. Neurosci Lett. 77:272-276.
65. **Myers, P. and M. Bastiani**. 1993. Growth cone dynamics during the migration of an identified commissural growth cone. J Neurosc. 13:127-143.
66. **Nixon, R.** 1993. The regulation of neurofilament protein dynamics by phosphorylation: Clues to neurofibrillary pathobiology. Brain Pathol. 3:29-38.
67. **Nixon, R.A. and R.K. Sihag**. 1991. Neurofilament Phosphorylation - A New Look at Regulation and Function. Trends Neurosci. 14:501-506.
68. **Okabe, S., H. Miyasaka and N. Hirokawa**. 1993. Dynamics of the neuronal intermediate filaments. J Cell Biol. 121:375-386.
69. **Okazaki, K., N. Obata, S. Inoue and H. Hidaka**. 1995. S100ß is a target protein of neurocalcin β, and abundant isoform in glial cells. Biochem J 306:551-556.
70. **Oppenheim, R.W., Q.W. Yin, D. Prevette and Q. Yan**. 1992. Brain-Derived neurotrophic factor rescues developing avian motoneurons from cell death. Nature. 360:755-759.
71. **Parhad, I., J. Scott, L. Cellars, J. Bains, C. Krekoshi and A. Clark**. 1995. Axonal atrophy in aging is associated with a decline in neurofilament gene expression. J Neurosc Res. 41:355-366.
72. **Patterson, P.** 1995. Neuronal growth and differentiation factors and synaptic plasticity, p. 619-629. In Bloom, F. and Kepfer D. (Ed.). Psychophamarcology: The fouth generation of progress. Raven Press, NY.
73. **Posmantur, R., R.L. Hayes, C.E. Dixon and W.C. Taft**. 1994. Neurofilament 68 and neurofilament 200 protein levels decrease after traumatic brain injury. J Neurotrauma. 11:533-545.
74. **Raphael, Y., G. Marshak and A. Barash, et al**. 1987. Modulation of intermediate-filament expression in developing cochlear epithelium. Differentiation. 35:151-162.
75. **Reiderer, B. and I. Barakat-Walter**. 1992. Differential distribution of two microtubule-associated proteins, MAP2 and MAP5, during chick dorsal root ganglion development in situ and in culture. Develop Brain Res. 68:111-123.
76. **Rose, J.E., H.M. Sobkowicz and B. Bereman**. 1977. Growth in culture of the peripheral axons of the spiral neurons in response to displacement of the receptors. J Neuroctyol. 6:49-70.
77. **Saidel, W., J. Presson and J. Chang**. 1990. S-100 immunoreactivity identifies a subset of hair cells in the utricule and saccule of a fish. Hear Res. 47:139-146.
78. **Schäfer, B. and C. Heizmann**. 1996. The S100 family of EF-hand calcium-binding proteins: Functions and pathology. TIBS. 21:134-140.
79. **Schwartz, M.L., P.S. Shneidman, J. Bruce and W.W. Schlaepfer**. 994. Stabilization of neurofilament transcripts during postnatal development. Mol Brain Res. 27:215-220.
80. **Sheng, J., R. Mrak and W. Griffin**. 1994. S100ß protein expression n Alzheimer disease: Potential role in the pathogenesis of neuritic plaques. J Neurosci Res. 39:398-404.
81. **Sobue, K.** 1993. Actin-based cytoskeleton in growth cone activity. Neurosci Res. 18:91-102.
82. **Takahashi, A., M. Mizutani and C. Itakura**. 1995. Acrylamide-induced peripheral neuropathy in normal and neurofilament-deficient japanese quails. Acta Neuropathol. 89:17-22.
83. **Tsukita, S. and H. Ishikawa**. 1981. The cytoskeleton in myelinated axons: serial section study. Biomed Res. 2:424-437.
84. **Usami, S., J. Hozawa, H. Shinkawa, S. Saito, A. Matsubara and S. Fujita**. 1993. Immunocytochemical localization of intermediate filaments in the guinea pig vestibular periphery with special reference to their alteration after ototoxic drug administration. Acta Oto-Laryngol. Suppl. 506:7-13.
85. **Usami, S., J. Hozawa, M. Tazawa, M. Igarashi, G.C. Thompson, J.Y. Wu and R.J. Wenthold**. 1989. Immunocytochemical study of the GABA system in chicken vestibular endorgans and the vestibular ganglion. Brain Res. 503:214-218.
86. **Usami, S.-I., M. Igarashi and G.C. Thompson**. 1987. GABA-like immunoreactivity in the squirrel monkey vestibular endorgans. Brain Res. 417:367-370.
87. **Usami, S.-I., H. Shinkawa, Y. Inoue, J. Kanzaki and M. Anniko**.

1995. Calbinding-28K localization in the primate inner ear. ORL. 57:94-99.

88. **Usami, S.I., J. Hozawa, H. Shinkawa, M. Tazawa, H. Jin, A. Matsubara, S. Fujita and J. Ylikoski**. 1993. Immunocytochemical localization of Substance-P and neurofilament proteins in the guinea pig vestibular ganglion. Acta Oto-Laryngol. Suppl. 503:127-131.
89. **Vallee, R.B. and G.S. Bloom**. 1991. Mechanisms of fast and slow axonal transport. Ann Rev Neurosci. 14:59-92.
90. **Veenman, C.L., R.L. Albin, E.K. Richfield and A. Reiner**. 1994. Distributions of $GABA_A$, $GABA_B$, and benzodiazepine receptors in the forebrain and midbrain of pigeons. J Comp Neurol. 344:161-189.
91. **von Bartheld, C., R.A. Code and E.W. Rubel**. 1989. GABAergic neurons in brainstem auditory nuclei of the chick: distribution, morphology, and connectivity. J Comp Neurol. 287:470-483.
92. **Von Bartheld, C.S., S.L. Patterson, J.G. Heuer, E.F. Wheeler, M. Bothwell and E.W. Rubel**. 1991. Expression of nerve growth factor (NGF) receptors in the developing inner ear of chick and rat. Development. 113:455-470.
93. **Whitlon, D.S. and H.M. Sobkowicz**. 1989. GABA-lLike immunoreactivity in the cochlea of the developing mouse. J neurocytol. 18:505.
94. **Yamasaki, H., G.S. Bennett, C. Itakura and M. Mizutani**. 1992. Defective expression of neurofilament protein subunits in hereditary hypotrophic axonopathy of quail. Lab Invest. 66:734-743.
95. **Yin, H. and M. Mim**. 1995. Distribution of non-phosphorylated and phosphorylated neurofilament proteins in the spinal cord of an anuran amphibian during development and regeneration. Exp Brain Res. 104:409-418.
96. **Yin, H.-S. and Y.-J. Lee**. 1994. Heterogeneity and differential expression of the ?-Aminobutyric $Acid_A$ ($GABA_A$)/benzodiazepine receptor in the avian brain during development. Cell Mol Neurobiol. 14:359-371.
97. **Ylikoski, J., U. Pirvola and O. Happola**. 1993. Characterization of the vestibular and spiral ganglion cell somata of the rat by distribution of neurofilament proteins. Acta Oto-Laryngol. 121-126.
98. **Zhao, J.X., A. Ohnishi, C. Itakura, M. Mizutani, T. Yamamoto, H. Hayashi and Y. Murai**. 1994. Greater number of microtubules per axon of unmyelinated fibers of mutant quails deficient in neurofilaments - possible compensation for the absence of neurofilaments. Acta Neuropathol. 87:332-336.
99. **Zhao, Y.G. and B.G. Szaro**. 1994. The return of phosphorylated and nonphosphorylated epitopes of neurofilament proteins to the regenerating optic nerve of xenopus laevis. J Comp Neurol. 343:158-172.
100. **Zheng, J., R.E. Buxbaum and S.R. Heidemann**. 1993. Investigation of microtubule assembly and organization accompanying Tension-Induced neurite initiation. J Cell Sci. 104:1239-1250.
101. **Zimmer, D., E. Cornwall, A. Landar and W. Song**. 1995. The S100 protein family: History, function, and expression. Brain Res Bull. 37:417-429.

Address correspondence to:

C. D. Fermin
Tulane University School of Medicine
Department of Pathology & Laboratory Medicine
1430 Tulane Avenue/SL79
New Orleans LA 70112-2699
Phone 504/584-2521
Fax 504/587-7389
E-Mail: Fermin@tmc.tulane.edu
Web: http://www.tmc.tulane.edu/ferminlab

[PSN049][27 Jan 1998][2:40 p.m.] [D][1] p. 1

Prim. Sensory Neuron, Vol. 0, No. 0, pp. 1–22 (1998)

IN PRESS !

Chicken (*Gallus domesticus*) inner ear afferents

HIROTAKA HARA,[1] XIANGDONG CHEN,[2] JERSHONDA F. HARTSFIELD,[3] JUN HARA,[1] DALE MARTIN[1] and CESAR D. FERMIN[1,*]

[1]*Department of Pathology & Laboratory Medicine, Tulane University, New Orleans, LA 70112-2699, USA*
[2]*Department of Otolaryngology, The Second Hospital of Henan Medical University, Zhengzhou, Henan, PRC*
[3]*MedRep Program, Tulane Medical School, New Orleans, LA ???-???, USA*

Au: place, supply

Abstract—Neurons from the vestibular (VG) and the statoacoustic (SAG) ganglion of the chick (*Gallus domesticus*) were evaluated histologically and morphometrically. Embryos at stages 34 (E8 days), 39 (E13 days) and 44 (E18 days) were sacrificed and temporal bones microdissected. Specimens were embedded in JB-4 methacrylate plastic, and stained with a mixture of 0.2% toluidine blue (TB) and 0.1% basic Fuschin in 25% ethanol or with a mixture of 2% TB and 1% PDA for axon and myelin measurement study. Images of the VIIIth nerve were produced by a V150® color imaging system and the contour of 200–300 neuronal bodies (perikarya) was traced directly on a video screen with a mouse in real time. The cross-sectional area of VG perikarya was 67.29 μm^2 at stage 34 (E8), 128.46 μm^2 at stage 39 (E13) and 275.85 μm^2 at stage 44 (E18). The cross-sectional area of SAG perikarya was 62.44 μm^2 at stage 34 (E8), 102.05 μm^2 at stage 39 (E13) and 165.02 μm^2 at stage 44 (E18). A significant cross-sectional area increase of the VG perikarya between stage 39 (E13) and stage 44 (E18) was determined. We randomly measured the cross-sectional area of myelin and axoplasm of hatchling afferent nerves, and found a correspondence between axoplasmic and myelin cross-sectional area in the utricular, saccular and semicircular canal nerve branches of the nerve. The results suggest that the period between stage 34 (E8) and 39 (E13) is a critical period for afferent neuronal development. Physiological and behavioral vestibular properties of developing and maturing hatchlings may change accordingly. The results compliment previous work by other investigators and provide valuable anatomical measures useful to correlate physiological data obtained from stimulation of the whole nerve or its parts.

Keywords: VIIIth nerve; development; perikarya; axoplasm; myelin; immunohistochemistry; morphometry.

1. INTRODUCTION

Even though transduction of mechanical energy into neural signals is mandatory for perception of head acceleration and sound, transmission of the signal from the inner

*To whom correspondence should be addressed.

ear to the brain stem must take place for organisms to successfully stay tuned to their environments. Recent work on the organization of the afferent neurons of the VIIIth nerve suggests that the more recent type I hair cells characteristic of birds and mammals, and not present in older vertebrates, added an additional level of complexity to vestibular functioning (Goldberg, 1991). The diversity of afferent morphology observed previously by others since the initial ultrastructural descriptions of the vestibular nerve appeared (Engström *et al.*, 1966; Hamilton, 1968; Ballantyne and Engström, 1969; Bergström, 1973a–c) suggests that vestibular afferents acquire distinct phenotypes that impart to them specific antigenic identity (Fermin and Martin, 1995; Fermin *et al.*, 1997). Expression of neurotrophic molecules such as S100β in selected groups of vestibular neurons may influence their repair and survival after partial deafferentation (Richter, 1981a, b; Fermin and Igarashi, 1984; Fermin *et al.*, 1989).

The phenotypic variability of vestibular perikarya may also be related to their regular and irregular discharge characteristics. The outstanding work from Goldberg and collaborators in rodents and primates clearly showed that perikarya innervating type I hair cells in the central portion of the crista have irregular discharge, whereas those in the periphery innervating mostly type II hair cells have regular discharge (Goldberg, 1981, 1991; Highstein *et al.*, 1987; Baird *et al.*, 1988; Fernández *et al.*, 1988, 1995; Goldberg *et al.*, 1990c; Boyle *et al.*, 1992; Lysakowski *et al.*, 1992).

The phenotypic heterogeneity of afferents and their functional diversity is probably related to innervation patterns of the peripheral dendrites contacting the hair cells. Moreover, there seems to be a differential expression of antigenic markers in different portions of the end organs where different types of hair cells are located (Meza *et al.*, 1982, 1992; Didier *et al.*, 1990; Lopez *et al.*, 1990, 1992; Wackym *et al.*, 1993; Ylikoski *et al.*, 1993; Fermin and Martin, 1995; Fermin *et al.*, 1997). The afferent innervation diversity starts early in development, and, at least in rodents, terminal mitosis leads to cell specialization that varies among linear and angular detecting organs. In the macula, older cells are located in the striola where most of the type I hair cells are located (Sans and Chat, 1982) and receive chalice endings from large diameter afferents. Since older species do not have true type I hair cells (Drescher *et al.*, 1989; Boyle *et al.*, 1991; Guth *et al.*, 1994), one may speculate that type II hair cells are phylogenetically older, but this has not been proven. Regardless of the significance of hair cell position along the evolutionary tree, in those species with non-true type I hair cells and lacking true chalice endings, afferent morphological diversity and functional variation exists (Honrubia *et al.*, 1981, 1984, 1985; Boyle *et al.*, 1991, 1992). Moreover, it seems that afferents innervating type I hair cells could be potentially regulated locally in the end organs of birds (Peusner *et al.*, 1988) and have mixed type synaptic contacts (Yamashita and Ohmori, 1991). Regardless, transmission of information from the hair cell to the nerve endings probably occurs through the release of neurotransmitters (Sans *et al.*, 1994) giving these cells a 'distributed modifying' rather than a 'channeled' pattern of innervation (Ross *et al.*, 1991).

Despite obvious morphological differences between avian and mammalian inner ear, the organization of the afferents is similar except for the central interconnections of several brain stem nuclei (Wold, 1975, 1976, 1981; Correia *et al.*, 1983; Cox

and Peusner, 1990a–c) and it is highly likely that peripheral to central connections in mature birds share similar features with mature mammals (Brodal *et al.*, 1962; Highstein and Mccrea, 1988; Gacek *et al.*, 1989; Newman *et al.*, 1992). We thus designed this study to fill in the gap left behind by previous studies and to establish normative data for chicken similar to data already established for the monkey (Fermin and Igarashi, 1982, 1987).

Previous analyses of the chick embryo VIIIth nerve demonstrated increased surface areas of the perikarya and axons (Ard and Morest, 1984) between E7 and hatching, and showed that cochlear neurons of chicken differ significantly from vestibular neurons. Other studies showed increased myelin lamellae thickness during critical periods of myelination (Fermin and Cohen, 1984a) and ultrastructural refinement of the inner ear epithelia (Fermin and Cohen, 1984b). These and other studies of avian afferents did not correlate the increase of axonal diameter with myelin thickness. For instance, Landolt *et al.* (1973) determined an average 8720 perikarya in the vestibular nerve of pigeon, and estimate that was later corroborated by Ard and Morest (1984) during development and Fischer *et al.* (1994) in adult chickens. This last work also showed that lagenar afferents have morphological characteristics that are indistinguishable from true vestibular afferents. Moreover, lagenar fibers (Jorgensen, 1970) peripheral to the ganglion are homogeneous in diameter, whereas vestibular fibers are not. The homogeneous organization of auditory afferents could be related to the relative equidistance that exists between the auditory perikarya and the auditory hair cells in the basilar papilla (Takasaka and Smith, 1971). In the vestibule where different end organs are located at different distances from the ganglion, fiber diameter may be another important variable that influences the functional attributes of each region. In fact, despite interspecies differences (i.e. amphibian–rodent–human) large myelinated fibers are generally located in the center of the organs where directionality (Wersäll *et al.*, 1965) affects receptor depolarization the greatest (Lewis *et al.*, 1985). The macula lagena hair cells are organized in striolar and extrastriolar regions in such a manner that movement of the bird head in flight could affect the sensitivity of the utricle (Jorgensen, 1970), but such an idea has not been investigated behaviorally or functionally. Finally, fiber diameter was previously correlated with myelin sheet thickness (Smith *et al.*, 1982; Friedrich and Mugnaini, 1983; Guy *et al.*, 1989a, b; Fraher *et al.*, 1990) and cytoskeletal proteins (Fermin *et al.*, 1997), and shown to influence axoplasmic diameter (Muma *et al.*, 1991; Dewaegh *et al.*, 1992; Sakaguchi *et al.*, 1993; Hsieh *et al.*, 1994; Zhao *et al.*, 1994).

Evidence exists that chickens are excellent models to evaluate vestibular function. The avian inner ear membranous structures are well characterized (Bissonenette and Fekete, 1995), chicken eyes convergence corresponds to frontal binocular fixation (Martinoya *et al.*, 1984), chickens have static and stato-kinetic reflexes also described in mammals (Kleitman and Koppanyi, 1926), and develop nystagmus upon rotatory stimulation (Winget and Smith, 1962). In addition, non-invasive far-field recording of short latency response to study functional responses of cochlear (Jones *et al.*, 1987; Jones and Jones, 1995a, b) and vestibular afferents (Jones and Pedersen, 1989; Jones and Schiltz, 1989; Jones, 1992) were employed successfully.

Due to the above properties of the afferent vestibular innervation we considered it important to characterize the nerve fibers in each branch of the vestibular nerve and to compare the cross-sectional area of the myelin and axoplasm. In the present study we corroborated previous morphometric parameters of the embryonic VIIIth nerve and compared the cross-sectional areas of the perikarya of the auditory (SAG) and vestibular ganglia (VG). These comparisons are necessary because myelin thickness influences speed of conduction (Sakaguchi *et al.*, 1993). Moreover, it was previously shown that refinement of the inner ear epithelia occurs at those critical developmental stages we chose for analysis. The data presented suggests the following. (a) Stages 34–39 (E8–E13 embryonic days) mark a very important critical period of development for the afferent innervation of the inner ear. (b) Afferent neuron cross-sectional area increases significantly after stage 39 (E13). (c) Perikarya nuclear and cytoplasmic cross-sectional area increase is gradual and proportional. (d) Axonal cross-sectional area is proportional to myelin cross-sectional area of the same fibers in each branch of the vestibular nerve, but myelin thickness to the posterior crista is significantly larger. (e) Perikaryal diversity seems greatest in the VG as compared to the SAG. The diversity was demonstrated with histological and with calcium binding proteins immunostains.

2. METHODS

2.1. Animals

White leghorn (*Gallus domesticus*) fertile eggs were used. All experiment were approved by the Tulane Medical School Advisory Committee for Animal Resources (ACAR). Eggs were incubated in a rotating, forced-draft incubator at 37°C and 90% humidity. Embryos were fixed by immersion with 10% neutral buffered formalin or 3% biological grade glutaraldehyde. Hatchlings were fixed by perfusion of the fixative through the heart after saline rinse of the blood. Tissues were kept in the same fixative until used. Embryonic stages were determined by staging the embryos according to the classification of Lille (Hamilton, 1952).

2.2. Tissue preparation

Samples were dehydrated in ascending alcohol concentrations from 50 to 100% and embedded in JB-4 methacrylate plastic. The tissues were cut at 5 μm thickness afixed to glass slides and stained with a mixture of 0.2% toluidine blue O (TB) and 0.1% basic Fuschin (BF) in 25% ethanol for perikarya measurement study and stained with a mixture of 2% TB and 1% PDA for axon and myelin measurement study. Sections can either be floated in warm water and picked up on glass slides, or placed on a drop of water on the glass slide and allowed to stretch. For perikarya measurement study, the sections were stained by quickly dipping them for 1–3 s into a Coplin jar with freshly filtered solution. Over-stained sections were destained by washing in running tap water for as long as needed with frequent observation under a microscope.

Deeply stained sections were destained with 1% glacial acetic acid. The differentiation between the blue TB and the red BF can be altered by varying concentrations and proportions of the dyes. Sections were dried by air drying or by placing them on a plate warmer and cover slipped with Permount when cooled.

2.3. Computerized morphometry

Stained slides were placed on an Olympus BH2 light microscope and the images of the neurons viewed in real time on a color monitor screen with a V150® (Oncor) color imaging system. The screen distance was calibrated for each objective and the features of interest traced with the mouse directly on the color screen (Fermin and DeGraw, 1995). The resulting measures were stored to an ASCII file and the average (mean and SD) of the measures printed to a screen. Values were stored as ASCII and analyzed with StatMost for Windows, StatView or InStat for the Macintosh and plotted with either StatMost or KaleidaGraph for the Macintosh.

2.4. Immunohistochemistry

To examine the expression pattern of S100β and calretinin on vestibular and statoacoustic ganglia, we used procedures similar to those already published (Fermin and Martin, 1995; Fermin *et al.*, 1997). Briefly: all incubations were done at room temperature in a humidity chamber with Tris buffer rinse in between: (1) 20 min in 1% hydrogen peroxide; (2) 10% goat serum for 20 min; (3) primary anti-S100β rabbit IgG diluted 1 : 4000 or primary anti-calretinin IgG diluted 1 : 200 in 2% bovine serum albumin–Tris (BSA–TMC/HCl) buffer for 18 h; (4) biotinylated goat-anti-rabbit IgG for 30 min; (5) streptavidin–horseradish peroxidase (Biogenex Laboratories, Location?, CA) for 30 min; (6) 3′,3′-diaminobenzidine tetrahydrochloride (DAB) for 5 min or 3-amino-9-ethylcarbazole (AEC); (7) counterstain in hematoxylin.

3. RESULTS

Development of peripheral auditory and vestibular neurons of the chick is characterized by a noticeable morphological change immediately after temporary synapses form. At stage 34 (E8) when the end organs are immature, afferent synapses are forming, myelination is just beginning and efferent fibers are scarce, perikarya in both ganglia are almost identical (Figs 1 and 2). Perikarya and Schwann cells are tightly packed and distinction between the two is difficult. A prominent nucleolar complex is apparent in the perikarya of both ganglia. By stage 39 (E13), however, the vestibular perikarya are larger (Figs 3 and 4), there is no myelin surrounding the perikarya, the cytoplasmic to nuclear ratio remains constant, and the separation between perikarya and Schwann cells is still difficult with the stain used. At stage 39 (E13) afferent temporary synapses are being replaced by permanent afferent synapses and the efferent terminals are common inside the epithelia. By stage 44 (E18), myelin surrounds both the axons and the perikarya (Figs 5 and 6) indicating that the neurons are ready for function. Table 1 shows that the greatest change in cross-sectional area

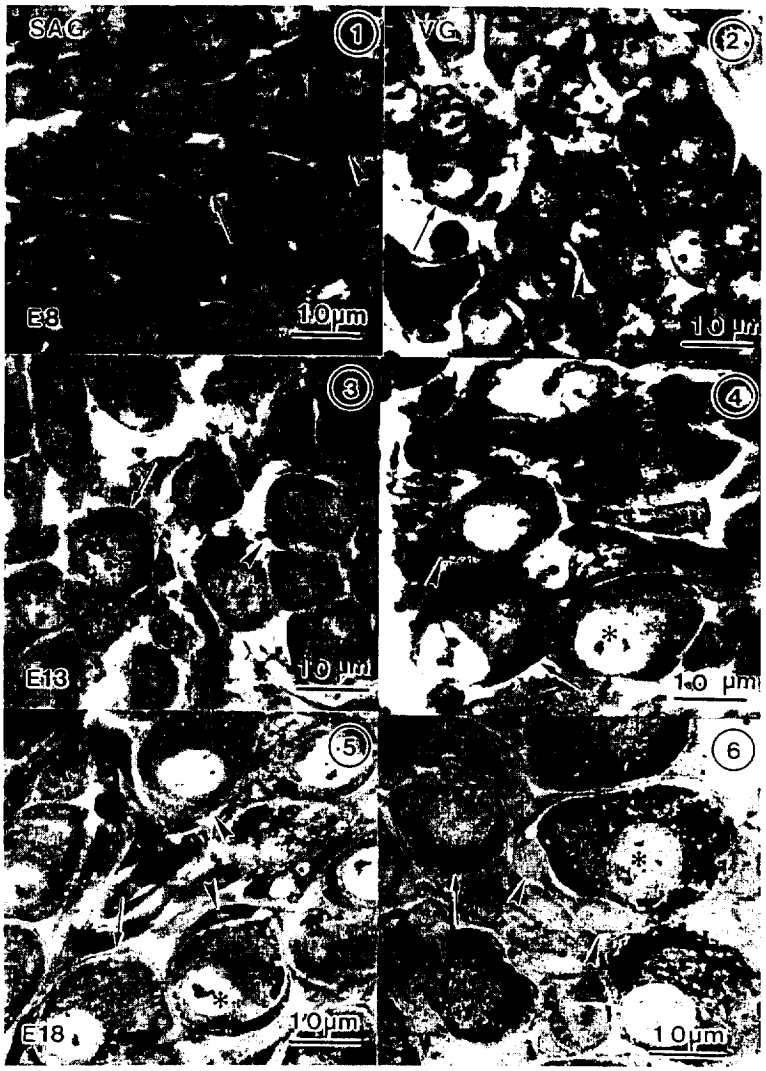
SAG
1
E8
1.0μm
VG
2
1.0 μm
3
E13
1.0 μm
4
1.0 μm
5
E18
1.0μm
6
1.0μm

and probably in volume of the perikarya occurs after stage 39 (E13), and it is greatest near hatching when the chick must be able to balance and walk. The greatest change in nuclear diameter takes place after stage 39 (E13) (Table 2) and peaks near hatching when the ratio of nuclear over perikaryal cross-sectional area was 0.35.

In newly hatched chicks the cross-sectional area of axon and myelin peripheral to the ganglion of the VIIIth nerve yielded a heterogeneity of fiber size in each vestibular branch (Figs 7–11). The cross-sectional area of the peripheral auditory fibers traveling

Table 1.
Mean cross-sectional area and perimeter of perikarya in the statoacoustic and ganglion neurons

Stage	Ganglion	Number measured	Mean area ± SD (μm^2)	Mean perimeter ± SD (μm)
34	SA	750	62.44 ± 15.03	30.65 ± 3.84
34	V	750	67.29 ± 17.73	31.77 ± 4.33
39	SA	250	102.05 ± 20.83	39.12 ± 4.43
39	V	250	128.46 ± 57.47	43.15 ± 9.07
44	SA	750	165.02 ± 56.39	49.58 ± 8.64
44	V	750	275.85 ± 103.39	64.99 ± 12.36

Table 2.
Mean cross-sectional area and perimeter of nuclei in the statoacoustic and vestibular ganglion neurons

Stage	Ganglion	Number measured	Mean area ± SD (μm^2)	Mean perimeter ± SD (μm)
34	SA	150	33.47 ± 6.07	21.73 ± 1.86
34	V	150	33.65 ± 9.10	21.80 ± 2.84
39	SA	50	40.06 ± 8.62	24.10 ± 2.47
39	V	50	54.08 ± 13.61	27.62 ± 3.28
44	SA	150	71.19 ± 19.64	31.07 ± 4.25
44	V	150	88.66 ± 32.33	35.15 ± 6.02

Composite I. Cross-sectional area of perikarya from the VG and the (auditory) SAG at E8, E13 and E18. **Figure 1.** SAG neuron during stage 34 (E8 days of incubation). Neurons are indistinguishable from each other (arrow), have prominent nuclei (asterisk) and are difficult to distinguish from Schwann cells (arrowheads). **Figure 2.** VG neuron from the same embryo as Fig. 1 showing that there is very little difference between VG and SAG neurons. **Figure 3.** By stage 39 (E13) packing of the perikarya in the SAG ganglionic matrix is looser, perikaryal (arrow) size increased and Schwann cells are difficult to distinguish from neurons (arrowhead). **Figure 4.** By stage 39 (E13) VG neurons (arrow) cross-sectional area is larger than SAG neurons and the cytoplasmic to nuclear (asterisk) ratio changes. Schwann cells (arrowhead) are still difficult to separate from the ganglionic matrix background. **Figure 5.** By stage 44 (E18) SAG neurons (arrow) have acquired about the size of stage 39 (E13) VG neurons (see Fig. 4), Schwann cells are clearly separated from the perikarya (arrowheads) and the nucleolar complex remains prominent (asterisk). **Figure 6.** VG perikarya (arrow) are clearly separated from Schwann cells (arrowheads) and the nuclear (asterisk) to cytoplasmic ratio changes considerably by stage 44 (E18). Note that the Nissl substance occupies a large portion of the cytoplasm and that its amount is larger in the VG than in the SAG neurons of Fig. 5.

Composite II. Cross-sectional area of fibers from each branch of the VG and SAG. **Figure 7.** Cross-section of myelinated afferent fibers from the peripheral branch of the utricular nerve with mixed large (arrowhead) and small diameter fibers (arrow). Some bundles contain large and small fibers whereas other (arrow) contain mainly small diameter fibers. **Figure 8.** Fibers from the saccular vestibular nerve branch contain large (arrowhead) and small (arrow) diameter fibers with little bundle organization and abundant ganglionic matrix. **Figure 9.** Fibers from the superior vestibular nerve branch contain more large (arrowhead) than small diameter fibers (arrow). A blood capillary (B) is shown. **Figure 10.** Fibers of the posterior vestibular branch are mixed in almost similar manner as those of the superior division, but myelin thickness is significantly larger (arrowhead) in larger than in thin fibers (arrow). **Figure 11.** Large (arrowhead) and small (arrow) fibers of the horizontal (lateral) vestibular branch are mixed in not well seggregate bundles. The large diameter fibers have, similar to those from the posterior branch, thicker myelin sheets. **Figure 12.** The fibers of the auditory basilar papilla are remarkably homogeneous in axoplasmic and myelin thickness cross-sectional area (arrows) and bundles are well segregated.

Table 3.
Mean of axon, myelin and axon/myelin cross-sectional area

Nerve branch	Axon ± SD (μm^2)	Myelin ± SD (μm^2)	Axon/myelin ± SD
Utricular nerve	2.045 ± 0.266	5.848 ± 0.602	0.495 ± 0.222
Saccular nerve	1.878 ± 0.19	6.186 ± 0.485	0.502 ± 0.269
Superior SC nerve	2.148 ± 0.211	7.349 ± 0.675	0.436 ± 0.182
Posterior SC nerve	4.007 ± 0.435	11.489 ± 1.017	0.538 ± 0.481
Horizontal SC nerve	3.182 ± 0.419	8.729 ± 0.872	0.466 ± 0.276
Auditory nerve	1.371 ± 0.707	2.351 ± 0.836	0.578 ± 0.205

SC, semicircular canal.

from the stato-acoustic ganglion toward the hair cells was homogeneous (Fig. 12). Large and small diameter fibers in all vestibular branches of the nerve were mingled

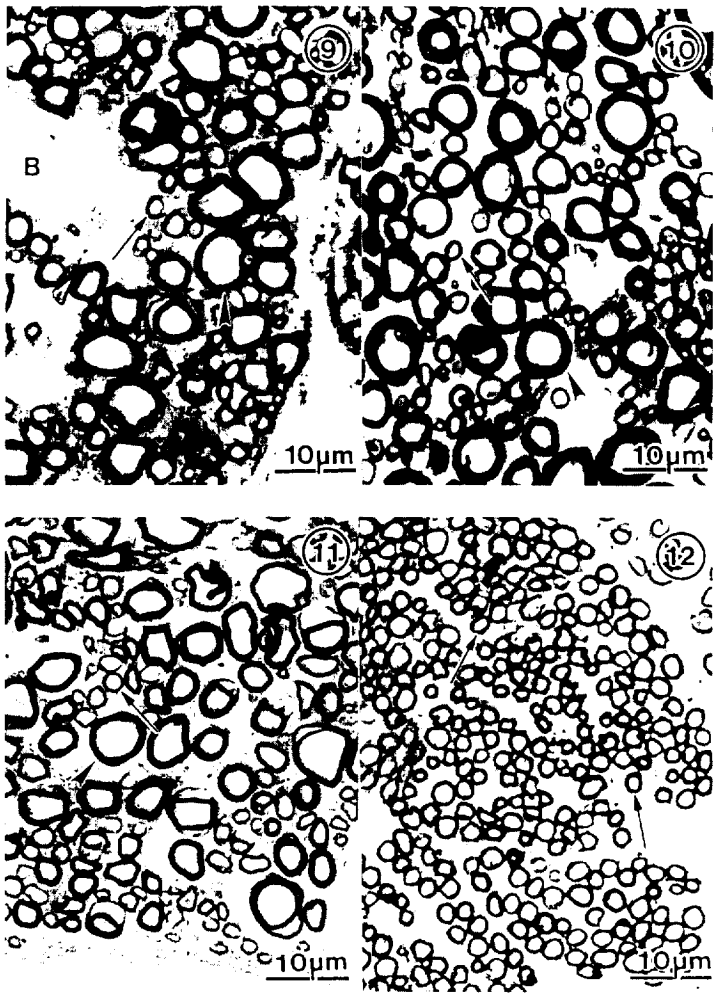

Composite II. (Continued).

and there was no clear bundle arrangement according to size (Figs 7–11), whereas in the auditory nerve fiber size and grouping were homogeneous (Fig. 12).

The morphological characteristics of the SAG and VG perikarya and fibers may reflect differential innervation pattern of the maculae and cristae central and periph-

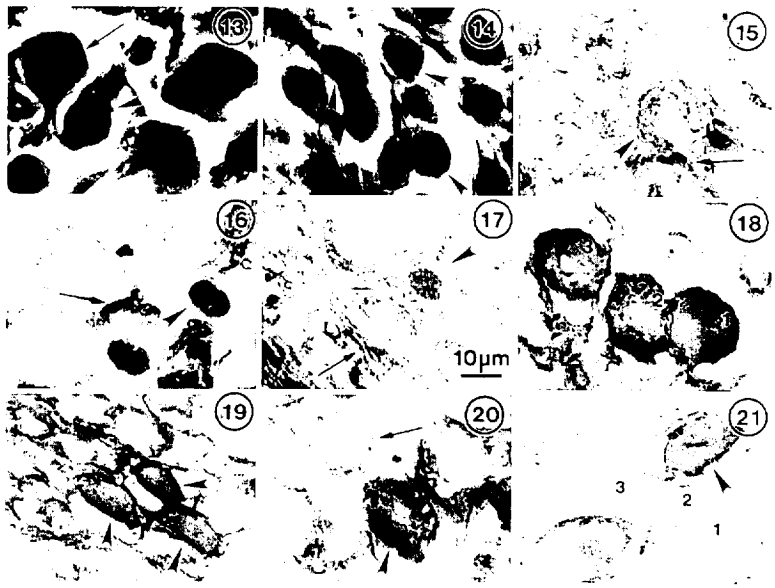

Composite III. Color montage of vestibular and auditory neurons stained with polychrome (Figs 13 and 14) and immunohistochemically for two calcium binding proteins (Figs 15–21). Magnification is the same in Figs 13–21 and indicated by a calibrate bar in Fig. 17. **Figure 13.** At least two distinct types of vestibular perikarya are apparent with polychrome stain: large (arrow) green neurons and yellow to red smaller (arrowhead). **Figure 14.** Auditory neurons appear to stain yellow to red, and are appear homogeneous in shape and size (arrowheads). **Figure 15.** When stained for S100β, a calcium binding and neurotrophic protein, SAG perikarya display only diffuse stain over the cytoplasm (arrowhead) and over myelin (arrow) which serves as a built-in positive control. **Figure 16.** The nuclei of certain VG perikarya express the S100β (arrow). Myelin stain (arrow) serves as a built-in positive control. **Figure 17.** Perikarya from the macular lagena nerve branch, which runs together with the SAG expressed the protein in their nuclei (arrowhead) more distinctly than the SAG perikarya. Myelin stain (arrow) serves as a built-in positive control. **Figure 18.** Double immunostaining of VG for anti-S100β (red) and anti-calretinin (brown) yields two distinct groups of perikarya. Perikarya 1 expressed more S100β than perikarya 2 and 3. **Figure 19.** SAG perikarya from the same nerve as Fig. 18 expressed both molecules equally (arrowheads). **Figure 20.** Lagenar perikarya (arrowhead) expressed the proteins like VG perikarya (see Fig. 18) and some perikarya did not express these proteins at all (arrow). **Figure 21.** The expression of calretinin alone over VG (arrowhead) neurons differs from the expression of S100β alone (see Fig. 16). Some neurons (1–3) did not express calretinin at all.

eral locations. VG and SAG perikarya have varying affinity for histological staining (Figs 13 and 14), a difference that goes hand in hand with their phenotypes and may be related to the differential immunostaining patterns of the perikarya in each ganglion. Well-characterized neuronal markers such as certain calcium binding proteins (Fermin and Martin, 1995; Fermin *et al.*, 1997) are expressed differentially on SAG and VG, and the expression varies in different portions of each ganglion. With anti-S100β

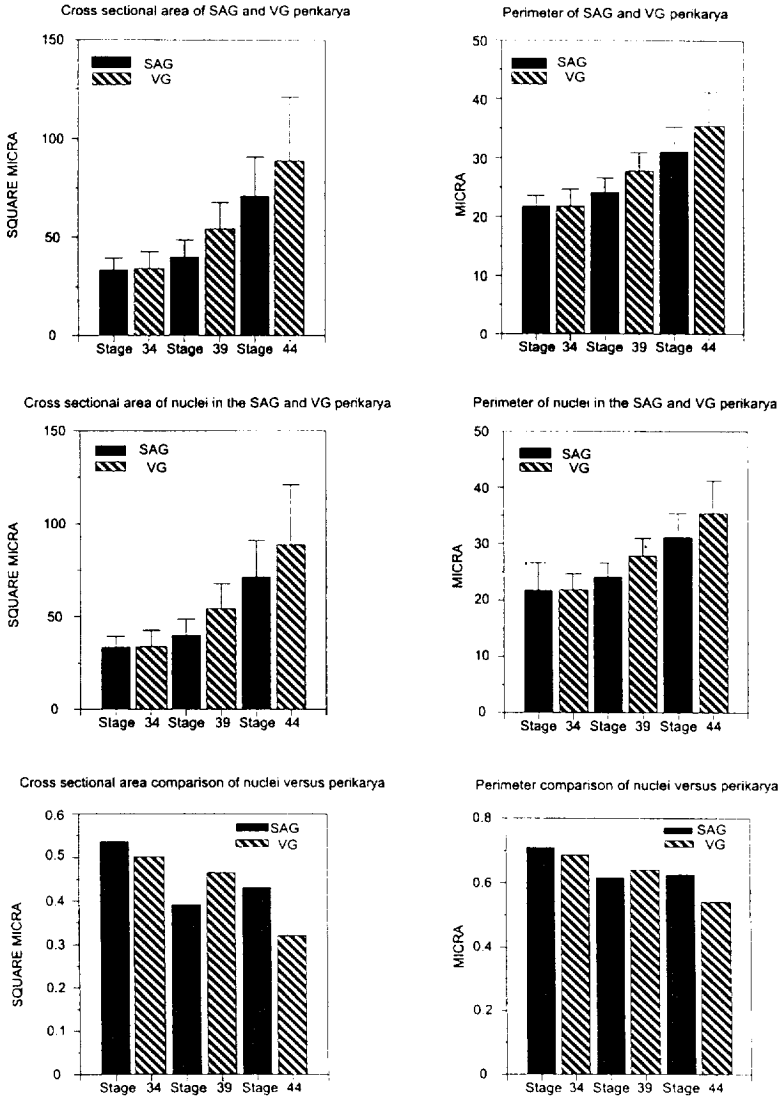

Figure 22. Cross-sectional area and perimeter of SAG and VG perikarya and nuclei. VG perikarya size increase surpass the SAG, but the nuclear size increase is proportional for perikarya in both ganglia.

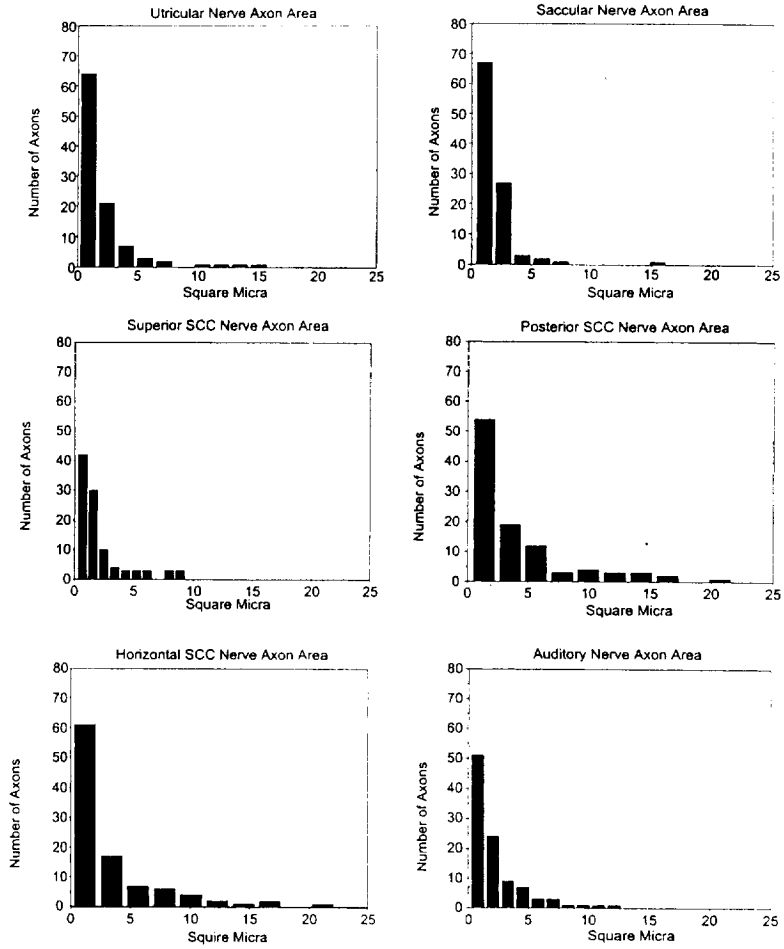

Figure 23. Cross-sectional area of axoplasm peripheral to the ganglia for each end organ and for the auditory nerve branch as comparison.

SAG perikarya stain in a diffuse manner (Fig. 15), whereas distinct groups of VG perikarya express the molecule in their nuclei only (Fig. 16). Neurons in the lagenar ganglion, which is assumed to be a vestibular structure, stain closer in appearance to VG than to SAG neurons (Fig. 17). When double immunostaining with anti-S100β and anti-calretinin, some VG groups of VG perikarya expressed both molecules and

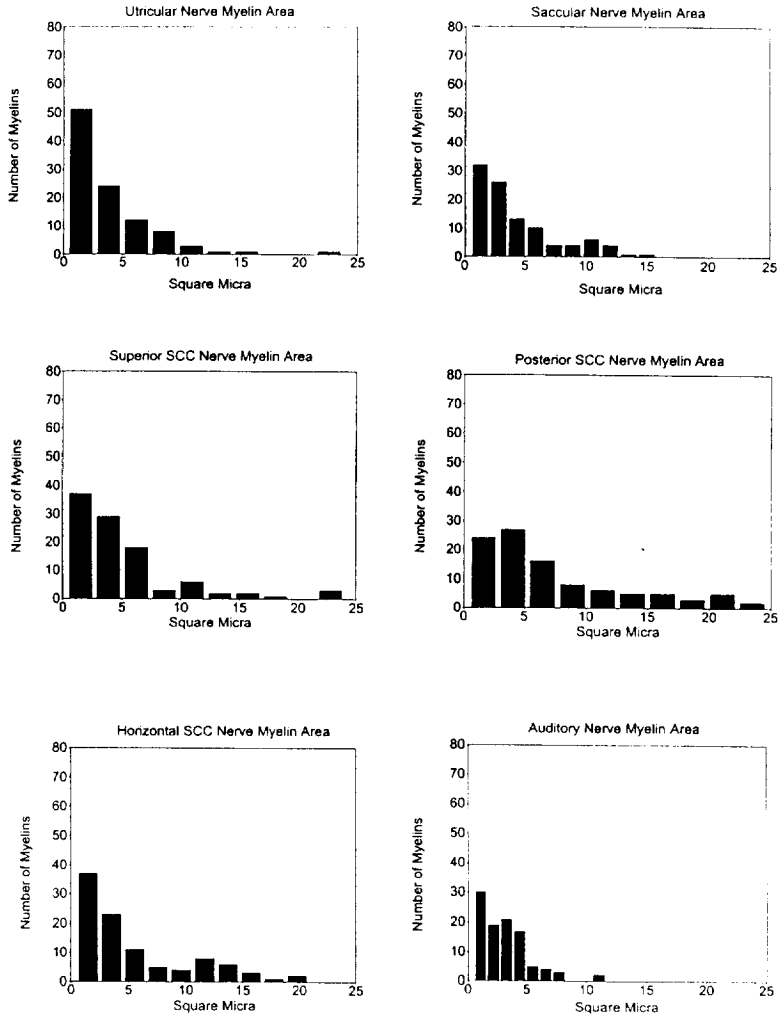

Figure 24. Cross-sectional area of myelin for those fibers shown in Fig. 23.

others did not (Fig. 18). In the same section SAG perikarya expressed both molecules differently (Fig. 19), and lagenar ganglion perikarya showed a propensity toward the VG pattern of stain rather than the SAG (Fig. 20). The expression of S100β over

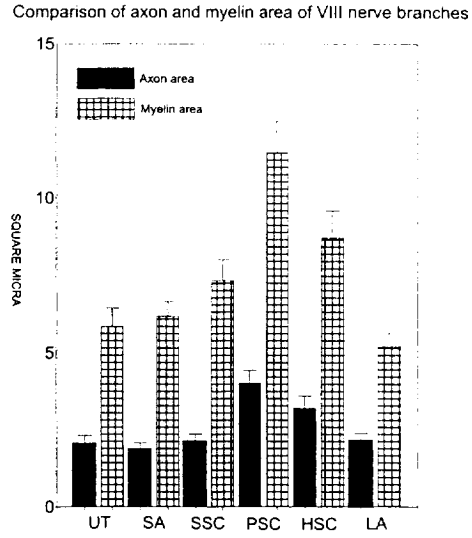

Figure 25. Comparison of cross-sectional area for axoplasm and myelin for each branch of the vestibular nerve peripheral to the ganglion. The axoplasms of fibers from the utricle (UT), saccule (SA), superior semicircular canal (SSC) and auditory or lagenar (LA) fibers were essentially similar. However, the axoplasm for the posterior semicircular canal (PSC) and horizontal (HSC) or lateral canal was larger as was the thickness of the myelin sheet around these fibers.

the nuclei of certain vestibular perikarya is unique (Fig. 16) and it differs from other calcium binding proteins. In the case of calretinin alone (Fig. 21) no specific nuclear stain over any perikarya was observed.

Morphometric measurements of the neurons at stages 34 (E8), 39 (E13) and 44 (E18) indicated a gradual increase of perikaryal and nuclear size that peaked near hatching (Fig. 22). Perikaryal size increase was not accompanied by shape deformation as evidenced by the proportional increase in perimeter. When Figs 1–6 were examined carefully there was a proportional increase in cytoplasm and nuclear size in neurons of both ganglia. The ratio of cytoplasmic to nuclear cross-sectional area changed but the changes were not skewed, an indication of smooth contour for neurons measured. The cross-sectional area of the axoplasm (Fig. 23) and myelin (Fig. 24) was skewed, and the distribution of fiber size followed almost identical patterns. When the raw data was compiled, the axoplasms of the utricular, saccular, superior crista and lagenar peripheral branch of the nerve shared very close values, but the posterior and horizontal crista fiber axoplasms were larger. Even though fibers appear first and are myelinated weeks later, myelin thickness, however, seemed to increase in proportion to axoplasmic diameter (Fig. 25). Figure 26 corresponds to linear regression plots of the cross-sectional areas of fibers for each branch of the vestibular nerve and the

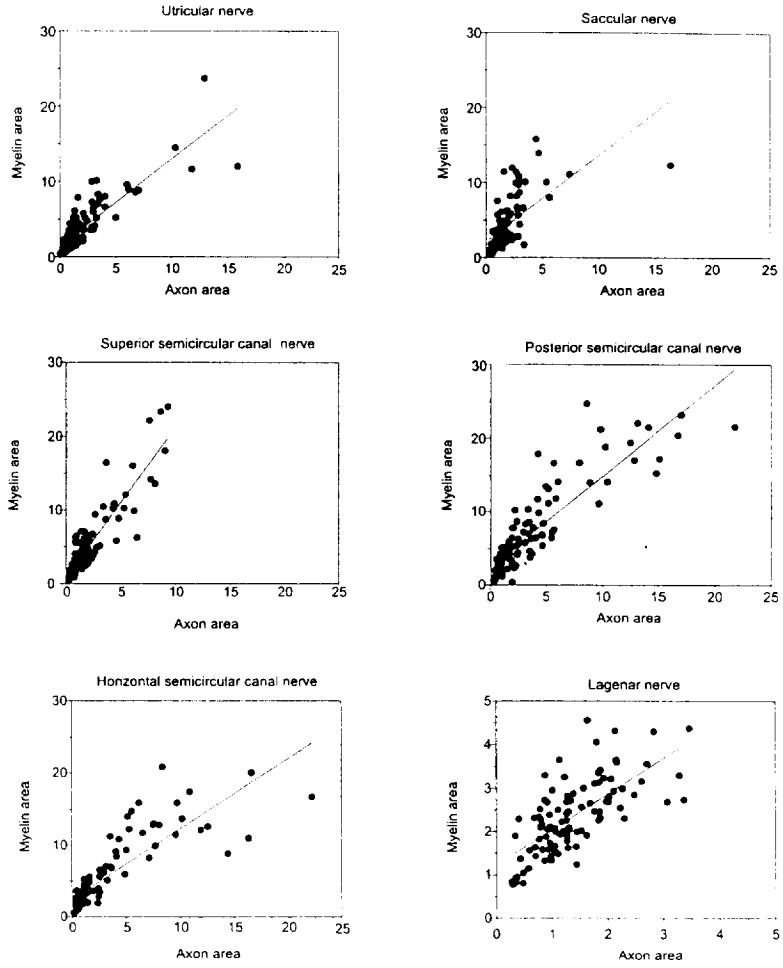

Figure 26. Correlation of axoplasm and myelin cross-sectional area for each branch of the vestibular nerve and auditory nerve as comparison. Note the scale difference on the lower right corner plot to accommodate the smaller auditory fibers.

basilar papilla nerve. These plots further corroborate that a proportional increase of axoplasm and myelin thickness takes place in the fibers of the VIIIth nerve even though fiber plus myelin thickness varies among its branches.

4. DISCUSSION

We designed the work presented because there is little information on the morphological characteristics of chick peripheral afferents that could be related to the well-known morphological and physiological diversity of mammalian afferents. Physiological and behavioral studies of function carried out by others in the past suggest that responses to vestibular inputs is greatly influenced by the end organ involved and hence the origin of the response (Brodal *et al.*, 1962; Gacek, 1980). It is established now that vestibular neurons fire at different rates (Fernández and Goldberg, 1971; Goldberg and Fernández, 1971; Fernández *et al.*, 1972; Goldberg *et al.*, 1990a, b; Boyle *et al.*, 1992) and respond to different tilts of the head and rotation of the body. It is also known that orientation (Wersäll and Lundquist, 1966; Lewis *et al.*, 1985) of vestibular receptors in the sensory epithelia greatly influences the response obtained from head tilt and/or body rotation (Fernández *et al.*, 1972; Baird and Lewis, 1986; Baird *et al.*, 1988; Meyers and Lewis, 1989). Moreover, chickens are now used extensively to measure vestibular evoked potentials non-invasively (Jones *et al.*, 1987; Jones, 1992), and the results may very well be influenced by the contributing end organs and branch of the nerve involved, because different diameter fiber and myelin thickness (Figs 7–12) would affect the speed of nerve conduction from the ear to the brain stem.

The present analysis of the chick afferents indicates that avian perikarya share similar morphological features with mammalian perikarya during development and near hatching (Figs 1–6). The characteristic Nissl substance abundance observed previously in mammalian vestibular perikarya is apparent in chicks even before hatching (Fig. 6). Such an increase in Nissl substance (polyribosomes) in the vestibular perikarya as compared to the auditory perikarya (Fig. 5) would suggest higher functional demand of the vestibular perikarya than auditory perikarya. The difference in protein synthesizing elements may in turn be related to constant demands on the vestibular perikarya to maintain body posture and muscle tone through tonic activity of the neurons. If this is correct, the survival advantage that vestibular neurons have demonstrated in several species after partial deafferentation (Igarashi *et al.*, 1970; Richter, 1981b; Ylikoski *et al.*, 1981; Fermin and Igarashi, 1984; Cass *et al.*, 1987; Fermin *et al.*, 1989; Gacek *et al.*, 1995) may also be related to differential molecular constituents in both neurons.

In fact, the expression of calcium binding proteins already characterized in Aves (Braun, 1990; Fermin and Martin, 1995) and mammals (Celio, 1986, 1990; Usami *et al.*, 1991) nervous system as reliable markers of neuronal bodies were expressed differently in auditory and vestibular perikarya (Figs 15 and 16). We suggested previously that S100β is probably one of several neurotrophic molecules with potential multiple functions in the inner ear (Fermin and Martin, 1995). We now know that the expression of S100β, GABA and GAD in the maculae of the chick is segregated along hair cell type I and II organization and types of innervation the cells receive (Fermin *et al.*, 1997). Morphological analysis of the mammalian utricle and saccule also showed similar segregation of hair cell type and it was related to discharge pattern characteristics of afferent neurons innervating each region (Goldberg, 1991).

Another interesting observation of the present study is that afferents innervating the lagenar macula display morphological, histochemical and immunohistochemical properties similar to true vestibular afferents rather than auditory afferents. Recent analysis of the lagenar macula afferents favors vestibular rather than auditory morphological and functional properties. Since the original observation of multiple type I hair cells surrounded by a single chalice (Jorgensen, 1970), it has been postulated that lagenar macula afferents may perform some vestibular function including additional detection of body torsion in flight. Indeed, a closer look at the morphological properties of the macula lagena indicates that its hair cells share many morphological properties with the saccule and utricle, particularly with the saccule, where it is not unusual to find up to 10 type I hair cells surrounded by a single chalice. In flight with head flexed dorsally, the hair cells of the lagena are arranged in such a pattern that would permit this organ to activate some cells regardless of the body torsion or flexion (Jorgensen, 1970). Thus, our observation of immunostaining afferents similar to true afferents supports the notion that afferents in the lagenar macula are probably derived from the same source and/or share antigenic properties (Fermin *et al.*, 1997).

The cross-sectional area of fibers differs in each branch of the vestibular nerve (Figs 23–26). Myelin sheet thickness is greatest for the posterior crista fibers that must travel the longest distance between the ganglion and the end organs. Thus, besides the strategic placement of hair cells in different portions of the end organs, the availability of more than one trophic and transmitter molecule, and polarization along strategic epithelial boundaries, fiber diameter and myelin thickness (Fig. 25) must be taken into account for interpreting functional measures. In fact, auditory fibers which travel a very short distance from the ganglion to the hair cells of the basilar papilla are thinner than most vestibular fibers and the myelin sheet thickness of auditory fibers is relatively constant through the nerve (Fig. 12), a property that can be best appreciated by comparing the correlation of vestibular and auditory fibers (Fig. 26). It is assumed that multiple hair cells innervated by a single neuron would provide a different pattern of activity than multiple hair cells innervated each mainly by one neuron. These results should prove useful for interpreting functional measures of the chicken vestibular system, in particular the role that peripheral afferents play in the transmission of neural signals from the inner ear receptors to the brain stem.

5. CONCLUSIONS AND RECOMMENDATIONS

(1) Chick afferents have similar morphological and morphometric features as mammalian afferents.

(2) There is a significant increase in neuronal (perikarya or soma and fibers) size in both ganglion between stage 34 (E8) and 44 (E18) but the increase is significantly larger in the vestibular than in the auditory neurons.

(3) The ratio of nuclear to cytoplasmic cross-sectional area and the amount of Nissl substance are greater for the vestibular than for the auditory perikarya.

(4) Vestibular perikarya express S100β in their nuclei whereas auditory perikarya express S100β primarily in the cytoplasm and in a diffuse manner.

(5) Macular lagenar perikarya express S100β and calretinin also in the nuclei, whereas adjacent auditory perikarya did not and may be vestibular rather than auditory neurons even though lagenar macula neurons coexist with auditory neurons.

(6) It is suggested that in the interpretation of functional vestibular avian measures the heterogeneity of fiber diameter and myelin sheet thickness shown here be taken into account.

Acknowledgements

This work was supported by NASA grant NAGW-2-999 to CDF, funds from the NIH and from Tulane Pathology.

REFERENCES

Ard, M. D. and Morest, D. K. (1984). Cell death during development of the cochlear and vestibular ganglia of the chick. *Int. J. Dev. Neurosci.* **2**, 535–547.

Baird, R. A., Desmadryl, G., Fernández, C. and Goldberg, J. M. (1988). The vestibular nerve of the chinchilla. II. Relation between afferent response properties and peripheral innervation patterns in the semicircular canals. *J. Neurophysiol.* **60**, 182–203.

Baird, R. A. and Lewis, E. R. (1986). Correspondences between afferent innervation patterns and response dynamics in the bullfrog utricle and lagena. *Brain Res.* **369**, 48–64.

Ballantyne, J. and Engström, H. (1969). Morphology of the vestibular ganglion cells. *J. Laryng. Otol.* **83**, 19–42.

Bergström, B. (1973a). Morphology of the vestibular nerve. I. Anatomical studies of the vestibular nerve in man. *Acta Otolaryngol.* **76**, 162–172.

Bergström, B. (1973b). Morphology of the vestibular nerve. II. The number of myelinated vestibular nerve fibers in man at various ages. *Acta Otolaryngol.* **76**, 173–179.

Bergström, B. (1973c). Morphology of the vestibular nerve. III. Analysis of the calibers of the myelinated vestibular nerve fibers in man at various ages. *Acta Otolaryngol.* **76**, 331–338.

Bissonenette, J. and Fekete, D. (1995). Standard atlas of the gross anatomy of the developing inner ear of the chicken. *J. Comp. Neurol.* **368**, 620–630.

Boyle, R., Carey, J. P. and Highstein, S. M. (1991). Morphological correlates of response dynamics and efferent stimulation in horizontal semicircular canal afferents of the toadfish. *Opsanus Tau. J. Neurophysiol.* **66**, 1504–1521.

Boyle, R., Goldberg, J. M. and Highstein, S. M. (1992). Inputs from regularly and irregularly discharging vestibular nerve afferents to secondary neurons in squirrel monkey vestibular nuclei. 3. Correlation with vestibulospinal and vestibuloocular output pathways. *J. Neurophysiol.* **68**, 471–484.

Braun, K. (1990). Calcium-binding proteins in avian and mammalian central nervous system: possible localization, development and possible functions. *Prog. Histochem. Cytochem.* **21**, 1–64.

Brodal, A., Pompeiano, O. and Walberg, F. (1962). *The Vestibular Nuclei and their Connections. Anatomy and Functional Correlations*. C. C. Thomas, Springfield, IL.

Cass, S. P., Goshgarian, H. G. and Stockwell, C. W. (1987). Vestibular compensation after labyrinthectomy and vestibular neurectomy in cats. In: *91st Meeting of the American Academy of Otolaryngology — Head & Neck Surgery*, Chicago, IL.

Celio, M. (1986). Parvalbumin in most gamma-aminobutyric acid-containing neurons of the rat cerebral cortex. *Science* **231**, 995–997.

Celio, M. (1990). Calbindin D-28k and paralbumin in the rat nervous system. *Neuroscience* **35**, 375–475.

Correia, M. J., Eden, A. R., Westlund, K. N. and Coulter, J. D. (1983). A study of some of the ascending and descending vestibular pathways in the pigeon (*Columba livia*) using anterograde transneuronal autoradiography. *Brain Res.* **278**, 53–61.

Cox, R. G. and Peusner, K. D. (1990a). Horseradish peroxidase labeling of the efferent and afferent pathways of the avian tangential vestibular nucleus. *J. Comp. Neurol.* **296**, 296–324.

Cox, R. G. and Peusner, K. D. (1990b). Horseradish peroxidase labeling of the central pathways in the medulla of the ampullary nerves in the chicken, *Gallus gallus*. *J. Comp. Neurol.* **297**, 564–581.

Cox, R. G. and Peusner, K. D. (1990c). Horseradish peroxidase labeling of the efferent and afferent pathways of the avian tangential vestibular nucleus. *J. Comp. Neurol.* **296**, 324–341.

Dewaegh, S. M., Lee, V. M. Y. and Brady, S. T. (1992). Local modulation of neurofilament phosphorylation, axonal caliber, and slow axonal transport by myelinating Schwann cells. *Cell* **68**, 451–463.

Didier, A., Dupont, J. and Cazals, Y. (1990). GABA immunoreactivity of calyceal nerve endings in the vestibular system of the guinea pig. *Cell Tissue Res.* **260**, 415–419.

Drescher, D. G., Khan, K. M., Arden, R. L. *et al.* (1989). Protein associated with the sensory cell layer of the rainbow trout saccular macula. *Brain Res.* **485**, 225–235.

Engström, H., Lindeman, H. H. and Ades, H. W. (1966). Anatomical features of the auricular sensory organs. In: J. Huertas and A. Graybiel (Eds), *2nd Symp. on the Role of the Vestibular Organs in Space Exploration*, Ames Research Center, Moffett Field, CA, pp. 33–46.

Fermin, C. D. and Igarashi, M. (1982). Vestibular ganglion of the squirrel monkey. *Ann. Otol. Rhino. Laryngol.* **91**, 44–52.

Fermin, C. D. and Cohen, G. M. (1984a). Development of the embryonic chick's statoacoustic ganglion. *Acta Otolaryngol.* **98**, 42–52.

Fermin, C. D. and Cohen, G. M. (1984b). Developmental gradients in the embryonic chick's basilar papilla. *Acta Otolaryngol.* **97**, 39–51.

Fermin, C. D. and Igarashi, M. (1984). Dendritic growth following labyrinthectomy in the squirrel monkey. *Acta Otolaryngol.* **97**, 203–212.

Fermin, C. and Igarashi, M. (1987). Morphometry and ultrastructure of the squirrel monkey (*Saimiri sciureus*) vestibular nerve. *Acta Anat.* **129**, 188–199.

Fermin, C. and DeGraw, S. (1995). Color thresholding in video imaging. *J. Anat.* **186**, 469–481.

Fermin, C. and Martin, D. (1995). Expression of S100β in sensory and secretory cells of the vertebrate inner ear. *Cell Mol. Biol.* **41**, 213–225.

Fermin, C., Igarashi, M., Martin, G. and Jenkins, H. (1989). Ultrastructural evidence of repair and neuronal survival after labyrinthectomy in the squirrel monkey. *Acta Anat.* **135**, 62–70.

Fermin, C., Martin, D. and Hara, H. (1997). Color threshold and ratio of S100β, MAP5, NF68/200, GABA & GAD. I. Distribution in inner ear afferents. *J. Cell Vision* **4** (in press).

Fernández, C., Baird, R. A. and Goldberg, J. M. (1988). The vestibular nerve of the chinchilla. I. Peripheral innervation patterns in the horizontal and superior semicircular canals. *J. Neurophysiol.* **60**, 167–181.

Fernández, C. and Goldberg, J. M. (1971). Physiology of peripheral neurons innervating semicircular canals of the squirrel monkey. II. Response to sinusoidal stimulation and dynamics of peripheral vestibular system. *J. Neurophysiol.* **34**, 661–675.

Fernández, C., Goldberg, J. M. and Abend, W. K. (1972). Response to static tilts of peripheral neurons innervating otolith organs of the squirrel monkey. *J. Neurophysiol.* **35**, 978–983.

Fernández, C., Lysakowski, A. and Goldberg, J. (1995). Hair-cell counts and afferent innervation patterns in the cristae ampullares of the squirrel monkey with a comparison to the chinchilla. *J. Neurosci.* **73**, 1253–1281.

Fischer, F. P., Eisensamer, B. and Manley, G. A. (1994). Cochlear and lagenar ganglia of the chicken. *J. Morphol.* **220**, 71–83.

Fraher, J. P., Oleary, D., Moran, M. A., Cole, M., King, R. H. M. and Thomas, P. K. (1990). Relative growth and maturation of axon size and myelin thickness in the tibial nerve of the rat. I. Normal animals. *Acta Neuropathol.* **79**, 364–374.

Friedrich, V. L. and Mugnaini, E. (1983). Myelin sheath thickness in the CNS is regulated near the axon. *Brain Res.* **274**, 329–331.

Gacek, R. R. (1980). Neuroanatomical correlates of vestibular function. *Ann. Otol. Rhinol. Laryngol.* **89**, 2–5.

Gacek, R. R., Lyon, M. J. and Schoonmaker, J. E. (1989). Morphologic correlates of vestibular compensation in the cat. *Acta Otolaryngol.* **462** (Suppl.), 1–16.

Gacek, R. R., Schoonmaker, J. and Lyon, M. J. (1995). Morphologic changes in superior vestibulo-ocular neurons and vestibular nerve following labyrinthectomy in the cat. *Acta Otolaryngol.* **518** (Suppl.), 3–12.

Goldberg, J. M. (1981). Thick and thin mammalian vestibular axons: Afferent and efferent response characteristics. In: *The Vestibular System: Function and Morphology*, Springer-Verlag, New York, pp. 187–205.

Goldberg, J. M. (1991). The vestibular end organs: morphological and physiological diversity of afferents. *Curr. Opin. Neurobiol.* **1**, 229–235.

Goldberg, J. M. and Fernández, C. (1971). Physiology of peripheral neurons innervating semicircular canals of the squirrel monkey. III. Variations among units in their discharge properties. *J. Neurophysiol.* **34**, 676–684.

Goldberg, J. M., Desmadryl, G., Baird, R. A. and Fernández, C. (1990a). The vestibular nerve of the chinchilla. V. Relation between afferent discharge properties and peripheral innervation patterns in the utricular macula. *J. Neurophysiol.* **63**, 791–804.

Goldberg, J. M., Desmadryl, G., Baird, R. A. and Fernández, C. (1990b). The vestibular nerve of the chinchilla. IV. Discharge properties of utricular afferents. *J. Neurophysiol.* **63**, 781–790.

Goldberg, J. M., Lysakowski, A. and Fernández, C. (1990c). Morphophysiological and ultrastructural studies in the mammalian cristae ampullares. *Hear. Res.* **49**, 89–102.

Guth, P., Fermin, C., Pantoja, R., Edwards, R. and Norris, C. (1994). Hair cells of different shapes and their placement along the frog crista ampullaris. *Hear. Res.* **73**, 109–113.

Guy, J., Ellis, E. A., Kelley, K. *et al.* (1989a). Spectra of G ratio, myelin sheath thickness, and axon and fiber diameter in the guinea pig optic nerve. *J. Comp. Neurol.* **287**, 446–454.

Hamilton, D. W. (1968). The calyceal synapse of tyoe I vestibular hair cells. *J. Ultrastruct. Res.* **23**, 98–114.

Hamilton, H. (1952). *Lillie's Development of the Chick*. Henry Hold, New York.

Highstein, S. M., Goldberg, J. M., Moschovakis, A. K. and Fernández, C. (1987). Inputs from regularly and irregularly discharging vestibular nerve afferents to secondary neurons in the vestibular nuclei of the squirrel monkey. II. Correlation with output pathways of secondary neurons. *J. Neurophysiol.* **58**, 719–738.

Highstein, S. M. and McCrea, R. A. (1988). The anatomy of the vestibular nuclei. In: *Neuroanatomy of the Oculomotor System*, Publisher, Location?, pp. 177–202.

Honrubia, V., Sitko, S., Kimm, J. *et al.* (1981). Physiological and anatomical characteristics of primary vestibular afferent neurons in the bullfrog. *Int. J. Neurosci.* **15**, 197–206.

Honrubia, V., Sitko, S. and Lee, R. (1984). Anatomical characteristics of the anterior vestibular nerve of the bullfrog. *Laryngoscope* **94**, 464–474.

Honrubia, V., Suarez, C., Kuruvilla, A. and Sitko, S. (1985). Central projections of primary vestibular fibers in the bullfrog. III. The anterior semicircular canal afferents. *Laryngoscope* **95**, 1526–1535.

Hsieh, S. T., Kidd, G. J., Crawford, T. O., Xu, Z. S., Lin, W. M., Trapp, B. D., Cleveland, D. W. and Griffin, J. W. (1994). Regional modulation of neurofilament organization by myelination in normal axons. *J. Neurosci.* **14**, 6392–6401.

Igarashi, M., Watanabe, T. and Maxian, P. M. (1970). Dynamic equilibrium in squirrel monkeys after unilateral and bilateral labyrinthectomy. *Acta Otolaryngol.* **69**, 247–253.

Jones, S. and Jones, T. (1995a). Neural tuning characteristics of auditory primary afferents in the chicken embryo. *Hear. Res.* **82**, 139–148.

Jones, S. and Jones, T. (1995b). The tonotopic map in the embryonic chicken cochlea. *Hear. Res.* **82**, 149–157.

Jones, T. A. (1992). Vestibular short latency responses to pulsed linear acceleration in unanesthetized animals. *Electroencephalogr. Clin. Neuro.* **82**, 377–386.

Jones, T. A. and Pedersen, T. L. (1989). Short latency vestibular response to pulsed linear acceleration. *Am. J. Otolaryngol.* **10**, 327–335.

Jones, T. A. and Schiltz, T. (1989). Pulsed linear acceleration as a vestibular stimulus in electrophysiological investigations. *J. Neurosci. Methods* **27**, 115–120.

Au: 1989? (Here or in 1989b)

Au: ptcav, supply

Au: OK?

Jones, T. A., Beck, M. M., Brown-Borg, M. M. and Burger, R. E. (1987). Far-field recordings of short latency auditory responses in the white leghorn chick. *Hear. Res.* **27**, 67–74.

Jorgensen, J. M. (1970). On the structure of the macula lagenae in birds with some notes on the avian maculae utriculi and sacculi. *Vidensk. Meddr. Dansk. Naturh. Foren.* **133**, 121–147.

Kleitman, N. and Koppanyi, T. (1926). Body-righting in the fowl (*Gallus domesticus*). *Am. J. Physiol.* **78**, 110–126.

Landolt, J. P., Topliff, E. D. L. and Silverberg, J. D. (1973). Size distribution analysis of myelinated fibers in the vestibular nerve of the pigeon. *Brain Res.* **54**, 31–42.

Lewis, E. R., Leverenz, E. L. and Bialek, W. (1985). In: *The Vertebrate Inner Ear*, CRC Press, Boca Raton, FL, pp. 13–83.

Lopez, I., Juiz, J. M., Altschuler, R. A. and Meza, G. (1990). Distribution of GABA-like immunoreactivity in guinea pig vestibular cristae ampullaris. *Brain Res.* **530**, 170–175.

Lopez, I., Wu, J. Y. and Meza, G. (1992). Immunocytochemical evidence for an afferent GABAergic neurotransmission in the guinea pig vestibular system. *Brain Res.* **589**, 341–348.

Lysakowski, A., McCrea, R. and Tomlinson, R. (1992). Anatomy of vestibular end organs and neural pathways. In: *Otolaryngology*, Mosby-Year Book, St Louis, MO, pp. 2525–2547.

Martinoya, C., LeHouezec, J. and Bloch, S. (1984). Pigeon's eyes converge during feeding: evidence for frontal binocular fixation in a lateral-eyed bird. *Journal* **45**, 335–339.

Meyers, S. F. and Lewis, E. R. (1989). Vestibular afferent responses to microrotational stimuli. *Ass. Res. Otolaryngol.* **13**, 246.

Meza, G., Carabez, A. and Ruiz, M. (1982). GABA synthesis in isolated vestibulary tissue of chick inner ear. *Brain Res.* **241**, 157–161.

Meza, G., Wu, J.-Y. and Lopez, I. (1992). GABA is an afferent vestibular neurotransmitter in the guinea pig. Immunocytochemical evidence in the utricular maculae. *Ann NY Acad. Sci.* **656**, 943–946.

Muma, N. A., Slunt, H. H. and Hoffman, P. N. (1991). Postnatal increases in neurofilament gene expression correlate with the radial growth of axons. *J. Neurocytol.* **20**, 844–854.

Newman, A., Suarez, C., Lee, W. S. and Honrubia, V. (1992). Afferent innervation of the vestibular nuclei in the chinchilla. 2. Description of the vestibular nerve and nuclei. *Brain Res.* **597**, 278–297.

Peusner, K. D., Lindberg, N. H. and Mansfield, P. F. (1988). Ultrastructural study of calycine synaptic endings of colossal vestibular fibers in the cristae ampullares of the developing chick. *Int. J. Dev. Neurosci.* **6**, 267–283.

Richter, E. (1981a). Quantitative study of Scarpa's ganglion and vestibular sense organs in endolymphatic hydrops. *Ann. Otol. Rhinol. Laryngol.* **90**, 121–125.

Richter, E. (1981b). Scarpa's ganglion in the cat one year after labyrinthectomy. *Arch. Otorhinolaryngol.* **230**, 251–255.

Ross, M. D., Cutler, L., Doshay, D. *et al.* (1991). A new theory of macular organization based on computer-assisted 3-D reconstruction, Monte Carlo simulation and symbolic modeling of vestibular maculas. *Acta Otolaryngol.* **481**, 11–14.

Sakaguchi, T., Okada, M., Kitamura, T. and Kawasaki, K. (1993). Reduced diameter and conduction velocity of myelinated fibers in the sciatic nerve of a neurofilament-deficient mutant quail. *Neurosci. Lett.* **153**, 65–68.

Sans, A. and Chat, M. (1982). Analysis of temporal and spatial patterns of rat vestibular hair cell differentiation by tritiated thymidine radioautography. *J. Comp. Neurol.* **206**, 1–8.

Sans, A., Griguer, C. and Lehouelleur, J. (1994). The vestibular type I hair cells — a self-regulated system. *Acta Otolaryngol.* **513** (Suppl.), 11–14.

Smith, K. J., Blakemore, W. F., Murray, J. A. and Patterson, R. C. (1982). Internodal myelin volume and axon surface area. A relationship determining myelin thickness. *J. Neurol. Sci.* **55**, 231–246.

Takasaka, T. and Smith, C. A. (1971). The structure and innervation of the pigeon's basilar papilla. *J. Ultrastruct. Res.* **35**, 20–65.

Usami, S.-C., Hozawa, J. and Ylikoski, J. (1991). Coexistence of substance P and calcitonin gene-related peptide-like immunoreactivities in the rat vestibular endorgans. *Acta Ololaryngol.* **481** (Suppl.), 166–169.

Wackym, P. A., Popper, P. and Micevych, P. E. (1993). Distribution of calcitonin gene-related peptide messenger RNA and immunoreactivity in the rat central and peripheral vestibular system. *Acta Otolaryngol.* **113**, 601–608.

Wersäll, J., Flock, A. and Lundquist, P.-G. (1965). Structural basis for directional sensitivity in cochlear and vestibular sensory recpetors. *Cold Spring Harbor Symp. Quant. Biol.* **30**, 122–132.

Wesäll, J. and Lundquist, P.-G. (1966). Morphological polarization of the mechanoreceptors of the vestibular and acoustic systems. In: J. Huertas and A. Graybiel (Eds), *2nd Symp. on the Role of the Vestibular Organs in Space Exploration*, Ames Research Center, Moffett Field, CA, pp. 57–72.

Winget, C. and Smith, A. H. (1962). Quantitative measurement of labyrinthine function in the fowl by nystagmography. *J. Appl. Physiol.* **17**, 712–718.

Wold, J. E. (1975). The vestibular nuclei in the domestic hen (*Gallus domesticus*). II. Primary afferents. *Brain Res.* **95**, 531–543.

Wold, J. E. (1976). The vestibular nuclei in the domestic hen (*Gallus domesticus*). I. Normal anatomy. *Anat. Embryol.* **149**, 29–46.

Wold, J. E. (1981). *Synopsis. The Vestibular Nuclei in the Domestic Hen. Anatomical Studies of their Structure and Fiber Connections.* Anatomical Institute, University of Oslo, Norway, 51 p., monograph.

Yamashita, M. and Ohmori, H. (1991). Synaptic bodies and vesicles in the calix type synapse of chicken semicircular canal ampullae. *Neurosci. Lett.* **129**, 43–46.

Ylikoski, J., Belal, A., Jr and House, W. F. (1981). Morphology of human cochlear nerve after labyrinthectomy. *Acta Otolaryngol.* **91**, 161–171.

Ylikoski, J., Pirvola, U. and Happola, O. (1993). Characterization of the vestibular and spiral ganglion cell somata of the rat by distribution of neurofilament proteins. *Acta Otolaryngol.* **503** (Suppl.), 121–126.

Zhao, J. X., Ohnishi, A. Itakura, C., Mizutani, M., Yamamoto, T., Hayashi, H. and Murai, Y. (1994). Greater number of microtubules per axon of unmyelinated fibers of mutant quails deficient in neurofilaments — possible compensation for the absence of neurofilaments. *Acta Neuropathol.* **87**, 332–336.